UNIVERSIDADE ESTADUAL DE CAMPINAS

Instituto de Geociências

RAPHAEL BIANCHI HUNGER

O DEPÓSITO DE ÓXIDO DE FERRO COBRE-OURO (IOGC) GROTA FUNDA, DOMÍNIO CARAJÁS (PA): ALTERAÇÃO HIDROTERMAL, REGIME DE FLUIDOS E IDADE DA MINERALIZAÇÃO

CAMPINAS

2017

RAPHAEL BIANCHI HUNGER

O DEPÓSITO DE ÓXIDO DE FERRO COBRE-OURO (IOGC) GROTA FUNDA, DOMÍNIO CARAJÁS (PA): ALTERAÇÃO HIDROTERMAL, REGIME DE FLUIDOS E IDADE DA MINERALIZAÇÃO

DISSERTAÇÃO APRESENTADA AO INSTITUTO DE GEOCIÊNCIAS DA UNIVERSIDADE ESTADUAL DE CAMPINAS PARA OBTENÇÃO DO TÍTULO DE MESTRE EM GEOCIÊNCIAS NA ÁREA DE GEOLOGIA E RECURSOS NATURAIS.

ORIENTADOR: PROF. DR. ROBERTO PEREZ XAVIER

COORIENTADORA: PROFA. DRA. CAROLINA PENTEADO NATIVIDADE MORETO

ESTE EXEMPLAR CORRESPONDE À VERSÃO FINAL DA DISSERTAÇÃO DEFENDIDA PELO ALUNO RAPHAEL BIANCHI HUNGER E ORIENTADA PELO PROF. DR. ROBERTO PEREZ XAVIER

CAMPINAS

2017

Agência(s) de fomento e nº(s) de processo(s): CAPES

Ficha catalográfica
Universidade Estadual de Campinas
Biblioteca do Instituto de Geociências
Marta dos Santos - CRB 8/5892

H894d

Hunger, Raphael Bianchi, 1990-
O depósito de óxido de ferro cobre-ouro (IOCG) Grota Funda, Domínio Carajás (PA) : alteração hidrotermal, regime de fluidos e idade da mineralização / Raphael Bianchi Hunger. – Campinas, SP : [s.n.], 2017.

Orientador: Roberto Perez Xavier.
Coorientador: Carolina Penteado Natividade Moreto.
Dissertação (mestrado) – Universidade Estadual de Campinas, Instituto de Geociências.

1. Depósitos de óxido de Fe-Cu-Au - Carajás, Serra dos (PA). 2. Alteração hidrotermal. 3. Inclusões fluidas. 4. Isótopos de boro. I. Xavier, Roberto Perez, 1958-. II. Moreto, Carolina Penteado Natividade, 1985-. III. Universidade Estadual de Campinas. Instituto de Geociências. IV. Título.

Informações para Biblioteca Digital

Título em outro idioma: The Grota Funda iron oxide copper-gold (IOCG) deposit, Carajás Domain (PA) : hydrothermal alteration, fluid evolution and mineralization age
Palavras-chave em inglês:
Iron oxide-copper-gold deposits - Carajas, Serra dos (PA)
Hydrothermal alteration
Fluid inclusions
Boron isotopes
Área de concentração: Geologia e Recursos Naturais
Titulação: Mestre em Geociências
Banca examinadora:
Roberto Perez Xavier [Orientador]
Maria José Maluf Mesquita
Luiz Henrique Ronchi
Data de defesa: 21-09-2017
Programa de Pós-Graduação: Geociências

UNIVERSIDADE ESTADUAL DE CAMPINAS
INSTITUTO DE GEOCIÊNCIAS

AUTOR: Raphael Bianchi Hunger

O DEPÓSITO DE ÓXIDO DE FERRO COBRE-OURO (IOCG) GROTA FUNDA, DOMÍNIO CARAJÁS (PA): ALTERAÇÃO HIDROTERMAL, REGIME DE FLUIDOS E IDADE DA MINERALIZAÇÃO

ORIENTADOR: Prof. Dr. Roberto Perez Xavier
COORIENTADORA: Profa. Dra. Carolina Penteado Natividade Moreto

Aprovado em: 21 / 09 / 2017

EXAMINADORES:

Prof. Dr. Roberto Perez Xavier - Presidente

Profa. Dra. Maria José Maluf de Mesquita

Prof. Dr. Luiz Henrique Ronchi

A Ata de Defesa assinada pelos membros da Comissão Examinadora, consta no processo de vida acadêmica do aluno.

Campinas, 21 de setembro de 2017.

SÚMULA CURRICULAR

RAPHAEL BIANCHI HUNGER

Possui graduação (2015) em Geologia pela Universidade Estadual de Campinas (UNICAMP). Tem experiência na área de Geociências, com ênfase em Metalogênese, Petrografia e Geologia de Campo. Atuou como monitor em diversas disciplinas da graduação, incluindo Mineralogia, Geologia Econômica, Sedimentologia, Estratigrafia e Elementos de Geologia (para biólogos). Auxiliou no desenvolvimento e execução de atividades em diversos projetos didáticos, como o XIV Ciência & Arte nas Férias (2016).

Atualmente está finalizando a dissertação de mestrado em Geociências através do programa de pós-graduação do Instituto de Geociências da UNICAMP, com ênfase em estudos petrográficos, isotópicos (isótopos de B em turmalina) e de inclusões fluidas do depósito de óxido de ferro-cobre-ouro Grota Funda, Província Carajás (PA – Brasil).

AGRADECIMENTOS

Meus sinceros agradecimentos a todos aqueles que de alguma maneira contribuíram com o desenvolvimento dessa pesquisa.

A Deus, por seu obstinado Amor.

A minha família: Elaine, Rodolpho, Fernanda, Lucas, Euterpia, Flavio e Carlos; pelo carinho, compaixão e incentivo nos momentos mais difíceis. Obrigado por nunca me deixarem esquecer de que sou capaz!

Aos amigos de longa data: Caroline Brandão, Anderson Yin, Tatiane e Rafael Baez, Lucas Di Salvo, Gabrieli Villela, Marcos Machado, Felipe Brandão, Beatriz Pavani, Alexandre Bliska e Guilherme Paes Leme. Obrigado por existirem!

Aos queridos amigos e companheiros de pós-graduação: José Henrique, Poliana Toledo, João Motta, Verônica Trevisan, Patrícia Caires, Danilo Barbuena e demais membros do SEG Student Chapter.

Aos meus orientadores: prof. Dr. Roberto Xavier e profa. Dra. Carolina Moreto, pelas experiências e conhecimentos compartilhados e por todo apoio oferecido ao longo desses últimos anos.

Ao grande amigo Gustavo Melo, por toda contribuição e orientação, pelas revisões textuais e discussões geológicas que aperfeiçoaram essa pesquisa.

Ao responsável pelos laboratórios do Instituto de Geociências da UNICAMP: Dailto Silva, por todas as vezes em que o incomodei e mesmo atarefado nunca recusou um pedido de ajuda. Agradeço em especial todo o suporte dado durante o período de análise das inclusões fluidas.

A Fundação de Amparo à Pesquisa (FADESP) em convênio com o INCT/GEOCIAM, pela bolsa auxílio concedida durante a etapa de campo. A Fundação CAPES, pela bolsa de mestrado com a qual fui contemplado.

A Vale, em especial a toda a equipe de funcionários do N5 e aos geólogos Ronan Barbosa e Samuel Nunes, por todo apoio logístico e operacional durante minha pesquisa de campo.

RESUMO

O depósito de óxido de ferro cobre-ouro (IOCG) Grota Funda está localizado na porção noroeste do Domínio Carajás, um segmento Arqueano (3,0 – 2,55 Ga) da Província Carajás, no sudeste do Cráton Amazônico. Situado em uma zona de cisalhamento regional de direção WNW-ESE (Sistema Transcorrente Pojuca), onde também se encontram os depósitos de Cu-Au Gameleira e Cu-Zn Pojuca, o depósito insere-se em sequências vulcano-sedimentares do Grupo Igarapé-Pojuca, compreendendo basalto, diabásio, gabro e dacito subordinado, além de formações ferríferas bandadas. Nesta sequência, as rochas metavulcânicas máficas correspondem às principais hospedeiras das mineralizações cupro-auríferas. A evolução paragenética do sistema hidrotermal do depósito Grota Funda engloba uma alteração hidrotermal cálcica-sódica de alta temperatura (albita-hastingsita-escapolita), seguida por intenso metassomatismo rico em Fe (magnetita-grunerita-almandina), alteração potássica com biotita, precipitação de clorita-quartzo-turmalina e veios de carbonato-quartzo tardios. Episódios de mineralizações de cobre (-ouro) associam-se espacialmente às zonas enriquecidas em ferro, de alteração potássica e cloritizas. A idade de 2530 ± 60 Ma, obtida através da datação Re-Os em molidenita associado a veios de grunerita-magnetita, é interpretada como a idade de formação do primeiro estágio de mineralização no depósito. A principal zona de minério está espacialmente associada às zonas de alteração potássica com brechas constituídas por calcopirita-magnetita-esfalerita-pirrotita-pentlandita. A paragênese do minério sugere condições de baixa fS_2 e fO_2 para os fluidos mineralizantes. O desenvolvimento da assembléia de alteração cálcica-sódica é atribuído à circulação regional de fluidos hipersalinos e metalíferos de alta temperatura (> 500°C). A mistura desses fluidos hipersalinos com fluidos mais frios e de salinidade moderada à elevada (24 a 29 wt% NaCl + CaCl2 equiv.), resultando em uma diminuição da temperatura e da atividade de Cl^- do sistema, é interpretado como o principal processo desencadeador da precipitação de metais na zona de minério principal. As associações de alteração pós-mineralização (clorita-quartzo-turmalina e carbonato-quartzo) refletem decréscimos graduais de temperatura, salinidade e pH dos fluidos. Além disso, as composições isotópicas de boro ($\delta^{11}B$ = +8,2‰ a + 13,6‰) em turmalina associada às zonas de alteração clorítica são atribuídas a fontes mistas, incluindo boro proveniente de salmouras marinhas (e.g. água do mar evoluída ou fluidos do tipo *bittern*) e boro lixiviado das rochas hospedeiras (e.g. metavulcânicas máficas).

Palavras-chave: Grota Funda; Carajás; Alteração hidrotermal; Inclusões fluidas; Isótopos de boro

ABSTRACT

The Grota Funda iron oxide copper-gold deposit (IOCG) is located at the northwestern portion of the Carajás Domain, an Archean (3.0 – 2.55 Ga) segment of the Carajás Province, in the southeastern sector of the Amazonian Cráton. Within the same regional WNW-ESE-striking shear zone (Pojuca Fault System) in which lie the Gameleira (Cu-Au) and Pojuca (Cu-Zn) deposits, volcano-sedimentary sequences of the Igarapé-Pojuca Group, comprising basalt, diabase, gabbro and dacitic rocks and banded iron formations, are the main lithotypes recognized in the deposit area. In this sequence, mafic metavolcanic rocks represent the main hosts to the copper(-gold) mineralizations. The paragenetic evolution of the Grota Funda hydrothermal system encompasses an early high-temperature calcic-sodic hydrothermal alteration (albite-hastingsite-scapolite), ensued by intense Fe-metasomatism (magnetite-grunerite-almandine), potassic alteration with biotite, chlorite-quartz-tourmaline precipitation, and late carbonate-quartz veining. Copper (-gold) mineralizations are spatially and temporally associated with iron-enriched, potassically-altered and chlorite-altered zones. Molybdenite from grunerite-magnetite veins yielded a Re-Os model age of 2,530 ± 60 Ma, which is interpreted as a mineralization age coeval with the Fe-metasomatism. The main sulfide ore is spatially associated with potassically-altered zones, and predominantly forms breccia bodies characterized by a chalcopyrite-magnetite-sphalerite-pyrrhotite-pentlandite assemblage. The ore paragenesis suggests a mineralizing fluid at low fS_2 and fO_2 conditions. Development of early and high temperature (> 500°C) alteration assemblages (albite, scapolite-hastingsite) is attributed to regional circulation of deep-seated hypersaline and metalliferous fluids. Mixing with moderate to high salinity (24 to 29 wt% NaCl + $CaCl_2$ equiv.) and cooler fluids, may have triggered ore precipitation in the main ore zone, due to a decrease in temperature and Cl^- activity. Post-ore alteration assemblages (chlorite-quartz-tourmaline, carbonate-quartz) resulted from considerable temperature, salinity and pH decrease. In addition, boron isotopic compositions ($\delta^{11}B$ = +8.2 to +13.6‰) of tourmaline from the chlorite alteration zone are attributed to mixed sources, including isotopically heavier boron sourced fluids, possibly represented by highly saline brines (e.g., evolved seawater, formation water or bittern fluids) and light boron leached from the host rocks (e.g mafic metavolcanic rocks).

Keywords: Grota Funda; Carajás; Hydrothermal alteration; Fluid inclusions; Boron isotopes

LISTA DE ILUSTRAÇÕES

APÊNDICE

LISTA DE TABELAS

APÊNDICE

SUMÁRIO

1. INTRODUÇÃO

A Província Carajás contempla uma ampla variedade de sistemas cupríferos formados durante o Neoarqueano e o Paleoproterozóico (Xavier et al. 2010, 2012). Dentre eles, os sistemas óxido de ferro-cobre-ouro (IOCG), localizados nos setores norte e sul do Domínio Carajás, têm sido alvos preferenciais da indústria de exploração mineral, dado seu potencial para formar depósitos de teor e tonelagem elevados. Atualmente este domínio conta com duas minas de cobre em operação, a de Sossego e Salobo, com produção anual de minério de cobre concentrado em torno de 100 Mt e de 160 Mt, respectivamente (VALE 2017).

O conhecimento atual acerca dos depósitos IOCG do Domínio Carajás permite concluir que a gênese desses sistemas está relacionada à atuação de múltiplos eventos hidrotermais no Neoarqueano (~ 2,71 Ga e 2,57 Ga) e no Paleoproterozóico (2,0 – 1,88 Ga) (Moreto et al. 2015a,b). Embora a origem dos fluidos mineralizantes seja ainda controversa, a mistura entre fluidos quentes (> 500°C), hipersalinos (~50 wt% NaCl + $CaCl_2$ equiv.) e portadores de metais, com fluidos mais diluídos (e.g. água meteórica) e de baixa salinidade, em diferentes níveis crustais, parece representar o principal mecanismo para a precipitação do minério de cobre e ouro nesses depósitos (Xavier et al. 2012). Contudo, a formação desses sistemas é dependente de uma série de fatores que atuam em escala regional e de depósito como, por exemplo, a disponibilidade de enxofre no sistema, condições redox dos fluidos, interação fluido-rocha, entre outros (Xavier et al. 2010, 2012). Adicionalmente, a contribuição de fluidos magmáticos e não-magmáticos caracteriza uma importante questão de debate no que se refere aos modelos metalogenéticos atuais. A importância de intrusões graníticas neoarqueanas (~ 2.75 ou 2.57 Ga) e paleoproterozóicas (~1.88 Ga) como potenciais fontes de calor e fluidos, têm sido enfatizada por uma série de autores (Huhn et al. 1999b; Réquia et al. 2003; Tallarico et al. 2005; Neves 2006; Pollard 2006; Villas et al. 2006; Grainger et al. 2008). Em contrapartida, a participação de fluidos bacinais que interagiram com evaporitos marinhos, ou derivados da evaporação da água do mar (fluidos do tipo *bittern*), e que poderiam explicar as elevadas salinidades observadas em fluidos mineralizantes na Província Carajás, é indicada por dados isotópicos (B, Cl, Sr) e de razões Cl/Br e Na/Cl em inclusões fluidas (Chiaradia et al. 2006; Xavier et al. 2008, 2009, 2013).

O depósito Grota Funda é formalmente conhecido como a extensão leste dos depósitos Gameleira e Pojuca, no setor noroeste do Domínio Carajás. Apesar de sua proximidade com esses depósitos, a evolução geológica e metalogenética do depósito Grota

Funda ainda é pouco conhecida. Uma evolução paragenética similar, marcada por estágios subsequentes de alteração sódica-cálcica, metassomatismo férrico e alteração potássica seguida por precipitação do minério cupro-aurífero, é reconhecida em outros depósitos IOCG localizados no setor norte do Domínio Carajás (e.g. Salobo; Melo et al. 2016), o que sugere a atuação de processos genéticos semelhantes. Desta forma, este estudo introduz o depósito Grota Funda, buscando definir suas rochas hospedeiras e a evolução paragenética de seu paleo-sistema hidrotermal, incluindo os principais estágios de mineralização. Adicionalmente, através de dados geocronológicos (Re-Os em molibdenita), isotópicos (B em turmalina) e de inclusões fluidas, esta pesquisa apresenta novas contribuições acerca da época de formação de sistemas IOCG no Domínio Carajás, e da origem e composição dos fluidos hidrotermais.

2. OBJETIVOS

O presente estudo tem como objetivo reconstruir a história evolutiva do depósito de óxido de ferro-cobre-ouro Grota Funda, comparando-o a sistemas semelhantes já descritos na Província Carajás, através da(o):

i. Caracterização detalhada das rochas hospedeiras do depósito, bem como dos tipos, distribuição temporal e associações minerais presentes nas diferentes zonas de alteração hidrotermal;

ii. Determinação dos principais estilos de mineralização, bem como as paragêneses de minério (incluindo fases acessórias), visando avaliar possíveis sobreposições temporais de eventos mineralizantes.

iii. Identificação da natureza e parâmetros físico-químicos (e.g. temperatura, densidade, salinidade) do(s) fluido(s) hidrotermal(is) responsável(is) pela formação das zonas de alteração hidrotermal e mineralizações;

iv. Estabelecimento da idade de formação da mineralização IOCG no depósito.

3. A PROVÍNCIA CARAJÁS: CONTEXTO GEOLÓGICO REGIONAL

A Província Carajás está localizada na porção sudeste do Cráton Amazônico (**Fig. 1A**), e representa atualmente uma das maiores e mais importantes províncias minerais do mundo, dado o seu diversificado potencial metalogenético. Formada e estabilizada tectonicamente no Arqueano (Teixeira et al. 1989; Tassinari 1996; Tassinari & Macambira 1999, 2004), a Província é compartimentada em dois domínios (**Fig. 1B**): Rio Maria, ao sul e Carajás (**Fig. 1C**), ao norte; separados, por sua vez, por uma região subdivida em dois domínios geológica e tectonicamente distintos, denominados Domínio Sapucaia e Domínio Canaã dos Carajás (Dall'Agnol et al. 2013).

As unidades mais antigas do Domínio Carajás foram originalmente associadas a rochas ortognáissicas e migmatitos de idade Mesoarqueana (2974 ± 15 Ma – Pb-Pb em zircão; Avelar et al. 1999) do Complexo Xingu e a ortogranulitos do Complexo Pium. Contudo, estudos recentes realizados na região de Canaã dos Carajás permitiram a individualização de novas unidades que originalmente eram consideradas partes do Complexo Xingu, mas que, no entanto, são formadas por diferentes tipos de granitóides (Moreto et al. 2011, 2015a,b; Feio et al. 2012, 2013). Dentre elas destacam-se o Granito Canaã dos Carajás (2,96 Ga), o Trondhjemito Rio Verde (2,93 Ga), o Tonalito Bacaba e o Granito Sequeirinho (3,0 Ga – U-Pb em zircão; Moreto et al. 2011, 2015a,b), o Tonalito Campina Verde (2,85 Ga), os granitos Bom Jesus, Cruzadão, e Serra Dourada (2,87 – 2,84 Ga; Moreto et al. 2011; Feio et al. 2013), as suítes graníticas Pedra Branca e Planalto e rochas charnockíticas associadas (2,74 – 2,73 Ga; Feio et al. 2012, 2013).

Adicionalmente, o Complexo Pium, originalmente descrito como um complexo granulítico Mesoarqueano (Pidgeon et al. 2000), foi reinterpretado como norito e quartzo-gabro (Oliveira et al. 2010) e redefinido por Vasquez et al. (2008) como Diopsídio-Norito Pium. Sendo assim, a unidade Ortogranulito Chicrim-Cateté foi proposta para designar o único embasamento granulítico do Domínio Carajás, que ocorre nas proximidades do rio Cateté (Ricci & Carvalho 2006; Vasquez et al. 2008).

Sobrepostas ao embasamento encontram-se as sequências metavulcano-sedimentares (*greenstone belts*) Neoarqueanas dos grupos Igarapé Salobo, Grão Pará, Igarapé Bahia e Igarapé Pojuca, que por sua vez compõem o Supergrupo Itacaiúnas (DOCEGEO 1988), e do Grupo Rio Novo (Hirata et al. 1982). O Grupo Igarapé Salobo (DOCEGEO 1988) foi redefinido por Vasquez et al. (2008), passando a incorporar apenas a sequência de rochas

metavulcano-sedimentares (quartzo-clorita xistos, granada-biotita xistos e quartzitos), além de metavulcânicas básicas à intermediárias subordinadas (DOCEGEO 1988; Siqueira 1990), expostas na serra do Salobo. O Grupo Grão Pará (CVRD/CMM 1972) é constituído por uma sequência de rochas vulcânicas máficas e félsicas subordinadas (Formação Paraupebas), sobrepostas a jaspilitos que hospedam as mineralizações de ferro de alto teor (< 65%) da Formação Carajás. O Grupo Igarapé Pojuca (DOCEGEO 1988) é composto por rochas metavulcânicas básico-intermediárias intercaladas com rochas metassedimentares psamo-pelíticas e formações ferríferas bandadas, por sua vez intrudidas por rochas máficas (DOCEGEO 1984, 1988; Farias et al. 1984; Medeiros Neto & Villas 1985; Saueressig 1988; Winter 1994; Lindenmayer et al. 2001; Galarza & Macambira 2002). O Grupo Igarapé Bahia (DOCEGEO 1988) inclui rochas metavulcânicas máfico-intermediárias, intercaladas com metavulcanoclásticas e formações ferríferas subordinadas. Por fim, o Grupo Rio Novo, localizado na porção nordeste do Domínio Carajás, inclui anfibolitos, xistos, metagrauvacas, rochas metavulcânicas tholeiíticas e gabros (Hirata et al. 1982).

Definindo uma inconformidade angular (Nogueira et al. 1995), a Formação Águas Claras sobrepõe-se ao Supergrupo Itacaiúnas e representa a cobertura siliciclástica arqueana não metamorfizada da sequência de *greenstone belts*. Nogueira et al. (1995), dividem essa formação em duas unidades litoestratigráficas distintas (Membro Inferior e Membro Superior), com contato gradacional. O Membro Inferior é composto por siltitos, pelitos e arenitos muito finos subordinados, e o Membro Superior é constituído por arenitos finos à grossos subordinados, ortoconglomerados e pelitos.

São definidos três eventos principais de magmatismo granítico no Domínio Carajás. O primeiro deles, contemporâneo à formação dos *greenstone belts* (2,76 – 2,73 Ga), é representado pela formação de granitos alcalinos à metaluminosos, similares aos do tipo-A, que compreendem o Complexo Granítico Estrela (Barros et al. 1997) e os granitos Plaquê (Araújo et al. 1988), Planalto (Huhn et al. 1999a; Feio et al. 2012), Serra do Rabo (Sardinha et al. 2006) e Igarapé Gelado (Avelar et al. 1999; Barros et al. 2004; Sardinha et al. 2006). O segundo, em 2,57 Ga, ainda muito contestado e restrito na Província, é definido exclusivamente pelos corpos graníticos peralcalinos a meta-aluminosos Old Salobo e Itacaiúnas (Machado et al. 1991; Souza et al. 1996), e o último, em 1,88 Ga, compreende os granitos alcalinos tipo-A a subalcalinos Central de Carajás, Young Salobo, Cigano, Pojuca e Breves (Machado et al. 1991; Lindenmayer and Teixeira 1999).

A estruturação geral do Domínio Carajás é demarcada por três principais sistemas de cisalhamento WNW-ESE: Carajás e Cinzento, ao norte, e Canaã ao sul (Pinheiro et al.

2013). Segundo Pinheiro et al. (2013), o formato sigmoidal (“S-shape”) característico desse domínio é atribuído a um sistema de falhas sinistrais NE-SW, análogas a estruturas do tipo-R (padrão de cisalhamento Riedel).

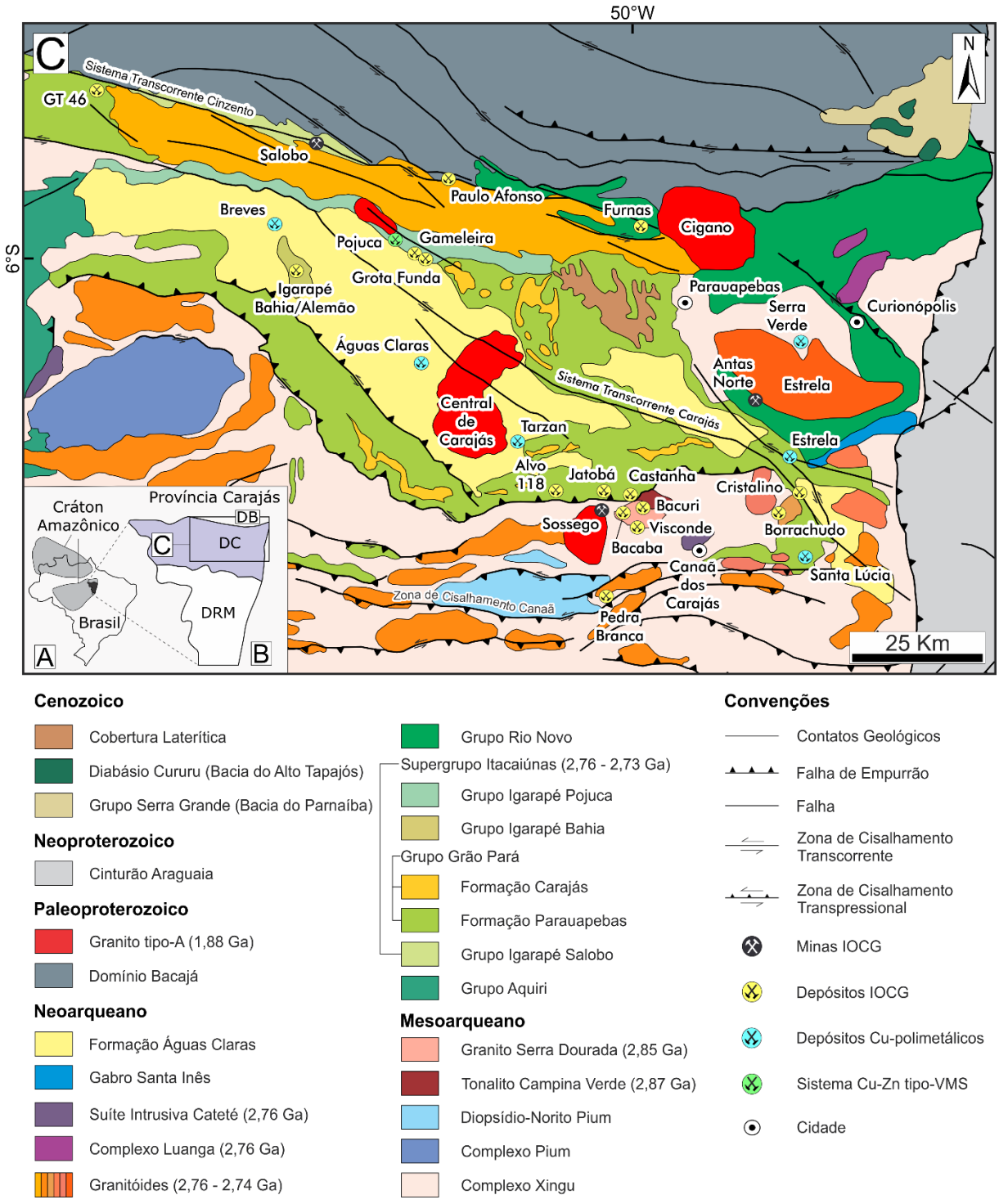

Fig. 1. (A) Localização da Província Carajás (preto) no Cráton Amazônico (cinza claro). (B) Compartimentação da Província Carajás nos domínios Rio Maria (sul) e Carajás (norte). (C)

Mapa geológico simplificado do Domínio Carajás, indicando a localização dos principais depósitos cupríferos e estruturas (modificado de Vasquez et al. 2008).

3.1. Depósitos IOCG

A Província Carajás representa um dos maiores e mais bem preservados núcleos cratônicos já conhecidos. Dentre os domínios que a compõem, o Domínio Carajás destaca-se por conter a maior concentração de depósitos IOCG de alta tonelagem do mundo (Monteiro et al. 2007; Xavier et al. 2012), tais como Salobo (1.112 Bt @ 0,69 wt.% Cu, 0,43 g/t Au; VALE 2012), Cristalino (482 Mt @ 0,65 wt.% Cu; 0,06 g/t Au; NCL Brasil 2005), Igarapé Bahia/Alemão (219 Mt @ 1,4 wt.% Cu, 0,86 g/t Au; Tallarico et al. 2005), Sossego (355 Mt @ 1.1 wt.% Cu, 0,28 g/t Au; Lancaster Oliveira et al. 2000), Gameleira (300 Mt @ 1.0 wt.% Cu; Carvalho 2004) e Alvo 118 (170 Mt @ 1.0 wt.% Cu, 0,3 g/t Au; Rigon et al. 2000). Conjuntamente a uma série de outros prospectos e alvos (e.g. Igarapé Cinzento/GT46, Bacaba, Bacuri, Visconde, Castanha e Borrachudo; Silva et al. 2005; Augusto et al. 2008; Melo et al. 2014; Costa Silva et al. 2015; Moreto et al. 2015a, b; Previato 2016), estes ainda em estágio de avaliação pela companhia Vale, os depósitos IOCG de Carajás compõem uma reserva estimada de mais de 8 bi de toneladas de minério cupro-aurífero.

De modo geral, os sistemas IOCG da Província Carajás compartilham vários atributos (Monteiro et al. 2007; Xavier et al. 2012), tais como: (i) forte controle estrutural com depósitos localizados ao longo de estruturas regionais (e.g. zonas de cisalhamento); (ii) proximidade a corpos intrusivos de diversas idades e composições químicas; (iii) presença de brechas hidrotermais; (iv) intensa alteração hidrotermal alcalina (Na-Ca-K); (v) precipitação de magnetita sucedida por precipitação de sulfetos; (vi) importantes concentrações de LREE, P, U, Ni, W, Sn, Co e Pd, e; (vii) coexistência entre fluidos hipersalinos e fluidos aquosos de salinidade moderada à baixa, por vezes aquo-carbônicos de baixa salinidade. Entretanto, os depósitos localizados no setor norte do Domínio Carajás apresentam características distintas em relação aos localizados no setor sul (e.g. rochas hospedeiras, tipos e assembleias de alteração hidrotermal, condições redox de precipitação do minério, influência estrutural e do metamorfismo regional), indicando uma evolução em diferentes condições crustais e a partir de distintas histórias de interação fluido-rocha e fluido-fluido (Xavier et al. 2012).

Estudos geocronológicos efetuados em depósitos IOCG localizados no setor sul do Domínio Carajás (Cinturão Sul do Cobre), demonstraram ainda que eventos hidrotermais podem ser episódicos no tempo, sendo nessa região relacionados a quatro épocas distintas (Moreto et al. 2015a,b): i) 2,76 Ga (Re-Os em molibdenita no depósito Bacuri); ii) 2,71 – 2,68

Ga (U-Pb em monazita nos depósitos Bacuri, Bacaba e corpo de minério Sequeirinho; Re-Os em concentrado de molibdenita no corpo de minério Pista); iii) 2,05 Ga (U-Pb em monazita no depósito Bacaba); iv) 1,90 – 1,88 Ga (U-Pb em monazita nos corpos de minério Sossego e Curral; U-Pb em xenotima do depósito Alvo 118; Tallarico 2003). No entanto, somente os eventos datados do Neoarqueano (2,71 – 2,68 Ga) e Paleoproterozóico (1,90 – 1,88 Ga), representam intervalos de idade associados à gênese de mineralizações IOCG no setor sul do Domínio Carajás (Moreto et al. 2015a,b).

Adicionalmente, dados geocronológicos que incluem Re-Os em molibdenita (depósito Salobo; Requia et al. 2003) e U-Pb em monazita (depósito Igarapé Bahia; Tallarico et al. 2005), apontam para um significativo evento metalogenético em 2,57 Ga, relacionado ao magmatismo Neoarqueano responsável pela colocação do granito Old Salobo na Província Carajás. Entretanto, o significado dessa idade ainda é polêmico, uma vez que este evento magmático se manifesta de maneira extremamente restrita e apenas no setor norte do Domínio Carajás. De acordo com Melo et al. (2016), a idade de 2,57 Ga pode representar um evento tectono-termal (e.g. reativação do sistema transcorrente Cinzento) associado a remobilização do minério no depósito Salobo, enquanto a idade de 2,705 ± 42 Ma (Pb-Pb em calcocita; Tassinari et al. 2003) estaria relacionada à mineralização primária IOCG no mesmo.

4. SISTEMAS IOCG E A ORIGEM DOS FLUIDOS: A SISTEMÁTICA DE ISÓTOPOS DE BORO EM TURMALINA

O termo IOCG (*sensu stricto*), inicialmente proposto por Hitzman et al. (1992), designa-se a uma classe de sistemas cupro-auríferos que progressivamente se tornaram importantes alvos da indústria de exploração mineral, visto seu elevado potencial para formar depósitos de metais base (Fe-Cu), e outros commodities associados (e.g. Ag, U, ETR), com tonelagem (100 Mt a 200 Mt) e teores (35% - 60% Fe; 0,5% - 3% Cu; 0,2 g/t a 3,6 g/t Au; Williams et al. 2005) de classe mundial. Em contrapartida, tais sistemas tornaram-se desafios ainda a serem explorados do ponto de vista científico, uma vez que nenhum dos modelos genético-descritivos propostos ainda é capaz de adequadamente contemplar todo o conjunto de aspectos relacionados a essa classe de depósitos, tampouco há consenso no que diz respeito aos processos responsáveis por sua gênese (Barton & Johnson 2004).

Nesse contexto, a fonte dos fluidos, metais e salinidade permanecem pontos críticos no que concerne à origem das mineralizações em depósitos IOCG nos vários distritos (Chiaradia et al. 2006; Xavier et al. 2008, 2010). Dentre os principais modelos metalogenéticos propostos para essa classe, destacam-se: (i) sistemas magmático-hidrotermais cujos fluidos são principalmente de origem magmática (ii) sistemas hidrotermais formados essencialmente a partir de fluidos terrestres (bacinais ou salmouras superficiais) circulados através de aquecimento crustal ou devido à atividade ígnea; (iii) sistemas metamórfico-hidrotermais cujos fluidos são derivados de distintas fontes crustais por interação fluido-rocha em profundidade, e; (iv) sistemas fundamentalmente magmáticos cujo fluido responsável pela precipitação do minério representa um fundido imiscível rico em voláteis e óxidos de ferro (Barton 2014).

No intuito de elucidar essas questões, a sistemática de isótopos de boro aplicada a caracterização de depósitos IOCG se mostrou uma importante e robusta ferramenta analítica. Uma amostra analisada através dessa técnica possui composição isotópica dada em termos de $\delta^{11}B$ (‰), este calculado com base na razão isotópica $^{11}B/^{10}B$. A diferença relativamente ampla entre as massas dos isótopos ^{11}B e ^{10}B, somada a elevada reatividade geoquímica do boro, definem, através do fracionamento isotópico, uma grande variedade de reservatórios naturais desse elemento na crosta, que por sua vez refletem distintos intervalos de $\delta^{11}B$ (Palmer et al. 1992; Barth 1993). Dessa forma, fluidos derivados de fontes magmático-hidrotermais evidenciarão assinaturas isotópicas de boro diferentes de fluidos originados a partir de fontes evaporíticas, por exemplo.

A turmalina contém aproximadamente 3 wt% de boro em sua estrutura, fato que a diferencia da maioria dos silicatos conhecidos, e possui natureza estável em um amplo intervalo de condições P-T (Marschall et al. 2009; Dutrow & Henry 2011; Hawthorne & Dirlam 2011). Devido a sua insignificante difusão intracristalina (von Goerne et al. 1999), pode registrar as condições químicas e isotópicas do meio em que se cristaliza, funcionando como uma espécie de "impressão digital" da composição dos fluidos (van Hinsberg et al. 2011a,b). Além disso, representa uma fase mineral extremamente comum em depósitos IOCG, podendo estar relacionada a diversos estágios de alteração hidrotermal em um mesmo paleosistema e diretamente associada à mineralização. Todos esses atributos em conjunto fazem com que a assinatura isotópica de cristais de turmalina represente uma excelente abordagem para discernir a fonte dos fluidos mineralizantes em sistemas IOCG.

Até o momento, estudos de isótopos de boro em depósitos IOCG ainda são escassos, tendo sido realizados apenas em sistemas pertencentes à Província Carajás (Xavier et al. 2008), sistemas Andinos (Tornos et al. 2012) e sistemas Fe-Cu descritos na Índia (Pal et al. 2010) e China (Su et al. 2016). De acordo com Tornos et al. (2012), análises em turmalinas pertencentes aos sistemas IOCG localizados na Cordilheira da Costa chilena (e.g. Tropezón, Silvita, Candelaria e Carola) demonstram valores de $\delta^{11}B$ variando entre -10,4‰ à 6,0‰ (**Fig. 2**), compatíveis com uma origem magmático-hidrotermal sem contribuição externa de salmouras bacinais relacionadas a evaporitos marinhos. Em contrapartida, cristais de turmalina pertencentes a quatros estágios distintos de alteração hidrotermal do depósito Dahongshan ($\delta^{11}B$ = -14,7‰ à 5,9‰; **Fig. 2**) indicam uma origem híbrida para a formação do minério, caracterizada pela mistura de fluidos originalmente magmáticos com fluidos de fontes marinhas (Su et al. 2016). Por fim, Pal et al. (2010) sugerem que a mistura entre fluidos de natureza marinha evaporítica e fluidos predominantemente gerados a partir de processos metamórficos, representa o principal mecanismo de precipitação do minério no depósito Jaduguda ($\delta^{11}B$ = -6,8‰ à 17,2‰; **Fig. 2**).

No que diz respeito à Província Carajás, estudos isotópicos realizados em turmalinas dos depósitos Salobo e Igarapé-Bahia revelam valores de $\delta^{11}B$ extremamente elevados (> 24‰; **Fig. 2**), sugerindo a interação dos fluidos mineralizantes com evaporitos marinhos (Xavier et al. 2008). Contudo, valores de $\delta^{11}B$ inferiores à 10‰ obtidos em turmalinas do corpo de minério ACPN do depósito Igarapé-Bahia, são atribuídos a fontes de boro mistas ou a uma possível mistura entre fluidos de composições isotópicas distintas (Xavier et al. 2008, 2013). De forma análoga, as composições isotópicas de turmalinas do depósito Sossego ($\delta^{11}B$ = -8‰ à 11‰; **Fig. 2**) são também associadas a fontes mistas,

evidenciando a interação entre fluidos de origem magmática granítica e fluidos derivados de salmouras evaporíticas (Xavier et al. 2008).

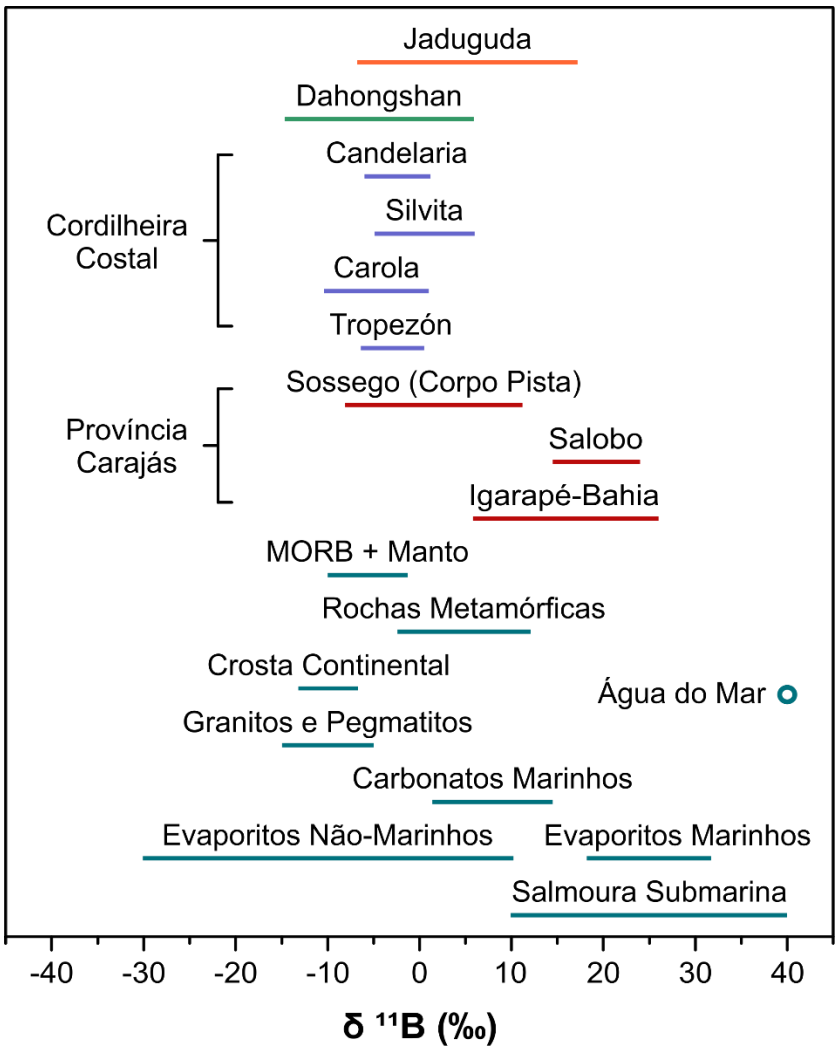

Fig. 2. *Composições isotópicas de boro obtidas em diferentes depósitos IOCG da Província Carajás (Xavier et al. 2008) e Cordilheira Costal do Chile (Tornos et al. 2012), além dos depósitos Dahongshan (China; Su et al. 2016) e Jaduguda (Índia; Pal et al. 2010). Intervalos de $\delta^{11}B$ de alguns dos principais reservatórios de boro naturais são exibidos como referência (Barth 1993; Marschall and Jiang 2011).*

Tendo em vista esses dados, é possível dizer que depósitos IOCG, em geral, revelam uma complexa história evolutiva que aponta para a contribuição de diferentes fontes de fluidos na sua formação. Tal fato pode estar diretamente associado à diversidade de características apresentadas por esses depósitos, tais como ambiente geotectônico, nível crustal, idades, rochas hospedeiras, paragêneses minerais, entre outros fatores (Hitzman et al. 1992; Williams et al. 2005; Barton 2014).

5. MATERIAIS E MÉTODOS

5.1. Trabalho de Campo

O trabalho de campo foi realizado no período entre os dias 22 a 31 de julho de 2015, concentrando-se na descrição detalhada e sistemática de testemunhos de sondagem (furos GRFUN_FD028, GRFUN_FD029, GRFUN_FD037, GRFUN_FD046 e PKO-09). Esta etapa visou o reconhecimento dos litotipos associados ao depósito Grota Funda (rochas hospedeiras) e a caracterização das zonas de alteração hidrotermal e mineralizadas, incluindo a identificação dos estilos, distribuição espacial e principais associações minerais, além da coleta de amostras para posteriores análises laboratoriais (**Tabela 1**).

Tabela 1 *Relação das amostras utilizadas em análises laboratoriais*

Furo	Profundidade (m)	Amostra	Análise
GRFUN_FD0037	339,70	Apatita	Inclusões Fluidas
GRFUN_FD0037	105,4	Molibdenita	Geocronologia Re-Os
GRFUN_FD0029	355,90	Turmalina	Isótopos de Boro

5.2. Estudos petrográficos e de microscopia eletrônica de varredura (MEV)

A partir das amostras de testemunho coletadas em campo, foram confeccionadas trinta e duas lâminas delgadas-polidas para estudos petrográficos tanto em luz transmitida como refletida. Essa etapa foi realizada no laboratório de microscopia do Instituto de Geociências da Universidade Estadual de Campinas (IG-UNICAMP), e visou a identificação dos litotipos hospedeiros e da evolução paragenética do depósito Grota Funda. Todas as fotomicrografias apresentadas neste trabalho foram obtidas com auxílio de uma câmera digital modelo Sony Cyber-shot DSC-W530 acoplada ao microscópio óptico Leica DM750P.

Análises de Microscopia Eletrônica de Varredura (MEV) acopladas a EDS (Energy Dispersive X-Ray Spectrometer) foram também realizadas no Instituto de Geociências da UNICAMP, com o objetivo de identificar fases minerais acessórias não reconhecidas através do microscópio óptico, relações microtexturais, zoneamentos composicionais, além de realizar análises químicas semi-quantitativas de determinados minerais hidrotermais e de minério.

5.3. Inclusões fluidas

Estudos de inclusões fluidas em cristais de apatita foram conduzidos e uma lâmina bipolida correspondente à principal zona de minério sulfetado do depósito Grota Funda. Os dados microtermométricos foram obtidos em platina modelo LINKAM THMSG600 acoplado a um microscópio óptico convencional (LEICA DMLP), este equipado com uma objetiva de 100x. A calibração do aparelho foi efetuada utilizando-se o conjunto de inclusões fluidas sintéticas padrão Synflinc, revelando uma precisão de ± 0.1°C para medidas entre -120°C e 21,2°C, e ± 2°C para medidas até 300°C. As análises foram realizadas no laboratório de Microtermometria do Instituto de Geociências da UNICAMP.

5.4. Isótopos de boro

Análises de isótopos de boro foram efetuados no State Key Laboratory of Geological and Mineral Resources (GPMR), China University of Geosciences (CUG), China. Duas amostras de turmalina associadas ao estágio de alteração clorítica foram investigadas *in situ* em lâmina bipolida, através de microscopia óptica e imagens de elétrons retroespalhados, visando a seleção de spots para a execução das análises. As composições isotópicas de boro foram então medidas através de um espectrômetro de massas com plasma indutivamente acoplado (LA-MC-ICP-MS) modelo Neptune Plus e um sistema auxiliar de ablação a laser (New Wave UP193). A descrição detalhada dos procedimentos analíticos e redução de dados é apresentada por Yang et al. (2015). As condições de operação do aparelho consistiram em uma densidade energética de 12 J/cm², frequência de repetição de 8 Hz e spots de 50 µm. O fracionamento isotópico e o *mass bias* foram calibrados utilizando-se o método SSB (*standard-sample-bracketing*). A turmalina IAEA B4 (Tonarini et al. 2003) foi utilizada como padrão externo. O fracionamento de massa instrumental (IMF) e a qualidade dos dados analíticos foram determinados através de análises sistemáticas dos padrões de referência internacional IMR RB1 (Hou et al. 2010) e interno Dai ($\delta^{11}B$ = -13.6‰). Os resultados reportados de $\delta^{11}B$ foram calculados com base na turmalina IAE B4 ($\delta^{11}B$ = -8.71‰; Tonarini et al. 2003).

5.5. Geocronologia Re-Os

Estudos geocronológicos através do método Re-Os ELAN DRC-e ICP-MS foram realizados no State Key Laboratory of Ore Deposit Geochemistry, Institute of Geochemistry, Guiyang (China). A descrição detalhada dos procedimentos analíticos é apresentada por Andao et al. (1995), Shirey and Walker (1995), Markey et al. (1998), Stein et al. (1998) e Qi et al. (2007, 2010). Aproximadamente 10 mg de concentrado de molibdenita foram inseridos em um tubo Carius reutilizável (120 ml) contendo concentrações conhecidas de *spykes* de ^{185}Re e ^{187}Os. A amostra foi então digerida e equilibrada utilizando-se 10 ml de HNO_3 concentrado e 2 ml de HCl. Posteriormente o tubo foi selado e posicionado em um suporte de aço inoxidável, sendo aquecido até 200° C por aproximadamente 12 h. Após o resfriamento, a separação do Os em sua forma oxidada (OsO_4) foi realizada através de destilação *in situ*. A extração do Re a partir da solução remanescente foi realizada utilizando-se uma resina de troca aniônica (Biorad AG 1-X8, 200 – 400 mesh). Íridio foi adicionado às soluções de Re e Os devido ao procedimento de correção para discriminação de massa (Schoenberg et al. 2000; Huang et al. 2013).

6. SÍNTESE DOS RESULTADOS E CONCLUSÕES

O depósito da Grota Funda, juntamente com os depósitos Gameleira e Pojuca, situa-se ao longo de uma zona de cisalhamento regional de direção WNW-ESE (Sistema Transcorrente Pojuca), na porção noroeste do Domínio de Carajás. Na área do depósito, rochas metavulcânicas máficas atribuídas ao Grupo Igarapé-Pojuca, representam os principais litotipos hospedeiros da mineralização de cobre (-ouro).

A sequência de alterações hidrotermais do depósito Grota Funda engloba: (i) uma alteração sódica-cálcica inicial, representada por albita, hastingsita e escapolita, seguida de; (ii) intenso metassomatismo rico em Fe, caracterizado pela precipitação maciça de magnetita, grunerita e almandina; (iii) alteração potássica com biotita, acompanhada de formação de quartzo e associada espacialmente à principal zona de minério sulfetado; (iv) alteração clorítica, com quartzo, turmalina, actinolita e carbonato associados; (V) veios de carbonato-quartzo tardios de desenvolvidos em ambiente rúptil. Mineralizações de cobre (-ouro) também foram reconhecidas associadas à zonas enriquecidas em ferro e cloritizadas. A idade de 2530 ± 60 Ma, obtida através da datação Re-Os em molidenita associado a veios de grunerita-magnetita, é interpretada como a idade de formação do primeiro estágio de mineralização no depósito associado ao metassomatismo férrico.

O principal corpo de minério sulfetado ocorre predominantemente associado à zonas brechadas, sendo subordinadamente reconhecido em vênulas, preenchendo fraturas e disseminado. A paragênese de minério inclui principalmente calcopirita, magnetita, pirrotita, pentlandita e esfalerita, com ilmenita, Ti-hematita, siegenita, cobaltita e melonita subordinados. A associação calcopirita-magnetita-pirrotita-esfalerita indica precipitação sob baixas condições de fS_2 e fO_2, enquanto que a substituição de calcopirita por bornita e a cristalização tardia de pirita são evidências que refletem uma evolução de fluidos para condições de fS_2 mais elevadas.

A evolução paragenética do depósito Grota Funda é caracterizada por mudanças significativas nas condições físico-químicas dos fluidos hidrotermais, tais como a diminuição de temperatura dos sistema de ~540°C (alteração Na-Ca) para abaixo de 200°C (veios de carbonato tardios), acompanhada pela diminuição na salinidade e pH. As assembléias de alteração hidrotermal iniciais (albita, hastingsita-escapolita), formadas em alta temperatura, podem estar intrinsecamente relacionadas a circulação regional de fluidos metalíferos quentes e hipersalinos profundos, enquanto que a precipitação do minério foi possivelmente

promovida devido ao influxo significativo de fluidos relativamente diluídos (salinidade moderada) e mais frios.

De forma geral, os dados de inclusões fluidas do depósito Grota Funda apontam para uma tendência na evolução dos fluidos que aparentemente envolveu a interação entre fluidos hidrotermais altamente salinos com fluidos mais frios e relativamente diluídos. Este processo pode ter induzido a diminuição de salinidade e temperatura do sistema, e consequentemente, a formação da principal zona de minério sulfetado. Adicionalmente, as composições isotópicas de boro dos cristais de turmalina pertencentes à zona de alteração clorítica são atribuídas a fontes mistas, incluindo boro proveniente de salmouras marinhas (e.g. água do mar evoluída ou fluidos do tipo *bittern*) e boro lixiviado das rochas hospedeiras (e.g. metavulcânicas máficas).

REFERÊNCIAS

Andao D., Hongliao H., Ningwan Y., Xiaoqiu Z., Yali S., Dezhong S., Shaozhen C., Wenjun Q. 1995. A Study of the Rhenium-Osmium Geochronometry of Molybdenites. *Acta Geologica Sinica*, **8**:171–181.

Araújo O. J. B., Maia R. G. N., Jorge-João X. S., Costa, J. B. S. 1988. A megaestruturação da folha Serra dos Carajás. In: *VII Congresso Latino Americano de Geologia*. Belém, p. 324–333.

Augusto R. A., Monteiro L. V. S., Xavier R. P., Souza Filho C. R. 2008. Zonas de alteração hidrotermal e paragênese do minério de cobre do Alvo Bacaba, Província Mineral de Carajás (PA). *Revista Brasileira de Geociências*, **38**:263–277.

Avelar V. G., Lafon J. M., Correia Jr. F. C., Macambira E. M. B. 1999. O magmatismo arqueano da região de Tucumã - Província Mineral De Carajás: Novos resultados geocronológicos. *Revista Brasileira de Geociências*, **29**:453–460.

Barros C. E. M., Dall'Agnol R., Barbey P., Boullier A.-M. 1997. Geochemistry of the Estrela Granite Complex, Carajás region, Brazil: an example of an Archaean A-type granitoid. *Journal of South American Earth Sciences*, **10**:321–330.

Barros C. E. M., Macambira M. J. B., Barbey P., Scheller T. 2004. Dados isotópicos Pb-Pb em zircão (evaporação) e Sm-Nd do Complexo Granítico Estrela, Província Mineral de Carajás, Brasil: Implicações petrológicas e tectônicas. *Revista Brasileira de Geociências*, **34**:531–538.

Barth S. 1993. Boron isotope variations in nature: a synthesis. *Geologische Rundschau*, **82**:640–651.

Barton M. D. 2013. Iron Oxide(-Cu-Au-REE-P-Ag-U-Co) Systems. In: Holland H., Turkian K. (eds.). *Treatise on Geochemistry: Second Edition*, Elsevier Ltd, p. 515-541.

Barton M. D., Johnson D. A. 2004. Footprints of Fe-oxide (-Cu-Au) systems. *University of Western Australia Special Publication*, **33**, p. 112–116.

Carvalho J. M. A. 2004. *Distritos Mineiros do Estado do Pará*, Belém, DNPM/CPRM.

Chiaradia M., Banks D., Cliff R., Marschik R., Haller A. 2006. Origin of fluids in iron oxide-copper-gold deposits: Constraints from δ37Cl, 87Sr/86Sr and Cl/Br. *Mineralium Deposita*, **41**:565–573.

Costa Silva A. R., Villas R. N. N., Lafon J.-M., Craveiro G. S., Ferreira V. P. 2015. Stable isotope systematics and fluid inclusion studies in the Cu–Au Visconde deposit, Carajás Mineral Province, Brazil: implications for fluid source generation. *Mineralium Deposita*, **50**:547–569.

CVRD/CMM. 1972. Distrito ferrífero da Serra dos Carajás. In: *XXVI Congresso Brasileiro de Geologia*. Belém, SBG-Núcleo Norte, p. 78–80.

Dall'Agnol R., Oliveira D. C., Guimarães F. V., Gabriel E. O., Feio G. R. L., Lamarão C. N., Althoff F. J., Santos P. A., Teixeira M. F. B., Silva A. C., Rodrigues D. S., Santos M. J. P., Silva C. R. P., Santos R. D., Santos P. J. L. 2013. Geologia do subdomínio de transição do Domínio Carajás - implicações para a evolução arqueana da Província Carajás - Pará. In: *XIII Simpósio de Geologia da Amazônia*. Belém, p. 1082–1085.

DOCEGEO. 1984. *Relatório de pesquisa do projeto Cobre Carajás-Pojuca*. Belém.

DOCEGEO. 1988. Revisão litoestratigráfica da Província Mineral de Carajás - Litoestratigrafia e principais depósitos minerais. In: *XXXV Congresso Brasileiro de Geologia*. Belém, SBG, p. 11–54.

Farias N. F., Santos A. B. S., Biagini D. O., Vieira E. A. P., Martins L. P. B., Saueressig R. 1984. Jazidas de Cu e Zn da área Pojuca, Serra dos Carajás - PA. In: *XXXIII Congresso Brasileiro de Geologia*. Rio de Janeiro, p. 3658–3668.

Feio G. R. L., Dall'Agnol R., Dantas E. L., Macambira M. J. B., Gomes A. C. B., Sardinha A. S., Oliveira D. C., Santos R. D., Santos P. A. 2012. Geochemistry, geochronology, and origin of the Neoarchean Planalto Granite suite, Carajás, Amazonian craton: A-type or hydrated charnockitic granites?. *Lithos*, **151**:57–73.

Feio G. R. L., Dall'Agnol R., Dantas E. L., Macambira M. J. B., Santos J. O. S., Althoff F. J., Soares J. E. B. 2013. Archean granitoid magmatism in the Canaã dos Carajás area: Implications for crustal evolution of the Carajás province, Amazonian craton, Brazil. *Precambrian Research*, **227**:157–185.

Galarza M. A., Macambira M. J. B. 2002. Geocronologia e evolução crustal da área do depósito de Cu-Au Gameleira, Província Mineral de Carajás (Pará), Brasil. *Revista do Instituto de Geociências da USP*, **2**:143–159.

von Goerne G., Franz G., Wirth, R. 1999. Hydrothermal synthesis of large dravite crystals by the chamber method. *European Journal of Mineralogy*, **11**:1061–1077.

Grainger C. J., Groves D. I., Tallarico F. H. B., Fletcher I. R. 2008. Metallogenesis of the Carajás Mineral Province, Southern Amazon Craton, Brazil: Varying styles of Archean through Paleoproterozoic to Neoproterozoic base- and precious-metal mineralisation. *Ore Geology Reviews*, **33**:451–489.

Hawthorne F. C., Dirlam D. M. 2011. Tourmaline the indicator mineral: From atomic arrangement to viking navigation. *Elements*, **7**:307–312.

van Hinsberg V. J., Henry D. J., Dutrow B. L. 2011. Tourmaline as a petrologic forensic mineral: A unique recorder of its geologic past. *Elements*, **7**:327–332.

van Hinsberg V. J., Henry, D. J., Marschall H. R. 2011. Tourmaline: An ideal indicator of its host environment. *Canadian Mineralogist*, **49**:1–16.

Hirata W. K., Rigon J. C., Kadekaru K., Cordeiro A. C. C., Meireles E. A. 1982. Geologia regional da Província Mineral de Carajás. In: *I Simpósio de Geologia da Amazônia*. Belém, SBG/NO, p. 100–110.

Hitzman M. W., Oreskes N., Einaudi M. T. 1992. Geological characteristics and tectonic setting of proterozoic iron oxide (Cu-U-Au-REE) deposits. *Precambrian Research*, **58**:241–287.

Hou K. J., Li Y. H., Xiao Y. K., Liu F., Tian Y. R. 2010. In situ boron isotope measurements of natural geological materials by LA-MC-ICP-MS. *Chinese Science Bulletin*, **55**:3305–3311.

Huang X.-W., Qi L., Gao J.-F., Zhou M.-F. 2013. First Reliable Re-Os Ages of Pyrite and Stable Isotope Compositions of Fe(-Cu) Deposits in the Hami Region, Eastern Tianshan Orogenic Belt, NW China. *Resource Geology*, **63**:166–187.

Huhn S. R. B., Macambira M. J. B., Dall'Agnol R. 1999. Geologia e geocronologia Pb-Pb do Granito Alcalino Planalto, Região da Serra do Rabo, Carajás-PA. In: *VI Simpósio de Geologia da Amazônia*. SBG-Núcleo Norte, p. 463–466.

Lancaster Oliveira J., Fanton J., Almeida A. J., Leveille R. A., Vieira S. 2000. Discovery and geology of the Sossego copper-gold deposit, Carajás district, Pará State, Brazil. In *31th International Geological Congress*. Rio de Janeiro, p. [CD-ROM].

Lindenmayer Z. G., Pimentel M. M., Ronchi L. H., Althoff F. J., Laux J. H., Araújo J. C., Fleck A., Baecker C. A., Carvalho D. B., Nowatzki A. C. 2001. Geologia do depósito de Cu-Au de Gameleira, Serra dos Carajás, Pará. In: Jost H., Brod J. A., Queiroz E. T. (eds.). *Caracterização de depósitos auríferos em distritos mineiros*. Brasília, DNPM/ADIMB, p. 81–139.

Lindenmayer Z. G., Teixeira J. B. G. 1999. Ore genesis at the Salobo copper deposit, Serra dos Carajás. In: Silva M. G., Misi A. (eds.). *Base metal deposits of Brazil*. Belo Horizonte, MME/CPRM/DNPM, p. 33–43.

Machado N., Lindenmayer Z. G., Krogh T. E., Lindenmayer D. 1991. U-Pb geochronology of Archean magmatism and basement reactivation in the Carajás area, Amazon shield, Brazil. *Precambrian Research*, **49**:329–354.

Markey R., Stein H., Morgan J. 1998. Highly precise Re-Os dating for molybdenite using alkaline fusion and NTIMS. *Talanta*, **45**:935–946.

Marschall H. R., Jiang S. Y. 2011. Tourmaline isotopes: No element left behind. *Elements*, **7**:313–319.

Marschall H. R., Meyer C., Wunder B., Ludwig T., Heinrich W. 2009. Experimental boron isotope fractionation between tourmaline and fluid: Confirmation from in situ analyses by secondary ion mass spectrometry and from Rayleigh fractionation modelling. *Contributions to Mineralogy and Petrology*, **158**:675–681.

Medeiros Neto F. A., Villas R. N. N. 1985. Geologia da jazida de Cu-Zn do corpo 4E-Pojuca, Serra dos Carajás. In: *II Simpósio de Geologia da Amazônia*. Belém, SBG-Núcleo Norte, p. 97–112.

Melo G. H. C., Monteiro L. V. S., Moreto C. P. N., Xavier R. P., Silva M. A. D. 2014. Paragenesis and evolution of the hydrothermal Bacuri iron oxide-copper-gold deposit, Carajás Province (PA). *Brazilian Journal of Geology*, **44**:73–90.

Melo G. H. C., Monteiro L. V. S., Xavier R. P., Moreto C. P. N., Santiago E. S. B., Dufrane S. A., Aires B., Santos A. F. F. 2016. Temporal evolution of the giant Salobo IOCG deposit, Carajás Province (Brazil): Constraints from paragenesis of hydrothermal alteration and U-Pb geochronology. *Mineralium Deposita*. Mineralium Deposita, **52**:709–739.

Monteiro L. V. S., Xavier R. P., Carvalho E. R., Hitzman M. W., Johnson C. A., Souza Filho C. R., Torresi I. 2007. *Spatial and temporal zoning of hydrothermal alteration and mineralization in the Sossego iron oxide–copper–gold deposit, Carajás Mineral Province, Brazil: paragenesis and stable isotope constraints. Mineralium Deposita*, **43**:129-159.

Moreto C. P. N., Monteiro L. V. S., Xavier R. P., Amaral W. S., Santos T. J. S., Juliani C., Filho, C. R. S. 2011. Mesoarchean (3.0 and 2.86 Ga) host rocks of the iron oxide-Cu-Au Bacaba deposit, Carajás Mineral Province: U-Pb geochronology and metallogenetic implications. *Mineralium Deposita*, **46**:789–811.

Moreto C. P. N., Monteiro L. V. S., Xavier R. P., Creaser R. A., DuFrane S. A., Melo G. H. C., Silva M. A. D., Tassinari C. C. G., Sato K. 2015. Timing of multiple hydrothermal events in the iron oxide–copper–gold deposits of the Southern Copper Belt, Carajás Province, Brazil. *Mineralium Deposita*, **50**:517–546.

Moreto C. P. N., Monteiro L. V. S., Xavier R. P., Creaser R. A., DuFrane S. A., Tassinari C. C. G., Sato K., Kemp A. I. S., Amaral W. S. 2015. Neoarchean and paleoproterozoic iron oxide-copper-gold events at the Sossego deposit, Carajás Province, Brazil: Re-Os and U-Pb geochronological evidence. *Economic Geology*, **110**:809–835.

NCL Brasil. 2005. *Revision de La Estimación del Proyecto Cristalino*.

Neves M. P. 2006. *Estudos isotópicos (Pb-Pb, Sm-Nd, C e O) do depósito Cu-Au do Sossego, Província Mineral de Carajás*. Ms Dissertation, Universidade Federal do Pará, Pará, 104 p.

Nogueira A. C. R., Truckenbrodt W., Pinheiro R. V. L. 1995. Formação Águas Claras, Pré-Cambriano da Serra dos Carajás: Redescrição e redefinição litoestratigráfica. *Boletim do Museu Paraense Emílio Goeldi - Série Ciências da Terra*, **7**:177–277.

Oliveira M. A., Dall'Agnol R., Scaillet B. 2010. Petrological constraints on crystallization conditions of Mesoarchean sanukitoid rocks, southeastern Amazonian Craton, Brazil. *Journal of Petrology*, **51**:2121–2148.

Pal D. C., Trumbull R. B., Wiedenbeck M. 2010. Chemical and boron isotope compositions of tourmaline from the Jaduguda U (-Cu-Fe) deposit, Singhbhum shear zone, India: Implications for the sources and evolution of mineralizing fluids. *Chemical Geology*, **277**:245–260.

Palmer M. R., London D., Morgan VI G. B., Babb H. A. 1992. Experimental determination of fractionation of 11B/10B between tourmaline and aqueous vapor: A temperature- and pressure-dependent isotopic system. *Chemical Geology*, **101**:123–129.

Pidgeon R. T., Macambira M. J. B., Lafon J. M. 2000. Th-U-Pb isotopic systems and internal structures of complex zircons from an enderbite from the Pium Complex, Carajás Province, Brazil: Evidence for the ages of granulite facies metamorphism and the protolith of the enderbite. *Chemical Geology*, **166**:159–171.

Pinheiro R. V. L., Kadekaru K., Soares A. V., Freitas C., Ferreira S. N., Matos F. M. V. 2013. Carajás, Brazil - a short tectonic review. In: *XIII Simpósio de Geologia da Amazônia*. Belém, p. 1086–1089.

Pollard P. J. 2006. An intrusion-related origin for Cu-Au mineralization in iron oxide-copper-gold (IOCG) provinces. *Mineralium Deposita*, **41**:179–187.

Previato M. 2016. *Evolução paragenética e regime de fluidos hidrotermais no sistema mineral Borrachudo: Implicações para a metalogênese de cobre na Província Carajás*. Ms Dissertation, Instituto de Geologia, Universidade de São Paulo, São Paulo, 132 p.

Qi L., Zhou M.-F., Gao J., Zhao, Z. 2010. An improved Carius tube technique for determination of low concentrations of Re and Os in pyrites. *Journal of Analytical Atomic Spectrometry*, **25**:585–589.

Qi L., Zhou M.-F., Wang C. Y., Sun M. 2007. Evaluation of a technique for determining Re and PGEs in geological samples by ICP-MS coupled with a modified Carius tube digestion. *Geochemical Journal*, **41**:407–414.

Réquia K., Stein H., Fontboté L., Chiaradia M. 2003. Re-Os and Pb-Pb geochronology of the Archean Salobo iron oxide copper-gold deposit, Carajás mineral province, northern Brazil. *Mineralium Deposita*, **38**:727–738.

Ricci P. S. F., Carvalho M. A. 2006. Rocks of the Pium-area, Carajás Block, Brazil - A deep seated high-T abbroic pluton (charnockitoid-like) with xenoliths of enderbitic gneisse dated at 3002 Ma - The basement problem revisited. In: *VIII Simpósio de Geologia da Amazônia*. Belém, SBG, p. [CD ROM].

Rigon J. C., Munaro P., Santos L. A., Nascimento J. A. S., Barreira C. F. 2000. Alvo 118 copper-gold deposit: Geology and mineralization, Serra dos Carajás, Pará, Brazil. In: *31th International Geological Congress*. Rio de Janeiro, p. [CD-ROM].

Sardinha A. S., Barros C. E. M., Krymsky R. 2006. Geology, geochemistry, and U-Pb geochronology of the Archean (2.74 Ga) Serra do Rabo granite stocks, Carajás Metallogenetic Province, northern Brazil. *Journal of South American Earth Sciences*, **20**:327–339.

Saueressig R. 1988. Depósito de cobre e zinco do Corpo Quatro, Pojuca. In: *XXXV Congresso Brasileiro de Geologia*. Belém, SBG, p. 115–119.

Schoenberg R., Nägler T. F., Kramers J. D. 2000. Precise Os isotope ratio and Re – Os isotope dilution measurements down to the picogram level using multicollector inductively coupled plasma mass spectrometry. *International Jounral of Mass Spectrometry*, **197**:85–94.

Shirey S. B., Walker R. J. 1995. Carius Tube Digestion for Low-Blank Rhenium-Osmium Analysis. *Analytical Chemistry*, **67**:2136–2141.

Silva M. G., Teixeira J. B. G., Pimentel M. M., Vasconcelos P. M., Arielo A., Rocha W. J. S. F. 2005. Geologia e mineralizações de Fe-Cu-Au do Alvo GT46 (Igarapé Cinzento), Carajás. In: Marini O. J., Queiroz E. T., Ramos B. W. (eds.). *Caracterização de depósitos minerais em distritos mineiros da Amazônia*. Brasília, p. 94–151.

Siqueira J. B. 1990. *Organização lito-estrutural do duplex Salobo-Mirim, Serra dos Carajás*. Ms Dissertation, Centro de Geociências, Universidade Federal do Pará, Pará, 125 p.

Souza S. R. B., Macambira M. J. B., Sheller, T. 1996. Novos dados geocronológicos para os granitos deformados do Rio Itacaiúnas (Serra dos Carajás, PA): implicações estratigráficas. In: *V Simpósio de Geologia da Amazônia*. Belém, SBG, p. 380–383.

Stein H. J., Sundblad K., Markey R. J., Morgan J. W., Motuza G. 1998. Re-Os ages for Archean molybdenite and pyrite, Kuittila-Kivisuo, Finland and Proterozoic molybdenite, Kabeliai, Lithuania: Testing the chronometer in a metamorphic and metasomatic setting. *Mineralium Deposita*, **33**:329–345.

Su Z. K., Zhao X. F., Li X. C., Zhou M. F. 2016. Using elemental and boron isotopic compositions of tourmaline to trace fluid evolutions of IOCG systems: The worldclass Dahongshan Fe-Cu deposit in SW China. *Chemical Geology*, **441**:265–279.

Tallarico F. H. B. 2003. *O cinturão cupro-aurífero de Carajás, Brasil*. PhD Thesis, Instituto de Geologia, Universidade Estadual de Campinas, São Paulo, 229 p.

Tallarico F. H. B., Figueiredo B. R., Groves D. I., Kositcin N., McNaughton N. J., Fletcher I. R., Rego J. L. 2005. Geology and SHRIMP U-Pb geochronology of the Igarapé Bahia deposit, Carajás copper-gold belt, Brazil: An Archean (2.57 Ga) example of Iron-Oxide Cu-Au-(U-REE) mineralization. *Economic Geology*, **100**:7–28.

Tassinari C. C. G. 1996. *O mapa geocronológico do Cráton Amazônico no Brasil: revisão dos dados isotópicos*. Tese de Livre Docência, Instituto de Geociências, Universidade de São Paulo, São Paulo, 139 p.

Tassinari C. C. G., Macambira M. J. B. 1999. Geochronological provinces of the Amazonian Craton. *Episodes*, **22**:174–182.

Tassinari C. C. G., Macambira M. J. B. 2004. A evolução tectônica do Craton Amazônico. In: Mantesso-Neto V., Bartorelli A., Carneiro C. D. R., Brito Neves B. B. (eds.). *Geologia do Continente Sul-Americano: Evolução da obra de Fernando Flávio Marques Almeida*. São Paulo, Beca, p. 471–485.

Tassinari C. C. G., Mellito K. M., Babinski M. 2003. Age and origin of the Cu (Au-Mo-Ag) Salobo 3A ore deposit, Carajás Mineral Province, Amazonian Craton, northern Brazil. *Episodes*, **26**:2–9.

Teixeira W., Tassinari C. C. G., Cordani U. G., Kawashita K. 1989. A review of the geochronology of the Amazonian Craton: Tectonic implications. *Precambrian Research*, **42**:213–227.

Tonarini S., Pennisi M., Adorni-Braccesi A., Dini A., Ferrara G., Gonfiantini R., Wiedenbeck M., Gröning M. 2003. Intercomparison of boron isotope and concentration measurements. Part I: Selection, preparation and homogeneity tests of the intercomparison materials. *Geostandards Newsletter*, **27**:21–39.

Tornos F., Wiedenbeck M., Velasco F. 2012. The boron isotope geochemistry of tourmaline-rich alteration in the IOCG systems of northern Chile: Implications for a magmatic-hydrothermal origin. *Mineralium Deposita*, **47**:483–499.

Torresi I., Xavier R. P., Bortholoto D. F. A., Monteiro L. V. S. 2012. Hydrothermal alteration, fluid inclusions and stable isotope systematics of the Alvo 118 iron oxide-copper-gold deposit, Carajás Mineral Province (Brazil): Implications for ore genesis. *Mineralium Deposita*, **47**:299–323.

VALE. 2012. *Internal Report on the Bacuri. Vale obtains operation license for Salobo*. Available at: http://saladeimprensa.vale.com/en/release/interna. asp?id=22000.

VALE. 2017. *Produção da Vale no 4T16*. Available at: http://www.vale.com/PT/investors/information-market/quarterly-results/ResultadosTrimestrais/2016 4Q Production Report_p.pdf.

Vasquez M. L., Rosa-Costa L. T., Silva C. M. G., Klein E. L., Ricci P. S. F., Barbosa J. P. O., Lopes E. C. S., Macambira E. M. B., Chaves C. L., Carvalho J. M. A., Oliveira J. G. F., Anjos G. C., Silva H. R., João X. S. J. 2008. In: Vasquez M.L., Rosa-Costa L. T. (eds.). *Geologia e Recursos Minerais do Estado do Pará: Sistema de Informações Geográficas - SIG: texto explicativo dos mapas Geológico e Tectônico e de Recursos Minerais do Estado do Pará. Escala 1:1.000.000*. Belém, CPRM, 328 p.

Villas R. N., Neves M. P., Moura C. V., Toro M. A. G., Aires B., Maurity C. 2006. Estudos isotópicos (Pb, C e O) no depósito Cu-Au do Sossego, Província Mineral de Carajás. In: *IX Simpósio de Geologia da Amazônia*. Belém, SBG-Núcleo Norte, p. [CD-ROM].

Williams P. J., Barton M. D., Johnson D. A., Fontboté L., Haller A., Mark G., Oliver N. H. S., Marschik R. 2005. Iron Oxide Copper-Gold Deposits: Geology, Space-Time Distribution, and Possible Modes of Origin. *Economic Geology*, **100th Anni**:371–405.

Winter C. J. 1994. *Geology and base-metal mineralization associated with Archean iron-formation in the Pojuca Corpo Quatro Deposit, Carajás, Brazil*. PhD Thesis, University of Southampton, 173 p.

Xavier R. P., Monteiro L. V. S., Moreto C. P. N., Pestilho A. L. S., Melo G. H. C., Silva M. A. D., Aires B., Ribeiro C., Silva F. H. F. 2012. The iron oxide copper-gold systems of the Carajás mineral province. *Economic Geology*, **16(Special Publication)**:433–454.

Xavier R. P., Monteiro L. V. S., Souza Filho C. R., Torresi I., Carvalho E. R., Dreher A. M., Wiedenbeck M., Trumbull R. B., Pestilho A. L. S., Moreto C. P. N. 2010. The iron oxide copper-gold deposits of the Carajás Mineral Province, Brazil: An update and critical review. In: Porter T. M. (eds.). *Hydrothermal Iron Oxide Copper-Gold & Related Deposits: A Global Perspective, v.3, Advances in the Understanding of IOCG Deposits*. Adelaide, PGC Publishing, p. ##.

Xavier R. P., Rusk B., Emsbo P., Monteiro L. V. S. 2009. Composition and source of salinity of ore-bearing fluids in Cu-Au systems of the Carajás Mineral Province, Brazil. In: *10th SGA Biennial Meeting*. Townsville, SGA, p. 272–274.

Xavier R. P., Trumbull R. B., Wiedenbeck M., Monteiro L. V. S. 2013. Sources of mineralizing fluids in Cu-Au systems from the Carajás Mineral Province (Brazil): constraints from in-situ microanalysis of hydrogen and boron isotopes in tourmaline. In: *12th SGA Biennial Meeting*. Uppsala, p. 1402–1405.

Xavier R. P., Wiedenbeck M., Trumbull R. B., Dreher A. M., Monteiro L. V. S., Rhede D., Araújo C. E. G., Torresi I. 2008. Tourmaline B-isotopes fingerprint marine evaporites as the source of high-salinity ore fluids in iron oxide copper-gold deposits, Carajás Mineral Province (Brazil). *Geology*, **36**:743–746.

Yang S. Y., Jiang S. Y., Palmer M. R. 2015. Chemical and boron isotopic compositions of tourmaline from the Nyalam leucogranites, South Tibetan Himalaya: Implication for their formation from B-rich melt to hydrothermal fluids. *Chemical Geology*, **419**:102–113.

APÊNDICE

Hydrothermal Alteration, Fluid Evolution and Re-Os Geochronology of the Grota Funda IOCG Deposit, Carajás Province, Brazil

RAPHAEL BIANCHI HUNGER,[1] ROBERTO PEREZ XAVIER[1], CAROLINA P. N. MORETO[1], ZHI-KUN SU[2], XIN-FU ZHAO[2], JIAN-FENG GAO[3]

[1]*Instituto de Geociências, Universidade Estadual de Campinas (UNICAMP), R. João Pandiá Calógeras, 51, 13083-970, Campinas (SP), Brazil*

[2]*State Key Laboratory of Geological Processes and Mineral Resources, and Faculty of Earth Resources, China University of Geosciences, Wuhan 430074, China*

[2]*State Key Laboratory of Ore Deposit Geochemistry, Institute of Geochemistry, Chinese Academy of Sciences, Guiyang, China*

ABSTRACT

The Grota Funda iron oxide copper-gold deposit (IOCG) is located at the northwestern portion of the Carajás Domain, an Archean (3.0 – 2.55 Ga) segment of the Carajás Province, in the southeastern sector of the Amazonian Cráton. Within the same regional WNW-ESE-striking shear zone (Pojuca Fault System) in which lie the Gameleira (Cu-Au) and Pojuca (Cu-Zn) deposits, volcano-sedimentary sequences of the Igarapé-Pojuca Group, comprising basalt, diabase, gabbro and dacitic rocks and banded iron formations, are the main lithotypes recognized in the deposit area. In this sequence, mafic metavolcanic rocks represent the main hosts to the copper(-gold) mineralizations. The paragenetic evolution of the Grota Funda hydrothermal system encompasses an early high-temperature calcic-sodic hydrothermal alteration (albite-hastingsite-scapolite), ensued by intense Fe-metasomatism (magnetite-grunerite-almandine), potassic alteration with biotite, chlorite-quartz-tourmaline precipitation, and late carbonate-quartz veining. Copper (-gold) mineralizations are spatially and temporally associated with iron-enriched, potassically-altered and chlorite-altered zones. Molybdenite from grunerite-magnetite veins yielded a Re-Os model age of 2,530 ± 60 Ma, which is interpreted as a mineralization age coeval with the Fe-metasomatism. The main sulfide ore is spatially associated with potassically-altered zones, and predominantly forms breccia bodies characterized by a chalcopyrite-magnetite-sphalerite-pyrrhotite-pentlandite assemblage. The ore paragenesis suggests a mineralizing fluid at low fS_2 and fO_2 conditions. Development of early and high temperature (> 500°C) alteration assemblages (albite, scapolite-hastingsite) is attributed to regional circulation of deep-seated hypersaline and metalliferous fluids. Mixing with moderate to high salinity (24 to 29 wt% NaCl + $CaCl_2$ equiv.) and cooler fluids, may have triggered ore precipitation in the main ore zone, due to a decrease in temperature and Cl^- activity. Post-ore alteration assemblages (chlorite-quartz-tourmaline, carbonate-quartz) resulted from considerable temperature, salinity and pH decrease. In addition, boron isotopic compositions ($\delta^{11}B$ = +8.2 to +13.6‰) of tourmaline from the chlorite alteration zone are attributed to mixed sources, including isotopically heavier boron sourced fluids, possibly represented by highly saline brines (e.g., evolved seawater, formation water or bittern fluids) and light boron leached from the host rocks (e.g mafic metavolcanic rocks).

Keywords: Grota Funda; Carajás; Hydrothermal alteration; Fluid inclusions; Boron isotopes

INTRODUCTION

The Carajás Mineral Province (CMP), in the southeastern sector of the Amazonian Craton, is among the world´s best-endowed provinces in metal deposits formed during the Neoarchean to Paleoproterozoic (Xavier et al. 2010, 2012). It contains a vast number of Cu-Au systems, of which world-class (> 200 Mt) iron oxide copper-gold (IOCG) deposits (e.g. Cristalino, Igarapé-Bahia, Sossego, Salobo; Huhn et al. 1999b; Tallarico et al. 2005; Monteiro et al. 2007; Melo et al. 2016), situated in both north and south portions of the Carajás Domain, have been the main targets of the mineral exploration industry. Currently, Sossego and Salobo are the two mines in operation by VALE in the Carajás Domain, with annual copper ore production of 100 Mt and 160 Mt, respectively (VALE 2017).

The present knowledge on the IOCG deposits of the Carajás Domain reveals that these systems are product of multiple hydrothermal episodes of Neoarchean (ca. 2.71 Ga and 2.57 Ga) and Paleoproterozoic (2.0 and 1.88 Ga) ages (Moreto et al. 2015a, b), with fluid circulation at different crustal levels (Xavier et al. 2010, 2012). Although the origin of mineralizing fluids is still controversial, mixing of hot (> 500°C), hypersaline (~ 50 wt% NaCl + $CaCl_2$ equiv.), metal-bearing fluids, with lower salinity and more diluted fluids (e.g. meteoric water), has been attributed as the main mechanism to copper-gold ore precipitation. However, the genesis of these systems is also dependent upon a series of other important factors, such as sulfur availability, fluid redox and sulfidation states, and degrees of fluid-rock interaction (Xavier et al. 2012). Noteworthy, the role of magmatic and non-magmatic fluids on the genesis of these systems has been a matter of debate which has precluded a more robust definition of metallogenic models for the Carajás Domain (Chiaradia et al. 2006; Xavier et al. 2008, 2012; Moreto et al. 2011). The importance of Archean (ca. 2.75 or 2.57 Ga) and Paleoproterozoic (ca. 1.88 Ga) granitic intrusions as potential sources of heat and fluids have been reinforced by several authors (Huhn et al. 1999b; Réquia et al. 2003; Tallarico et al. 2005; Neves 2006; Pollard 2006; Villas et al. 2006; Grainger et al. 2008). Nonetheless, the participation of bittern-type evaporite fluids, which may explain the characteristic high salinity of the ore fluids has been shown by boron, chlorine and strontium isotopes data, and halogen ratios (e.g. Cl/Br, Na/Cl) in fluid inclusions (Chiaradia et al. 2006; Xavier et al. 2008, 2009, 2013).

The Grota Funda copper-gold deposit is formally known as the east extension of the Gameleira and Pojuca deposits, in the northwestern sector of the Carajás Domain. Despite its proximity to these deposits, the geological and metallogenic evolution at Grota Funda is

still poorly understood. Similar paragenetic evolution marked by early sodic-calcic alteration, Fe-metasomatism and potassic alteration, followed by ore precipitation, has also been recognized in other important IOCG deposits located in the northern sector of the Carajás Domain (e.g. Salobo; Melo et al. 2016), suggesting an analogous evolutionary history. Thus, this study aims to introduce the Grota Funda deposit, focusing on characterizing its host rocks, distribution and types of hydrothermal alteration, and modes of occurrence of copper(-gold) mineralization. Moreover, this paper presents new B-isotopic, fluid inclusions and geochronological data that contribute to the current knowledge on the timing of IOCG genesis in the Carajás Domain, and the origin and composition of the hydrothermal fluids.

THE CARAJÁS PROVINCE: GEOLOGICAL SETTING

The Carajás Province constitutes one of the most well-preserved Archean segments of the world. Situated in the southeastern sector of the Amazonian Craton (**Fig. 1A**), it is segmented into the Meso- to Neoarchean Carajás Domain (3.0 – 2.55 Ga; Dall'Agnol et al. 2006), in the north, and the Mesoarchean Rio Maria granite-greenstone terrane (3.0 – 2.86 Ga; Almeida et al. 2010), in the south (**Fig. 1B**). A major and geophysically constrained E-W tectonic discontinuity is interpreted to be the approximate limit between the Rio Maria and Carajás domains (Feio et al. 2013).

The Carajás Domain (Vasquez et al. 2008; **Fig. 1C**), anteriorly known as the Itacaiúnas Shear Belt (Araújo et al. 1988), was recently subdivided into the northern Carajás Basin and the southern Canaã dos Carajás and Sapucaia subdomains (Feio et al. 2013). Basement rocks of the Canaã dos Carajás subdomain comprise recently individualized Mesoarchean granitic units, originally considered portions of the Xingu Complex (Avelar et al. 1999), which include the Bacaba (3.0 Ga; Moreto et al. 2011) and Campina Verde tonalites, the Rio Verde Trondhjemite and the Canaã dos Carajás (2.96 – 2.93 Ga; Feio et al. 2013), Cruzadão, Bom Jesus and Serra Dourada granites (2.87 – 2.83 Ga; Moreto et al. 2011; Feio et al. 2013; Rodrigues et al. 2014). In contrast, the Sapucaia subdomain encompasses Mesoarchean tonalite-trondhjemite units, high-magnesium granitoids and leuco- granodiorites and granites (Teixeira et al. 2013; Gabriel and Oliveira 2014; Silva et al. 2014).

The Carajás Basin represents the Neoarchean (2.76 – 2.74 Ga) metavolcanic-sedimentary cover that overlies the basement rocks. It is divided into the Igarapé Salobo, Grão Pará, Igarapé Bahia and Pojuca groups, collectively known as the Itacaiúnas Supergroup (Wirth et al. 1986; DOCEGEO 1988; Machado et al. 1991), and the Rio Novo Group (Hirata et al. 1982). The Itacaiúnas Supergroup, which hosts an extensive number of Cu-Au deposits, including the world-class IOCG systems (e.g. Salobo, Igarapé-Bahia/Alemão, Cristalino, Sossego and Alvo 118), consists of basic to felsic metavolcanic rocks, banded iron formations and metavolcanoclastic, amphibolite and metasedimentary units (CVRD/CMM 1972; DOCEGEO 1988; Vasquez et al. 2008). The Rio Novo Group comprises amphibolites, schists, metagreywackes, tholeiitic metavolcanic rocks and gabbros (Hirata et al. 1982).

The Águas Claras Formation (Nogueira et al. 1995) defines the Archean non-metamorphosed siliciclastic cover that overlies the Itacaiúnas Supergroup. This unit is mainly consisted of sandstones, siltstones and orthoconglomerates which were originated in fluvial to shallow marine environments. Minimum deposition ages were obtained through dating of

detrital zircon grains extracted from sandstones (2,681 ± 5 Ma; Trendall et al. 1998) and metagabbro sills (2,645 ± 12 and 2,708 ± 37 Ma; Dias et al. 1996; Mougeot et al. 1996).

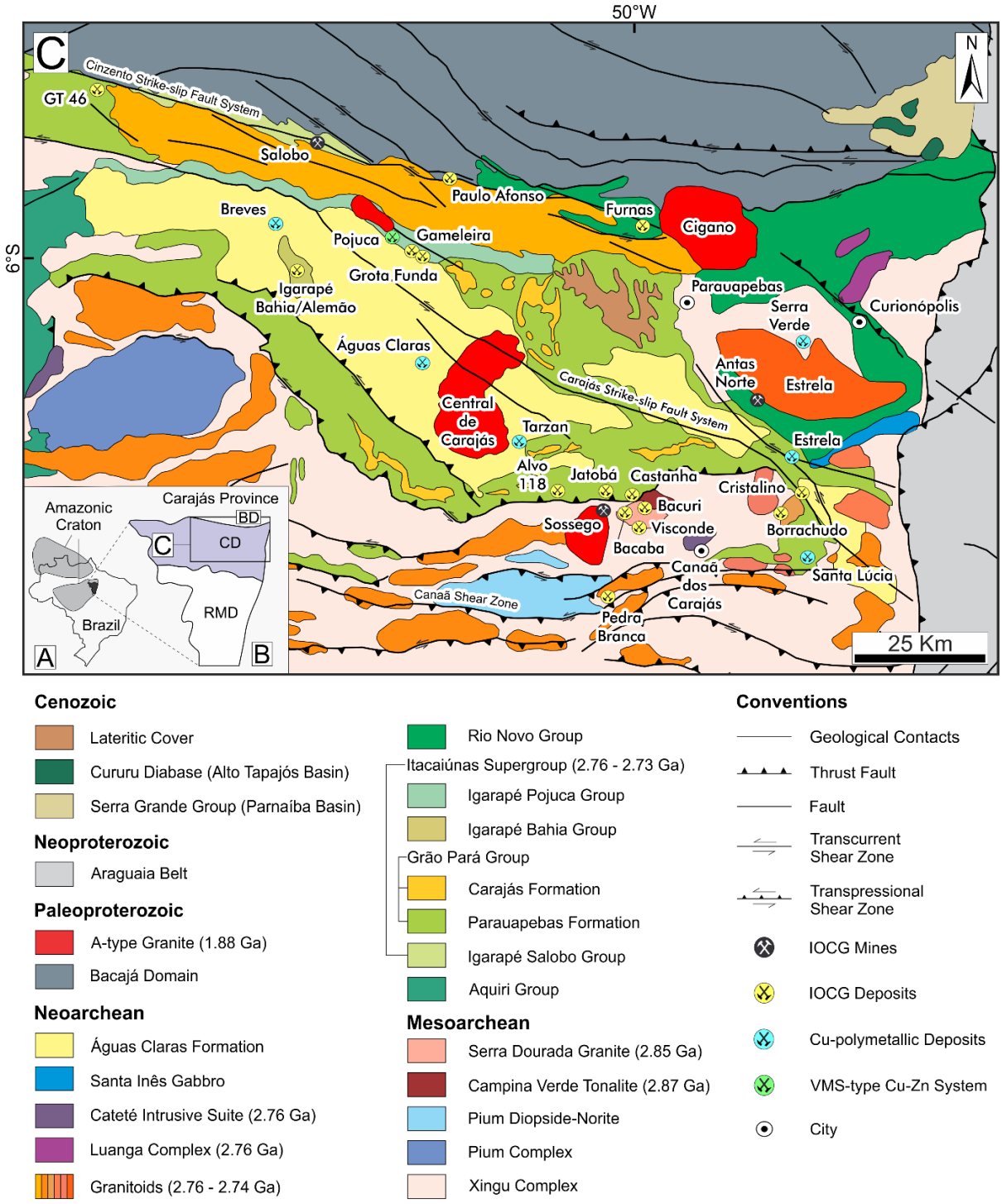

Figure 1. *(A) Location of the Carajás Province (black) in the Amazonian Craton (light grey). (B) Compartmentation of the Carajás Province into the Rio Maria (RMD) domain (south) and the Carajás Domain (north), this limited to the north by the Bacajá Domain (BD). (C) Simplified geological map of the Carajás Domain, showing the location of the main copper deposits and structures (modified from Vasquez et al. 2008).*

Widespread felsic to mafic-ultramafic magmatism has been reported in the Carajás Domain. Archean granitic episodes are attributed to ca. 2.76 – 2.73 Ga syn-tectonic, foliated alkaline intrusions (e.g. Plaquê, Planalto, Estrela, Serra do Rabo, Igarapé-Gelado and Pedra Branca suites; Avelar et al. 1999; Huhn et al. 1999a; Barros et al. 2004, 2009; Sardinha et al. 2006; Feio et al. 2012, 2013) and to ca. 2.57 Ga peralkaline to metaluminous granitoids, represented by the Old Salobo and Itacaiúnas granites (Machado et al. 1991; Souza et al. 1996). Paleoproterozoic (ca. 1.88 Ga) A-type alkaline to subalkaline and metaluminous to slightly peraluminous granites (e.g. Central de Carajás, Young Salobo, Cigano, Pojuca, Breves, and Rio Branco; Machado et al. 1991; Tallarico et al. 2004) are also broadly recognized in the Province. Mafic-ultramafic intrusions are mainly characterized by the Luanga layered complex (2,763 ± 6 Ma; Machado et al. 1991), and the Cateté Intrusive Suite, which includes the Serra da Onça, Serra do Puma, Serra do Jacaré-Jacarezinho, Vermelho and Igarapé Carapanã bodies (Macambira and Vale 1997; Macambira and Ferreira Filho 2002; Ferreira Filho et al. 2007).

The tectonic evolution of the Carajás Basin is ascribed to at least three main hypothesis, including the formation during a dextral transtension, subsequently tectonically inverted to positive flower structures by sinistral transpression (Araújo et al. 1988), during continental rifting related to mantle-plume activity (Tallarico 2003) and in a volcanic arc setting related to subduction processes (Meirelles 1986; Dardenne et al. 1988; Meirelles and Dardenne 1991; Teixeira 1994; Lobato et al. 2005; Silva et al. 2005; Teixeira et al. 2010). Major discontinuities recognized in the Carajás Domain comprise the northern Cinzento and Carajás transcurrent shear zones, and the southern Canaã shear zone (Pinheiro et al. 2013), products of a regional NNE-SSW shortening also responsible for the widespread E-W trending foliation observed in this domain.

PREVIOUS STUDIES ON THE POJUCA AND GAMELEIRA DEPOSITS

The Pojuca and Gameleira deposits are situated in the northwestern sector of the Carajás Domain, within the same WNW-ESE-trending regional discontinuity (Pojuca Fault System; **Fig. 2**). Among them, the Gameleira deposit is by far the most well documented, having been studied by several authors in the past and thus possessing an extensive set of published data (e.g. Lindenmayer et al. 2001; Galarza and Macambira 2002; Pimentel et al. 2003; Marschik et al. 2005; Chiaradia et al. 2006). The Pojuca deposit, on the other hand, was preliminarily studied in the late 80's (Medeiros Neto and Villas 1985; Saueressig 1988) and most recently detailed by Winter (1994) and Schwarz and Frantz (2013).

Gameleira

The Gameleira deposit (300 Mt @ 1.0 wt.% Cu; Carvalho (2004), previously known as Pojuca Leste (Pimentel et al. 2003), is hosted by the late Archean metavolcano-sedimentary rocks of the Igarapé Pojuca Group. These rocks consist mostly of mafic to intermediate metavolcanic units (meta-andesite and metagabbro), amphibolite, biotite schist, clastic sediments and ironstones (Lindenmayer et al. 2001; Marschik et al. 2005). Local metamorphic grade is greenschist to amphibolite facies. Available geochronological data for the meta-andesite and metagabbro (2,719 ± 80 Ma and 2,757 ± 81 Ma, respectively; whole-rock Sm-Nd isochrons; Pimentel et al. 2003), constrain the age of crystallization of the original calc-alkaline to tholeiitic, basic to intermediate magmas. Lindenmayer et al. (2001) have recognized two generations of granitic intrusions at Gameleira, comprising an older quartz-syenite to alkali-feldspar granitic aplite, correlated with the 1.87 Ga Pojuca Granite, and a younger muscovite-bearing, alkali-rich leucocratic syenogranite (1,583 +9/-7 Ma; U-Pb in zircon; Pimentel et al. 2003). The region is also intruded by Neoarchean mafic intrusions (ca. 2.70 Ga) and the 2.56 Ga Itacaiúnas granite (Galarza and Macambira 2002).

The mineralization at Gameleira is essentially epigenetic and predominantly ascribed to two veining styles, both associated with pervasive potassic (biotite) alteration (Lindenmayer et al. 2001; Galarza and Macambira 2002; Pimentel et al. 2003; Marschik et al. 2005): (i) early quartz-grunerite veins with minor sulfides; and (ii) crosscutting sulfide-rich veins containing chalcopyrite, pyrite, bornite, quartz, biotite and albite. Breccia bodies and disseminations within the meta-andesite and gabbro are also recognized.

Sulfur isotope analyses in chalcopyrite, bornite and molybdenite yielded values of $\delta^{34}S_{CDT}$ ranging from 2.0‰ to 4.81‰, which are consistent with a magmatic sulfur source

(Lindenmayer et al. 2001; Marschik et al. 2002). Complementarily, oxygen and carbon isotopes in calcite have $\delta^{18}O_{SMOW}$ values between 9.1 and 10.0‰ and $\delta^{14}C_{PBD}$ from -8.41 to -9.45‰, indicating (Lindenmayer et al. 2001), indicating a deep-seated magmatic source. Vein quartz associated with chalcopyrite and biotite shows a $\delta^{18}O_{SMOW}$ value of 8.8‰ (Marschik et al. 2002).

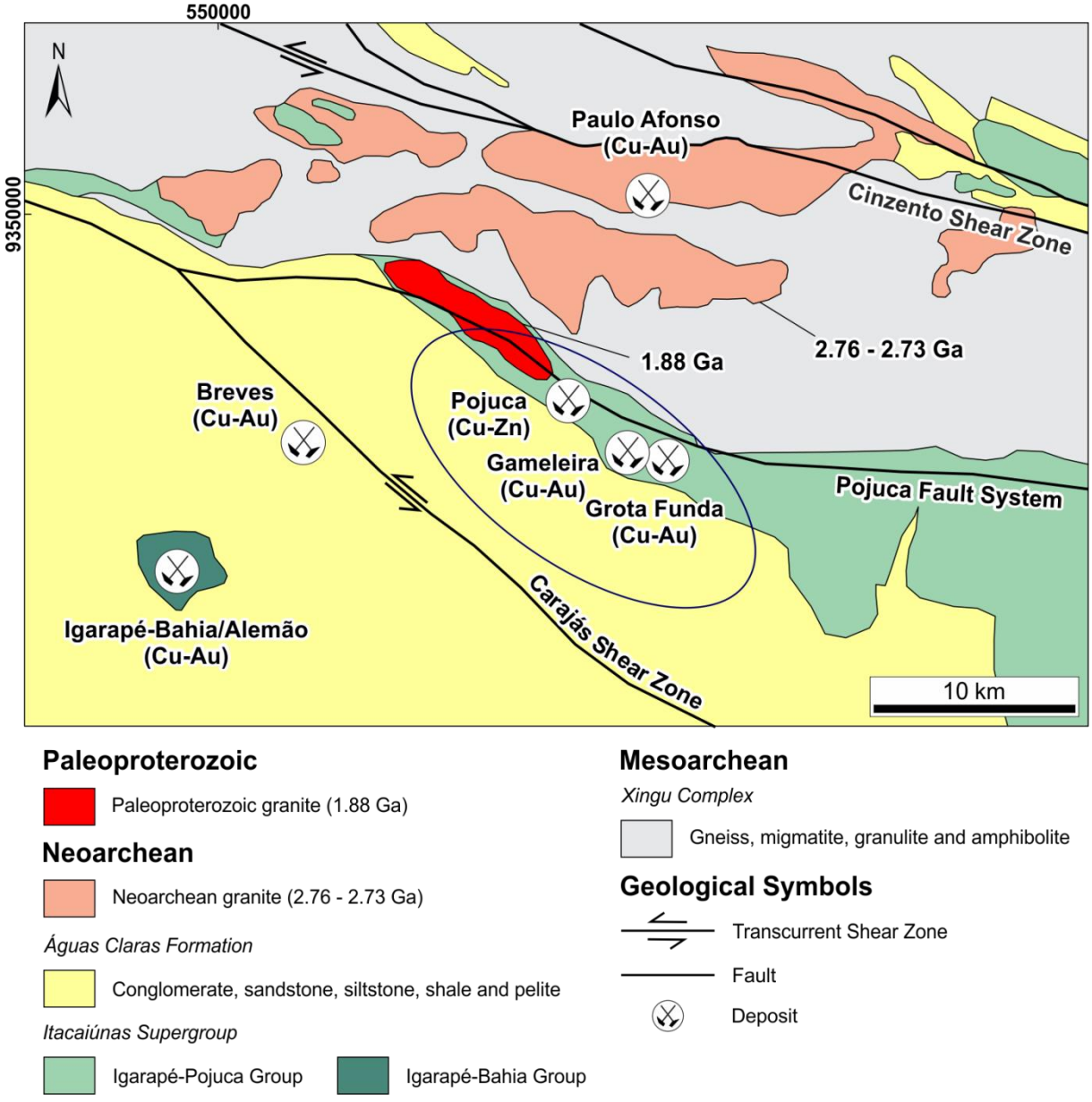

Figure 2. *Geological map of the north-western sector of the Carajás Domain, evidencing the main shear zones and the location of Pojuca, Gameleira and Grota Funda deposits (modified from VALE).*

Fluid inclusion studies in quartz, fluorite, tourmaline and calcite reveal the co-existence of aqueous two-phase inclusions with remarkably variable salinities (1 – 21 wt%

NaCl equiv), and hypersaline three-phase inclusions (30 – 40 wt% NaCl equiv). These data suggest that the mixing of magmatic-hydrothermal and low salinity non-magmatic fluids represents a reasonable mechanism for the ore formation (Lindenmayer et al. 2001; Ronchi et al. 2001).

Lindenmayer et al. (2001) indicate that Gameleira represents a magmatic end-member of the IOCG class of deposits, based on alteration mineral assemblages and metal associations (Fe-Cu-Au-Mo-Co-U-F-REE), originated in moderately deep crustal levels. The age of mineralization is, however, controversial. Marschik et al. (2005) presented a Re-Os molybdenite age of 2,614 ± 14 Ma for the Cu-Au ore, which configures a more reliable mineralization age than the Proterozoic Sm-Nd and Ar-Ar alteration ages (ca. 1.7 Ga) obtained by Pimentel et al. (2003). In this scenario, the Gameleira deposit is more likely to be genetically related to Neoarchean alkaline granitoids (ca. 2.56 – 2.76 Ga) or to calc-alkaline to tholeiitic volcanic-arc magmatism, instead of Paleoproterozoic (ca 1.8 – 1.9 Ga) anorogenic granites (Marschik et al. 2005).

Pojuca

The Pojuca deposit (58.2 Mt @ 0.78 – 0.89 wt.% Cu and 8.4 Mt @ 0.49 – 1.11 wt.% Zn; Carvalho (2004), commonly known as Corpo Quatro Cu-Zn orebody, is hosted by a metamorphosed (upper greenschist to lower amphibolite grade), conformable sequence of metavolcano-sedimentary rocks including metabasalts (2,757 ± 81 Ma, whole rock Sm-Nd; Pimentel et al. 2003) schists, banded iron formation, sand- and siltstones (Medeiros Neto and Villas 1985; Saueressig 1988; Winter 1994). Two events of granitic intrusions have been reported in the Pojuca area (Winter 1994): (i) post peak-metamorphism granitic veins; and (ii) the Pojuca Granite. Furthermore, at least four styles of quartz veining are described in the deposit, comprising early barren quartz veins, post-dated by quartz + chalcopyrite (Q2-A-type), quartz + biotite (Q2-B-type) and late barren quartz + calcite or calcite-only veins (Winter 1994). Microthermometric data conducted on fluid inclusions from these four generations of quartz veins revealed a similar Na-Ca-K-rich chemical composition for both aqueous two-phase and hypersaline multiphase inclusions. This similarity suggests an unique source of fluids for their formation (Winter 1994).

The ore at Pojuca is predominantly concentrated along the iron formation (stratabound), and consists of pyrite, pyrrhotite, chalcopyrite, sphalerite and minor molybdenite, pentlandite, gold and nickel-arsenides (Winter 1994). This primal sulfide mineralization is interpreted to be associated with intense sodic-calcic alteration (albite +

chlorite ± hornblende; Winter 1994; VALE 2009). Secondarily, late disseminations and quartz-carbonate vein-type mineralizations are also recognized and interpreted as remobilizations (Schwarz and Frantz 2013).

Although not consensual, a syngenetic volcanogenic massive sulfide (VMS) origin is indicated as the best suitable metallogenetic model for the genesis of the Pojuca deposit (Medeiros Neto and Villas 1985; Schwarz and Frantz 2013). According to Schwarz and Frantz (2013), evidences that support this hypothesis include: (i) stratabound ore bodies concordant to volcanogenic sequences and the presence of stockwork vein-systems; (ii) specific ore assemblage (pyrrhotite + chalcopyrite + sphalerite) and; (iii) inferior tonnage when compared with other important Cu-Au systems already described in the Carajás Province (e.g. IOCG deposits).

ANALYTICAL METHODS

Systematic and detailed descriptions of five drill cores from the Grota Funda deposit (GRFUN_FD028, GRFUN_FD029, GRFUN_FD037, GRFUN_FD046 and PKO-09) were performed to determine the host rocks, spatial distribution and stages of hydrothermal alteration and modes of occurrence of the copper-gold ore. Thorough petrographic analyses were carried out in thirty-two polished thin sections and accessory mineral phases were identified by Scanning Electron Microscope (SEM) coupled with EDS (Energy-Dispersive X-Ray Spectrometer). Fluid inclusions analyses in apatite were conducted on a doubly polished thin section representative of the chalcopyrite + pyrrhotite ± magnetite ± sphalerite ± pentlandite ore zone. Microthermometric data were obtained on a LINKAM THMSG600 heating-freezing stage attached to a LEICA DMLP petrographic microscope, equipped with a 100x objective. Calibration was performed using the Synflinc set of synthetic fluid inclusions and revealed a precision of ± 0,1°C for freezing runs down to -21,2°C, and to ± 2°C for heating runs up to 300°C. These studies were respectively executed at the laboratories of Microscopy, Scanning Electron Microscope and Microthermometry of the Institute of Geosciences, University of Campinas (UNICAMP), Brazil.

Boron isotope analyses were carried out in the State Key Laboratory of Geological and Mineral Resources (GPMR), China University of Geosciences (CUG), China. A double polished thin section containing tourmaline samples were investigated by optical microscopy and SEM backscattered electron imaging, in order to select spots for laser ablation shots. Boron isotopic compositions of two tourmaline crystals were measured in situ using a Neptune Plus Laser Ablation Multi-Collector Inductively Coupled Plasma Mass Spectrometry (LA-MC-ICP-MS) and a matching New Wave UP193 laser ablation system. Detailed analytical procedures and data reduction followed those of Yang et al. (2015). Operating conditions consist of an energy density of 12 J/cm², 8 Hz repetition rates and spot diameters of 50 μm. Mass bias of the instrument and the fractionation of isotopes were calibrated using the standard-sample-bracketing method (SSB). The tourmaline IAEA B4 (Tonarini et al. 2003) was used as an external standard. Instrumental mass fractionation (IMF) and analytical quality were determined by replicate analyses of international tourmaline reference material IMR RB1 (Hou et al. 2010) and an in-house standard Dai ($\delta^{11}B$ = -13.6‰). Individual uncertainty (2σ) for 100-cycle individual analyses was typically around 0.5‰. The reported $\delta^{11}B$ results were calculated relative to tourmaline IAE B4 of $\delta^{11}B$ = -8.71‰ (Tonarini et al. 2003).

Molybdenite for Re-Os analyses was manually separated from a drill core sample (GRFUND_FD037/105,40) representative of the grunerite-magnetite veins, using a diamond-tipped, slow-speed, handheld drill. The analyses were performed at the State Key Laboratory of Ore Deposit Geochemistry, Institute of Geochemistry, Chinese Academy of Sciences (Guiyang), on an ELAN DRC-e ICP-MS instrument. Detailed analytical procedures followed those of Andao et al. (1995), Shirey and Walker (1995), Markey et al. (1998), Stein et al. (1998), and Qi et al. (2007, 2010). Approximately 10 mg of concentrated molybdenite was weighed and loaded into a 120 ml re-usable Carius tube with known amounts of ^{185}Re and ^{190}Os spikes. Samples were then digested and equilibrated using 10 ml of concentrated HNO_3 and 2 ml HCl. The tube was posteriorly placed in a stainless-steel jacket and heated at 200℃ for about 12 h. After cooling, Osmium was separated from the matrix as OsO_4, using the *in-situ* distillation equipment, and Re was extracted from the remaining solution utilizing an anion exchange resin (Biorad AG 1-X8, 200 – 400 mesh). Iridium was added to the Re and Os solutions for mass discrimination correction (Schoenberg et al. 2000; Huang et al. 2013).

THE GROTA FUNDA IRON OXIDE-COPPER-GOLD DEPOSIT

Geological setting and host rocks

The Grota Funda deposit is located at the northwestern portion of the Carajás Domain, within the same regional WNW-ESE-striking shear zone in which lie the Pojuca and Gameleira deposits (Pojuca fault system; **Fig. 2**). The deposit is also intersected by NE-SW- and E-W-trending subsidiary faults associated with the Carajás fault system. Mafic metavolcanic rocks (basalt, diabase) correlated with the Igarapé-Pojuca group represent the main hosts to the Cu-Au mineralization (**Fig. 3**). Other lithotypes recognized in the deposit area include gabbro, a felsic subvolcanic rock and banded iron formations (BIF). Original features (e.g. textures, mineralogy) of the Grota Funda lithotypes have been partial to completely obliterated due to intense and widespread hydrothermal and brittle-ductile deformation.

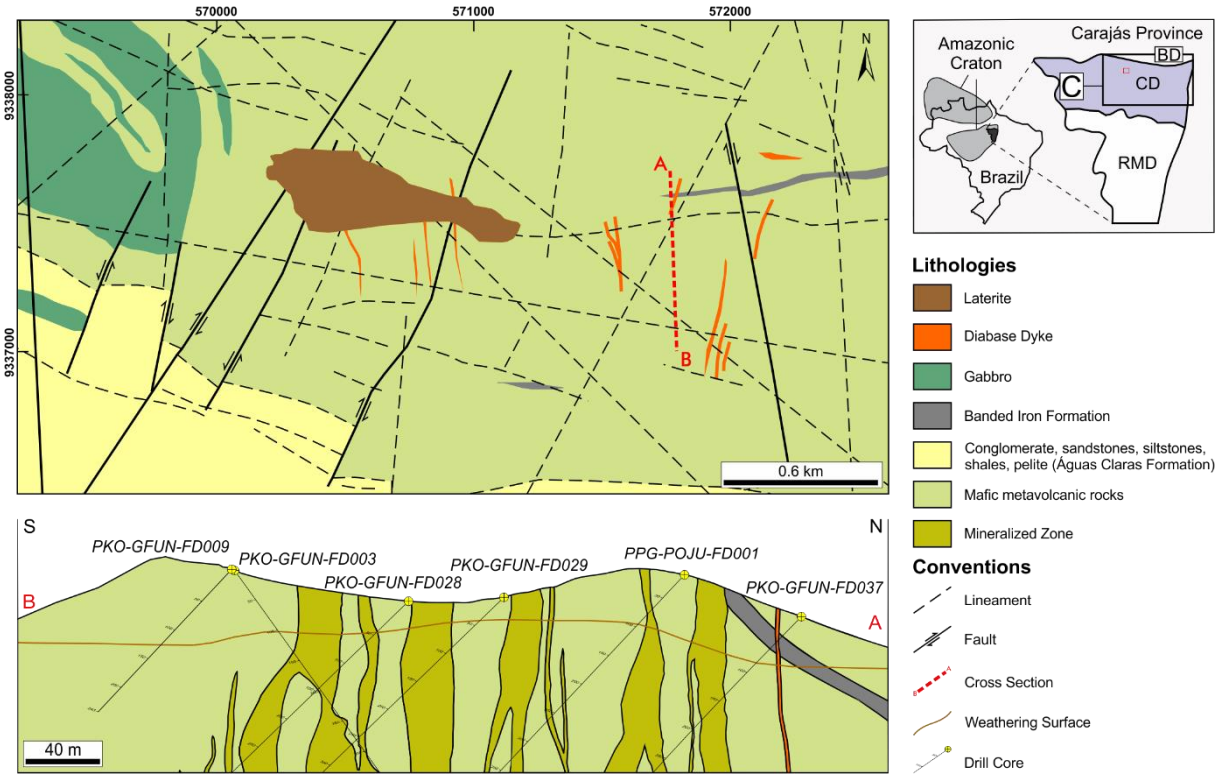

Figure 3. *Simplified geological map and cross-section of the Grota Funda deposit, showing the spatial distribution of the main lithotypes described in the deposit area, and the mineralized zones (modified from VALE).*

The occurrence of basaltic rocks in the deposit area was inferred based on the presence of amygdaloidal textures observed in extremely fine-grained rock samples

essentially composed of chlorite and quartz. These amygdaloidal cavities are filled with microcrystalline quartz and involved by a fine-grained rim of chlorite (**Fig. 4A**). Least-altered diabase and gabbro display similar compositions and fairly preserved subophitic textures, differing only in grain-size (**Figs. 4B-4D**). Both rocks are dark gray to green in color and predominantly composed of plagioclase and augite crystals, the latter intensively altered to hastingsite and biotite. Least-altered plagioclase crystals are generally tabular with poorly-preserved twinning, but most commonly converted into scapolite, and posteriorly mantled by biotite and chlorite. When preserved, augite grains commonly display cleaved and simple twinned basal sections (**Fig. 4E**).

The banded iron formation at Grota Funda belongs to the oxide facies. Compositional layering is typically marked by the alternation of grayish-white quartz + grunerite and dark magnetite-rich microbands, both up to 0.5 mm thick (**Fig. 4F-G**). Contact between microbands is usually diffuse. Magnetite is mostly fine-grained and generally displays different degrees of martitization. Grunerite crystals are typically acicular and randomly oriented within quartz-rich microbands.

The felsic subvolcanic rock was only locally observed in drill cores, although intensively affected by potassic and chlorite alteration (**Fig. 4H**). It is greenish-to-greyish in color and displays a fine-grained (< 1 mm) matrix composed of quartz and plagioclase (**Fig. 4I**), with subordinated potassium feldspar (microcline), that locally involves euhedral (bipyramidal) phenocrysts of bluish quartz (**Fig. 4J**). Bulk mineralogy indicates a dacitic composition. Trace amounts of zircon and epidote are also recognized within this rock. Chalcopyrite occurs as disseminations and fracture infillings.

Hydrothermal alteration and mineralization

The evolution of the paleo-hydrothermal system at Grota Funda is marked by intense and widespread hydrothermal activity, including stages of: (i) sodic-calcic alteration; (ii) Fe-metasomatism; (iii) potassic alteration with biotite; (iv) chlorite-quartz-tourmaline formation and; (v) carbonate-quartz veining. At least three main episodes of copper (-gold) mineralizations have been recognized in the deposit area, respectively associated with Fe-metasomatism, potassic and chlorite alteration stages.

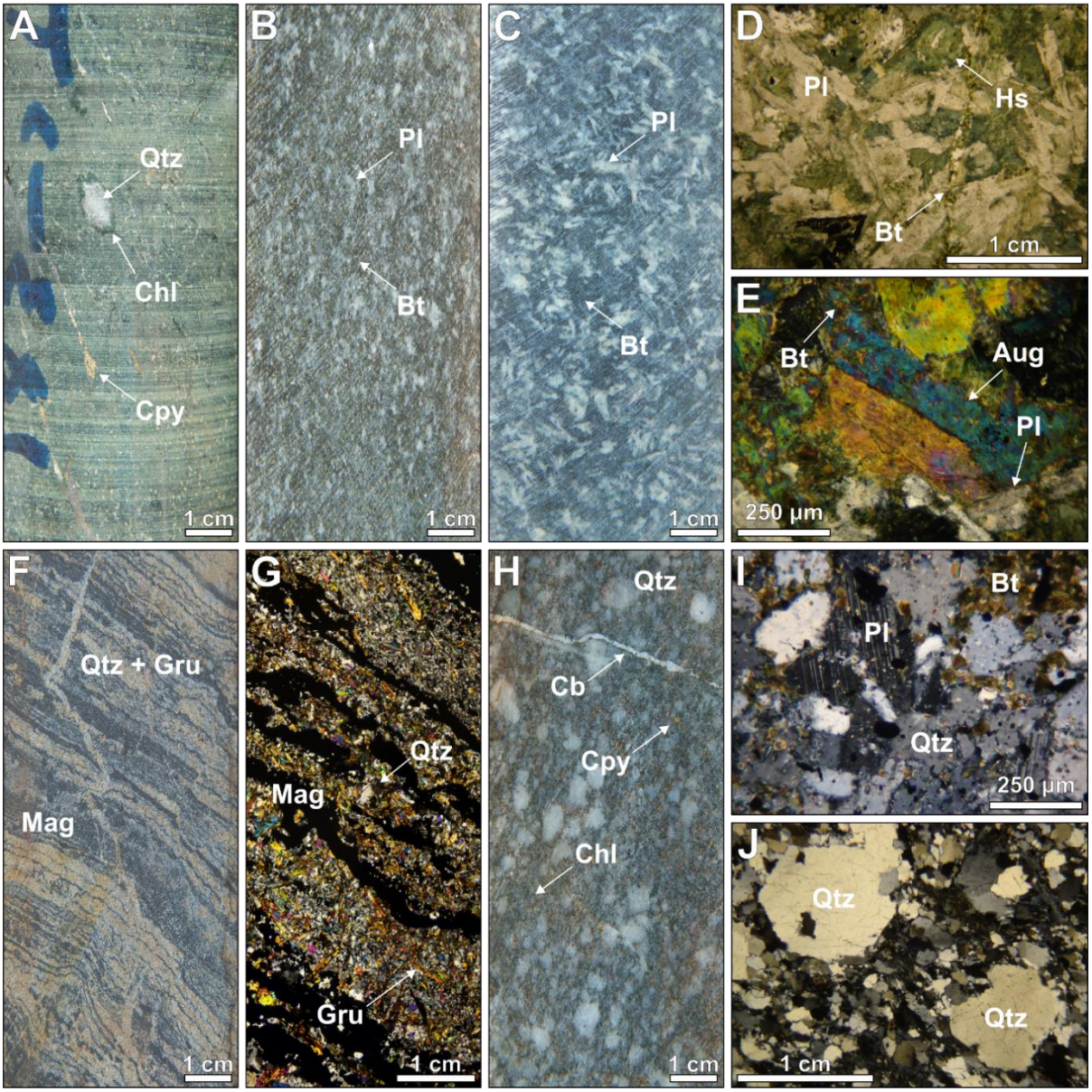

Figure 4. *Lithotypes of the Grota Funda deposit. (A) Mafic metavolcanic rock, possibly basalt, showing amygdaloidal texture. (B) and (C) Partially preserved sub-ophitic texture in diabase and gabbro, both affected by potassic alteration with biotite. (D) Subophitic texture in diabase, showing plagioclase crystals intergrown with hydrothermal hastingsite. (E) Simple twinned augite crystal in basal section. (F) and (G) Drill core picture and photomicrograph displaying the intercalation of quartz-grunerite and magnetite-rich microbands in banded iron formation. (H) Felsic rock of dacitic composition, displaying pervasive chlorite alteration. (I) Photomicrograph showing a fine-grained quartz-plagioclase matrix in dacite. (J) Dacitic rock with bipyramidal quartz phenocrysts involved by a fine-grained matrix of quartz. Mineral abbreviations: Qtz quartz; Chl chlorite; Cpy chalcopyrite; Pl plagioclase; Bt biotite; Hs hastingsite; Aug augite; Mag magnetite; Gru grunerite; Cb carbonate.*

Sodic-calcic alteration

Sodic-calcic alteration zones are represented by two different assemblages. The first is characterized by fracture-controlled veinlets of fine- to medium-grained albite ± quartz that crosscut the dacitic rock (**Fig. 5A**). Pervasive Na-rich alteration domains containing albite were only locally observed in the mafic metavolcanic rocks, although already obliterated due to scapolite (**Fig. 5B**), biotite and chlorite (**Fig. 5C**) overprinting. Albite crystals are generally xenoblastic to subidioblastic and when limpid exhibit evidences of stress-related deformation processes, including stretching, undulose extinction, twin boundary migration and tapered deformation twins. These crystals usually contain tiny inclusions of hematite, which impart a reddish color to the altered rocks.

A distinct assemblage of hastingsite + scapolite overprints zones with hydrothermal albite. This alteration stage is better recognized in mafic protoliths, where hastingsite and marialitic ($[Na,Ca]_4[Al_3Si_9O_{24}]Cl$) scapolite replace the igneous clinopyroxene and plagioclase grains, respectively. Hastingsite is typically bluish-green and forms subidioblastic to idioblastic prismatic crystals, frequently displaying diamond-shaped basal sections (**Fig. 5D**). It apparently reveals a relation of mutual replacement with grunerite (**Fig. 5E**), which suggests that the latter could have been formed earlier in the hydrothermal system. Scapolite is light-yellow in thin section and generally occurs as xenoblastic crystals or as albite pseudomorphs (**Fig. 5F**).

Fe-metasomatism

The central zone of the Grota Funda deposit is marked by intense iron-rich metasomatism, depicted by massive precipitation of magnetite(I)-grunerite-almandine ± chlorite(I)-quartz. Veins containing coarse grunerite, magnetite and minor molybdenite (1 – 2 cm in size) intersect previous zones of sodic-calcic alteration (**Figs. 6A-B** and **7A**), and are also associated with the Fe-metasomatism process. Grunerite replaces hastingsite (**Fig. 7B**), forming a fine-grained mass of frequently twinned prismatic crystals, often in diamond-shaped basal sections, which involves idioblastic almandine porphyroblasts (up to 5mm in diameter; **Fig. 7C**).

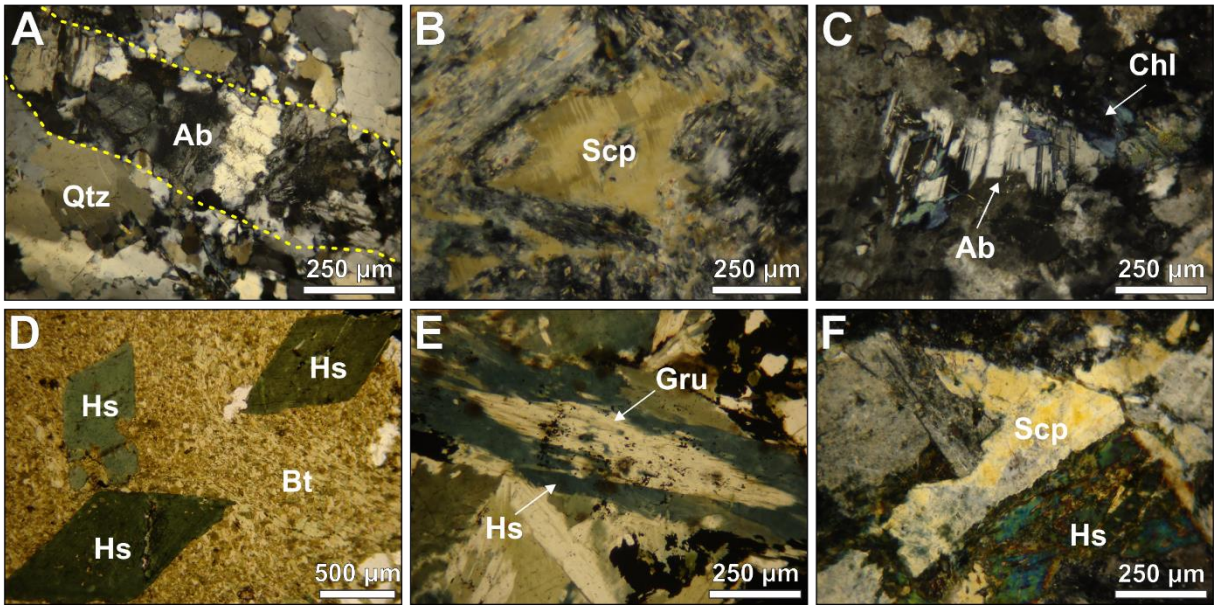

Figure 5. *Photomicrographs showing the main features of the Na-Ca alteration. (A) Albite vein crosscutting dacite matrix. (B). Scapolite pseudomorph after albite. (C) Xenoblastic crystal of albite mantled by chlorite. (D) Diamond-shaped hastingsite crystals involved by fine-grained biotite. (E) Grunerite crystal replaced by hastingsite along its rims. (F) Marialitic scapolite in association with hastingsite. Mineral abbreviations: Qtz quartz; Ab albite; Scp scapolite; Chl chlorite; Hs hastingsite; Bt biotite; Gru grunerite.*

Magnetite is perhaps the most important mineral phase associated with the iron metasomatism stage. Massive magnetite bodies (**Fig. 6C**), locally comprising up to 55 % of the rock mass, can reach thickness up to 10m in drill holes. Magnetite (I) is subidioblastic to idioblastic, commonly exhibiting granular to massive habit.

Towards iron-enriched zones, almandine content becomes progressively higher (**Fig. 6D**). The Fe-rich garnet is generally poikiloblastic, riddled with grunerite, magnetite and quartz inclusions. Individual crystals are also extremely fractured and selectively replaced by biotite. Elongated almandine grains with pressure shadows are observed in intensely deformed zones of the deposit.

A first generation of chalcopyrite formation is also recognized within these magnetite-rich zones. Chalcopyrite (I) is predominantly xenoblastic and typically intergrown with magnetite, grunerite and molybdenite (**Figs. 6E** and **7D-F**). LREE-bearing (La-Ce-Nd) monazite, allanite, uraninite (UO_2) and Te-bismuthite are common accessory phases associated with this mineralization stage (**Fig. 7G**). They usually form tiny inclusions in magnetite and chalcopyrite. Gold occurs essentially as inclusions in magnetite (**Fig. 7H**).

Potassic alteration with biotite

Widespread potassic alteration affects all rock types and overprints both sodic-calcic and Fe-rich alteration assemblages. Strongly potassically-altered zones are well developed in high strain domains dominated by biotite + quartz association (**Figs. 6F-H**), with subordinate amounts of apatite, tourmaline (I), allanite, ilmenite, and Ti-hematite (**Figs. 7I**). In this case, biotite usually occurs as a fine- to medium-grained mass of brownish tabular crystals intergrown with stretched quartz grains and tourmaline aggregates, defining a mylonitic foliation (**Figs. 7J-K**). Selective replacement of hastingsite and grunerite by brown biotite is commonly observed (**Figs. 7L-M**). Millimeter-scale veinlets of fine-grained greenish to brownish biotite flakes are also recognized as fracture-infillings in the mafic metavolcanic rocks, frequently altering almandine (**Figs. 7N**). They also crosscut the coarse grunerite-magnetite veins (**Figs. 7O**). Tourmaline (I) crystals are mainly dark greenish-blue and display clear internal zonation. In the felsic rocks, biotite generally mantles the igneous feldspar (**Fig. 7P**) and shows evidences of later replacement by chlorite.

Main sulfide ore

The main sulfide ore at Grota Funda is chiefly represented by breccia bodies (**Fig. 8A**) that may reach up to 15m thickness in drill holes. Subordinately, the mineralization can occur in veinlets (**Fig. 8B**) and as disseminations. These breccias are spatially associated with potassic alteration and essentially hosted by mafic metavolcanic rocks. The ore consists primarily of massive chalcopyrite (II) (up to 70%), followed by magnetite, pyrrhotite, pentlandite and sphalerite. Gangue minerals include apatite, quartz, tourmaline, biotite, chlorite and allanite. In this case, chalcopyrite represents the breccia matrix which involves other sulfides and gangue minerals (**Fig. 8C**).

Differently from the iron-enriched zones, magnetite (II) represents a secondary mineral phase when compared to sulfide abundance. It generally occurs as subidioblastic to idioblastic crystals, commonly exhibiting octahedral basal sections (**Fig. 8D**). Pyrrhotite usually forms xenoblastic crystals which may present fine-grained pentlandite exsolutions along its rims and cores (**Fig. 8E**). Sphalerite is mainly granular, commonly exhibiting chalcopyrite inclusions (chalcopyrite disease; **Fig. 8F**). Under transmitted light, sphalerite grains are typically translucid and orange-brownish, indicating low iron contents. Among the sulfides, bornite is exceptionally subordinate and generally replaces chalcopyrite along its rims (**Fig. 8G**). Ilmenite represents a common accessory phase, especially in biotite-rich

zones, and frequently displays Ti-hematite exsolutions (Fig. 8H). Minor pyrite (Fig. 8I), siegenite (Fig. 8J), cobaltite (Fig. 8K) and melonite (NiTe2) are also recognized in ore samples, occurring as inclusions in chalcopyrite.

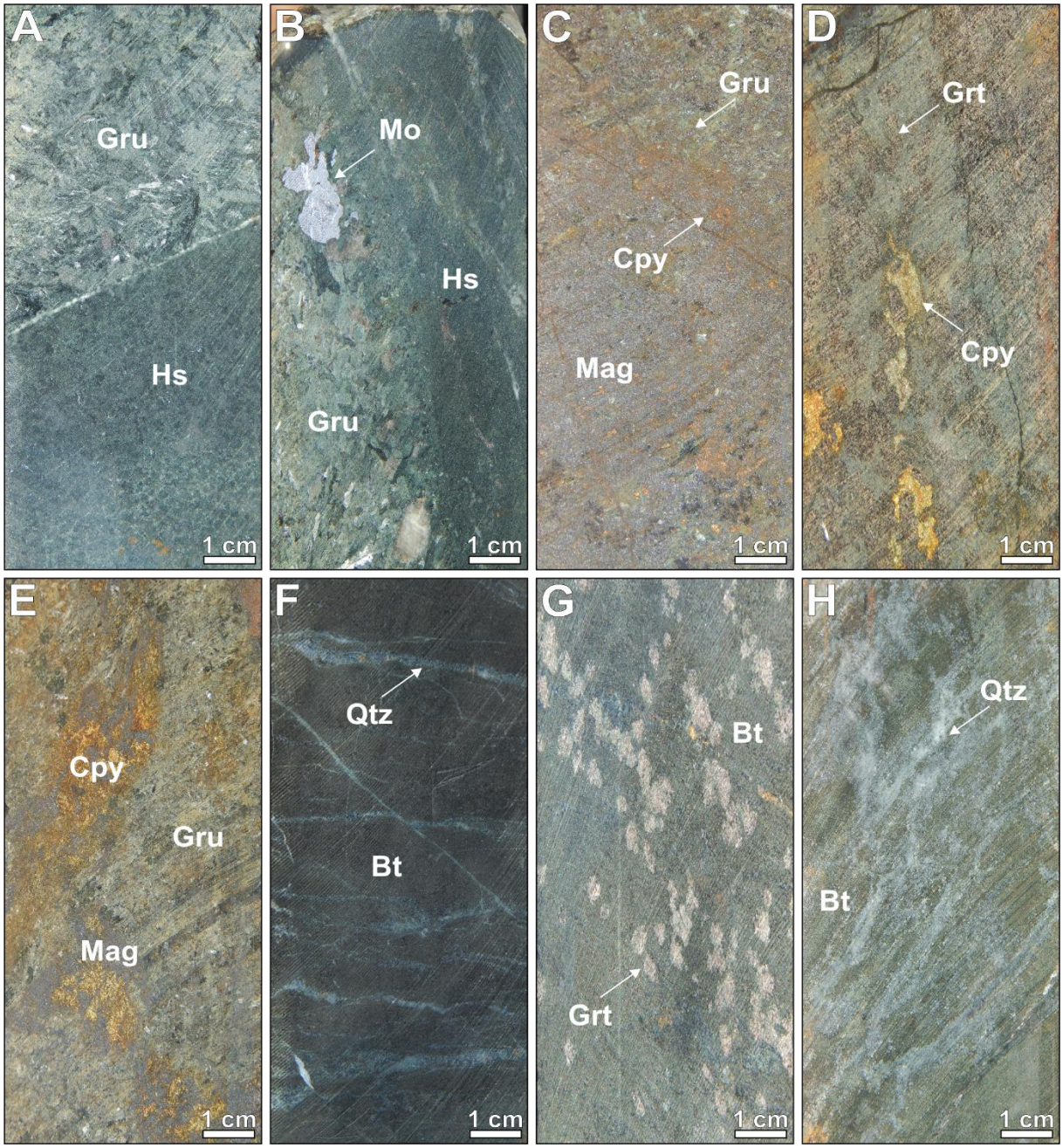

Figure 6. *Drill core pictures showing the main features of the Fe-metasomatism and potassic alteration. (A) Grunerite vein crosscutting Na-Ca altered rock with hastingsite. (B) Coarse-grained molybdenite crystal within grunerite-rich vein, intersecting Na-Ca altered rock with hastingsite. (C) Massive magnetite associated with grunerite and chalcopyrite. (D) Almandine-rich zone, with chalcopyrite, marking the transition to the massive magnetite zones. (E) Mineralized zone containing chalcopyrite intergrown with magnetite and grunerite.*

(F) and (G) Strongly mylonitized rock with biotite, quartz veinlets and stretched almandine crystals aligned with the foliation. (H) Silicification associated with the potassic alteration. Mineral abbreviations: Gru grunerite; Hs hastingsite; Mo molybdenite; Cpy chalcopyrite; Mag magnetite; Grt garnet (almandine); Bt biotite; Qtz quartz.

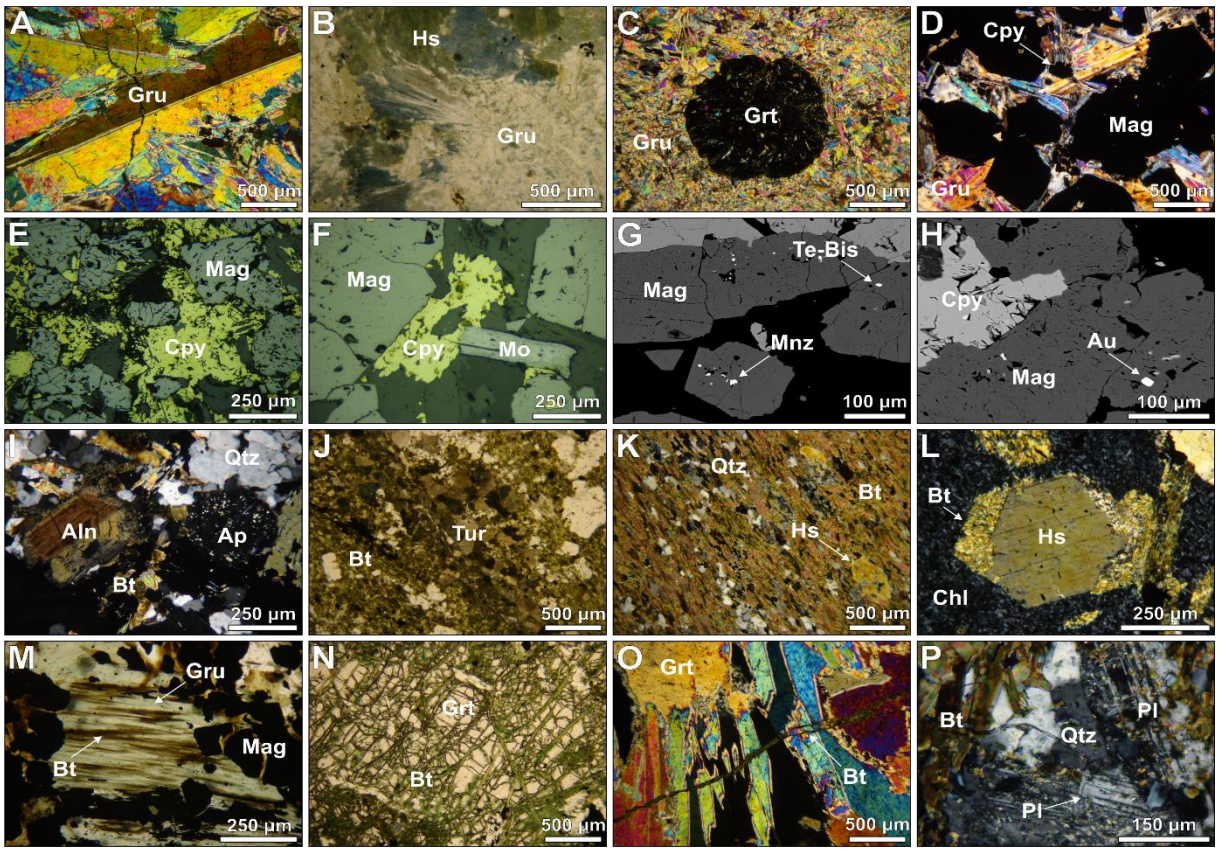

Figure 7. *Photomicrographs showing the main features of the Fe-metasomatism and potassic alteration. (A) Twinned coarse-grained grunerite crystal within vein. (B) Front of acicular grunerite crystals replacing hastingsite. (C) Almandine porphyroblasts involved by fine-grained grunerite. (D), (E) and (F) Chalcopyrite mineralization associated with magnetite, grunerite and molybdenite. (G) SEM image of monazite and Te-bismuthite inclusions in magnetite. (H) SEM image of native gold inclusion in magnetite. (I) Allanite-quartz-apatite-biotite association in potassically-altered rock. (J) Tourmaline aggregates associated with biotite-rich zone. (K) Pervasive potassic alteration with biotite, quartz and hastingsite aligned with the rock foliation. (L) Diamond-shaped hastingsite crystal altered to biotite and involved by fine-grained chlorite. (M) Grunerite crystal partially altered to biotite. (N) Green biotite fracture-infillings in almandine. (O) Coarse grunerite vein crosscutted by green biotite veinlet. (K) Igneous plagioclase crystals from dacitic rock mantled by biotite. Mineral abbreviations: Gru grunerite; Hs hastingsite; Grt garnet, Cpy chalcopyrite; Mag magnetite;*

Mo molybdenite; Mnz monazite; Te-bis Te-bismuthite; Au gold; Aln allanite; Ap apatite; Bt biotite; Qtz quartz; Tur tourmaline; Chl chlorite; Pl plagioclase.

Chlorite alteration

Chlorite alteration is widespread at Grota Funda, being better recognized in areas distal to the central zone of the deposit. Strongly chloritized domains, in which biotite and amphiboles are converted into Fe-rich chlorite (chamosite), are also accompanied by silicification and tourmaline(II)-magnetite(III)-carbonate-actinolite precipitation (**Fig. 9A**). The mafic metavolcanic rocks are particularly affected by this intense chloritization, having their original igneous texture completely obliterated (**Fig. 9B**). Veinlets of chlorite ± quartz-carbonate-chalcopyrite-epidote are commonly observed as fracture infillings within the felsic rocks (**Fig. 9C**).

Magnetite and tourmaline represent significant products of the chloritization process. Magnetite (III) is usually massive, occurring as fine- to medium-grained subidioblastic to idioblastic crystals, intergrown with tourmaline, chlorite, quartz and actinolite (**Fig. 9D**). Tourmaline (II) is black to dark brown and typically occurs as xenoblastic to subidioblastic coarse-grained prismatic crystals (up to 4 mm in length), often crystallized in triangular basal sections. Differently from tourmaline (I), this second generation of B-rich silicate shows no evident internal zonation and is generally poikiloblastic, riddled with chlorite, quartz and carbonate inclusions. Tourmaline-rich domains (up to 70 vol.%) are recurrent along strongly chloritized zones (**Fig. 9E**).

Carbonate-rich veins containing coarse (up to 3cm in length) prismatic actinolite crystals, with associated chalcopyrite and magnetite, were locally recognized within chlorite-altered zones (**Fig. 9F**). Although uncertain, the paragenetic association between chlorite, tourmaline and actinolite, observed in thin sections, suggest that these veins may have been coeval with the chloritization process (**Fig. 9G**). In this context, galena and Ag-tellurides occurs as inclusions in chalcopyrite.

A third stage of chalcopyrite crystallization is spatially related to chlorite-altered domains. The mineralization, in this case, consists of massive chalcopyrite (up to 50%) that occurs with quartz, chlorite, epidote, carbonate and minor Ti-bearing minerals (e.g. titanite, ilmenite and rutile). Two generations of chlorite were recognized within these mineralized zones, including a Mg-rich phase (anomalous dark brown birefringence colors; **Fig. 9H**) which apparently replaces the early-formed chamosite.

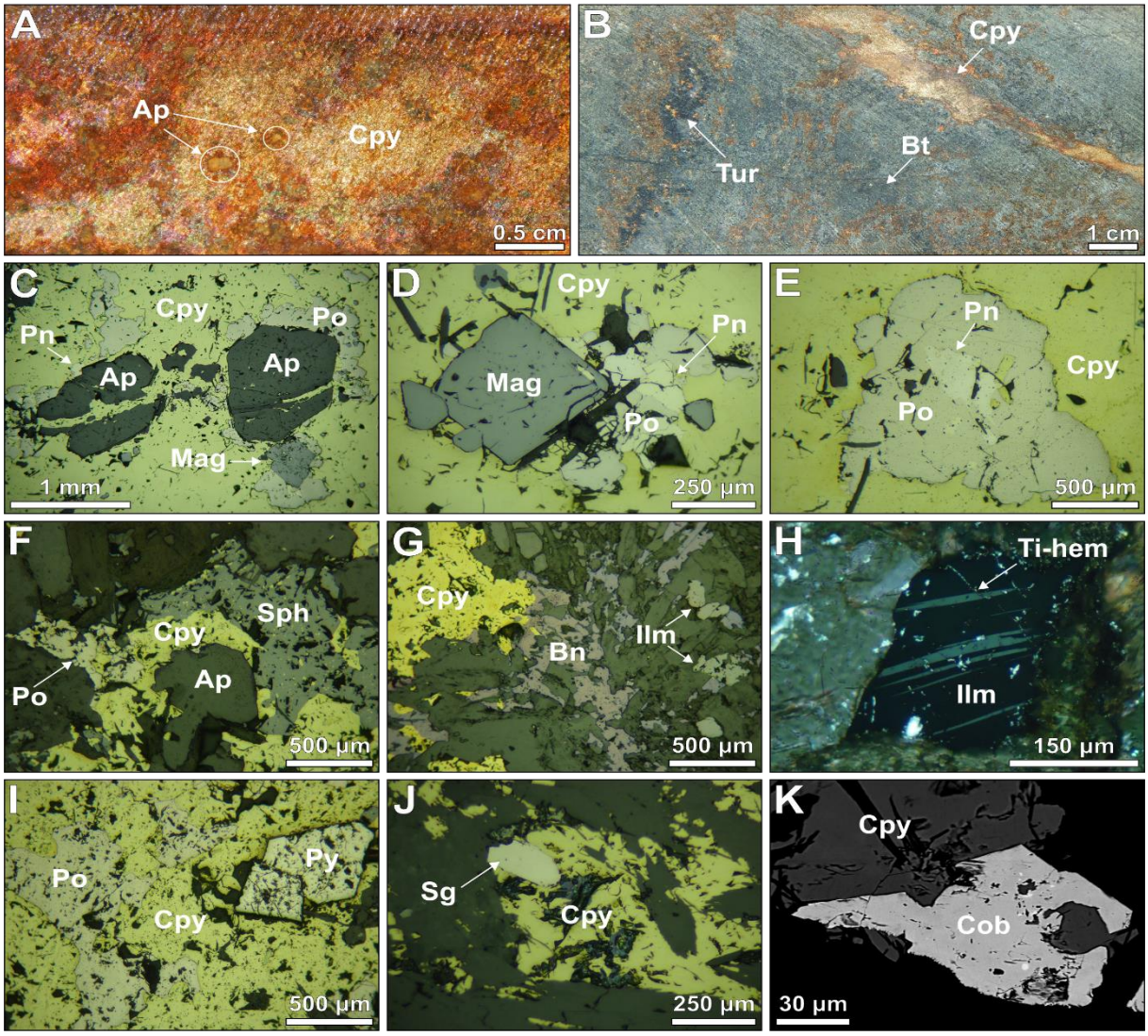

Figure 8. *Drill core pictures (A – B) and photomicrographs (C – K) displaying the characteristics of the main copper sulfide ore zone. (A) Mineralized breccia with massive chalcopyrite involving fine-grained apatite crystals. (B) Chalcopyrite-tourmaline(I) veinlets in a biotite-rich groundmass (C) Chalcopyrite-pyrrhotite-magnetite-pentlandite-apatite association in ore sample. (D) Magnetite crystal along its octahedral basal section within chalcopyrite and in contact with pyrrhotite and pentlandite. (E) Pentlandite exsolution in pyrrhotite as inclusions in chalcopyrite. (F) Xenoblastic sphalerite crystal with chalcopyrite disease, in association with chalcopyrite, pyrrhotite and apatite. (G) Bornite replacing chalcopyrite along its rims. Note the presence of ilmenite crystals. (H) Ti-hematite exsolutions in ilmenite crystal. (I) Chalcopyrite-pyrrhotite-pyrite in ore sample. (J) Siegenite crystal as inclusion in chalcopyrite. (K) SEM image showing cobaltite crystal in contact with chalcopyrite. Mineral abbreviations: Ap apatite; Cpy chalcopyrite; Tur tourmaline; Bt biotite; Pn pentlandite; Mag magnetite; Po pyrrhotite; Sph sphalerite; Bn bornite; Ilm ilmenite; Ti-hem Ti-hematite; Py pyrite; Sg siegenite; Cob cobaltite.*

Late carbonate veins

The latest stage of hydrothermal activity recognized at Grota Funda is represented by millimeter-scale veinlets (< 4 mm) consisting of calcite-quartz ± chalcopyrite(IV)-pyrite(II), which overprints previous zones of alteration and crosscuts all host rocks (**Fig. 9I**). These calcite-quartz veins are commonly brecciated (**Fig. 9J**) and evidencing open-space filling textures. In pervasive carbonate-altered domains, calcite usually replaces both igneous and hydrothermal feldspar crystals, Ca-amphiboles and also tourmaline.

Fluid inclusions

Petrography and inclusion types

Fluid inclusions studies were performed in two apatite crystals from the main sulfide ore. The investigated apatite grains are semi-rounded, up to 800 µm in length, slightly to moderately fractured and display a poikilitic texture mainly characterized by smaller chalcopyrite inclusions. Two types of fluid inclusions were recognized in the selected samples, based on phases present at room temperature: (i) multiphase, saline-aqueous inclusions (Type 1) and; (ii) aqueous two-phase inclusions (Type 2). Both types of inclusions display sizes rarely larger than 10 µm and may be faceted, rounded or irregularly shaped. They are usually randomly distributed within the apatite crystals (**Fig. 10A**), although thin intragranular planar arrays containing exceptionally smaller fluid inclusions were locally distinguished (**Fig. 10B**).

Type 1 inclusions contain a liquid phase (L_{H_2O}), one or multiple solid phases (S) and a vapor bubble (V_{H_2O}), which together may correspond to more than 50% of the inclusion volume. Among the solids, opaque phases are by far the most abundant (**Fig. 10C**), followed by rectangular to irregularly shaped translucent solids (**Figs. 10D-E**) and possibly hematite grains, given their reddish colour (**Fig. 10F**). Type 2 inclusions are dominant (> 80% vol.) among inclusion types, being characterized by a liquid phase (L_{H_2O}) and a vapor bubble (V_{H_2O}) that usually accounts for 10 to 20% of the inclusion volume (**Fig. 10G**).

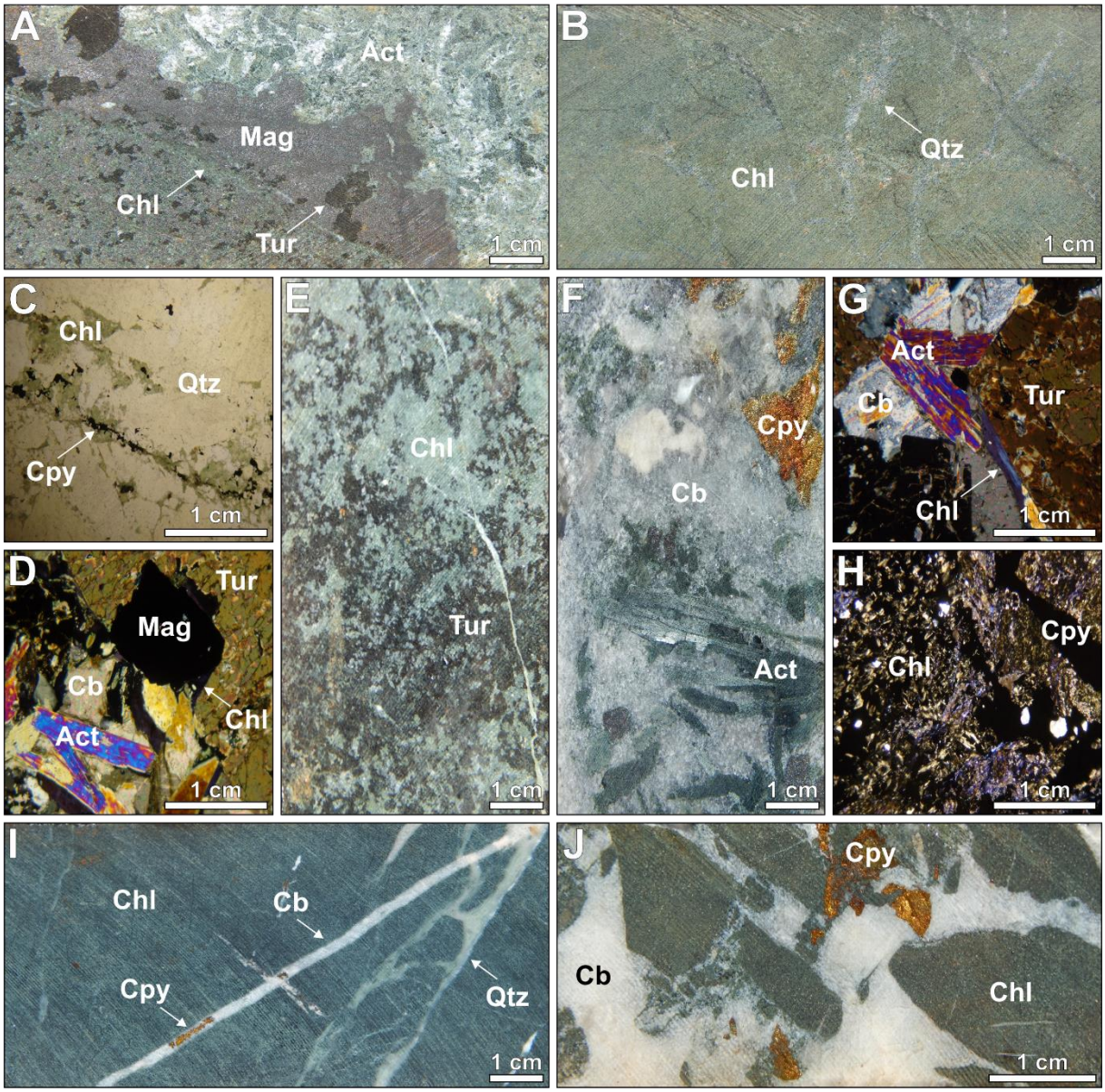

Figure 9. *Photomicrographs and drill core pictures showing the main features of the chlorite alteration and late carbonate veining. (A) Chlorite-magnetite-tourmaline-actinolite association in pervasively chlorite-altered zone. (B) Mafic metavolcanic rock strongly altered to chlorite-quartz. (C) Chlorite-chalcopyrite veinlet crosscutting dacitic rock. (D) Idioblastic magnetite crystal associated with tourmaline, actinolite, chlorite and carbonate. (E) Tourmaline-rich domain in chlorite-altered rock. (F) Carbonate vein containing coarse-grained prismatic actinolite crystals and associated chalcopyrite. (G) Actinolite crystals in association with chlorite and tourmaline, partially replaced by carbonate. (H) Mg- and Fe-rich chlorites in mineralized zone with chalcopyrite. (I) Carbonate-quartz-chalcopyrite veinlets crosscutting mafic rock. (J) Brecciation associated with late carbonate-chalcopyrite veining. Mineral abbreviations: Chl chlorite; Tur tourmaline; Mag magnetite; Act actinolite; Qtz quartz; Cpy chalcopyrite; Cb carbonate.*

Microthermometic Results

The results of microthermometric measurements are listed in **Table 1**. Data have only been recorded from Type 2 fluid inclusions, once the observation of phase change temperatures for Type 1 inclusions was precluded due to their small size and poor visibility. During low-temperature runs, most of the investigated aqueous inclusions froze completely at temperatures between -65 to -85°C, displaying either granular or clear appearances. Upon heating, first melting (Te) and ice melting temperatures (Tm_{ice}) were systematically registered. Due to the metastable behavior of hydrohalite, its melting temperature (Tm_{hh}) was not precisely recognized, and therefore discarded from the data.

The great majority of Te and Tm_{ice} values are respectively confined within the -75°C to -80°C and -25°C to -35°C ranges (**Figs. 11A-B**). These data suggest the presence of a complex mixture of metal chlorides, specially NaCl, $CaCl_2$ and LiCl (Crawford 1981; Roedder 1984), within the trapped fluids. The bulk salinity results for the aqueous two-phase inclusions were therefore estimated in terms of wt.% NaCl + $CaCl_2$ equivalent, revealing values ranging from 24 to 29 (**Fig. 11C**). Concentrations of NaCl (3.30 wt.% to 19.90 wt.%) and $CaCl_2$ (3.86 wt.% to 25.87 wt.%) were calculated following the method of Steele-MacInnis et al. (2011). It is important to point out that once the real hydrohalite melting temperatures were not considered in the salinity, NaCl and $CaCl_2$ calculations, Tm_{ice} was used as the utmost possible Tm_{hh} values (Tm_{ice} = Tm_{hh}). According to Chi and Ni (2007), this approximation is valid and provides a maximum error in salinity estimation inferior to 2 wt%, which is insignificant to most geological issues.

Total homogenization temperatures (Th_{LV-L}) for Type 2 fluid inclusions span from 113.2°C to 293 °C, with most of the values confined within the 120°C - 200° C interval (**Fig. 11D**). Homogenization, in this case, invariably occurs via disappearance of the vapor phase.

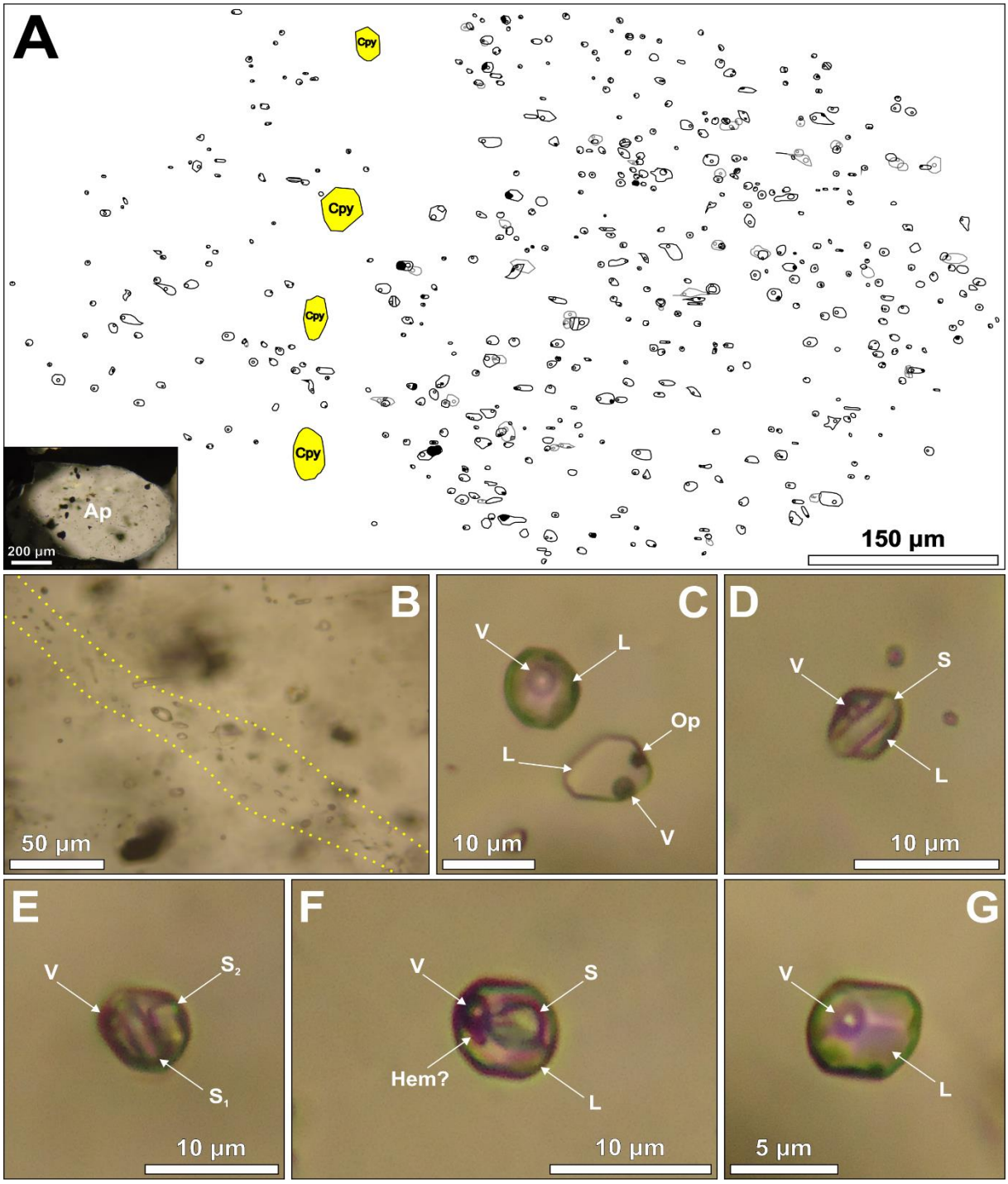

Figure 10. *Schematic representation and photomicrographs of modes of occurrence and types of fluid inclusions in apatite. (A) Overview distribution of fluid inclusions within apatite crystal. (B) Intragranular planar array containing extremely small (< 2µm) fluid inclusions. (C) Coexistence of Type 1 ($LH_2O + VH_2O + S$) and Type 2 ($LH_2O + VH_2O$) fluid inclusions, the former bearing an opaque phase. (D) and (E) Multiphase Type 1 fluid inclusions, respectively displaying one and two daughter crystals (S). (F) Multiphase Type 1 fluid inclusion, containing an irregularly shaped solid phase and a hematite(?) crystal. (G) Euhedral Type 2 fluid inclusion.*

Table 1 *Microthermometric data for Type 2 fluid inclusions of the Grota Funda deposit*

N°	Te (°C)	Tm_{ice} (°C)	Th_{LV-L} (°C)	Salinity (wt.% NaCl + $CaCl_2$ equiv.)[a]	NaCl (wt.%)[a]	$CaCl_2$ (wt.%)[a]
1	-79.6	-27.3	142.5	25	10.78	14.62
2	-81.8	-28.8	122.9	26	9.08	16.79
3	-76.9	-22.9	197	24	18.65	5.29
4	-79.1	-34	182.6	27	5.30	22.08
5	-76.1	-36.9	185.9	28	4.09	24.08
6	-86.5	-31.3	146.5	27	6.94	19.68
7	-92.7	-30.1	163.5	26	7.87	18.39
8	-78.9	-28.6	205.2	26	9.28	16.52
9	-75	-32.5	186.2	27	6.14	20.82
10	-78.9	-32.3	173.3	27	6.26	20.64
11	-81.1	-30.5	184.9	26	7.54	18.83
12	-81.3	-26	212	25	12.59	12.39
13	-79.1	-33	188.3	27	5.84	21.26
14	-79.6	-31	148.4	27	7.16	19.37
15	-79.8	-29.8	157.4	26	8.13	18.04
16	-84.4	-39.6	113.2	29	3.30	25.54
17	-95.7	-39.1	144.2	29	3.43	25.29
18	-81.8	-35.1	148.9	28	4.79	22.90
19	-76.6	-28.7	140.7	26	9.18	16.65
20	-75.4	-33.9	134.2	27	5.36	22.00
21	-77.3	-22.4	293	24	19.90	3.86
22	-71	-31.5	-	27	6.79	19.88
23	-74.5	-33.8	137.9	27	5.41	21.92
24	-78.8	-30.6	177.1	26	7.46	18.94
25	-74	-27.1	-	25	11.04	14.30
26	-77.7	-28	-	26	9.94	15.68
27	-80.4	-28.5	140.2	26	9.39	16.38
28	-79.5	-23.5	171.1	24	17.26	6.90
29	-78.8	-24.1	178.7	24	15.98	8.38
30	-78.1	-33.6	142.6	27	5.51	21.76
31	-89.8	-40.3	137.6	29	3.14	25.87
32	-83.8	-34.7	-	28	4.97	22.61
33	-77.7	-23.5	145.1	24	17.26	6.90
34	-83.9	-29.2	147.4	26	8.68	17.30
35	-75.8	-23.8	149.8	24	16.60	7.65
36	-74	-23.5	149.7	24	17.26	6.90
37	-93	-38.8	-	29	3.50	25.14
38	-77.2	-35.6	153.9	28	4.58	23.24
39	-94.6	-37.4	137.2	28	3.92	24.37

Samples: 1081A/B – GRFUN_FD037/339.70 m; Te – First melting or eutectic melting; Tm_{ice} – ice melting; Th_{LV-L} – homogenization to liquid

[a] *Estimated following the method of Steele-MacInnis et al. (2011).*

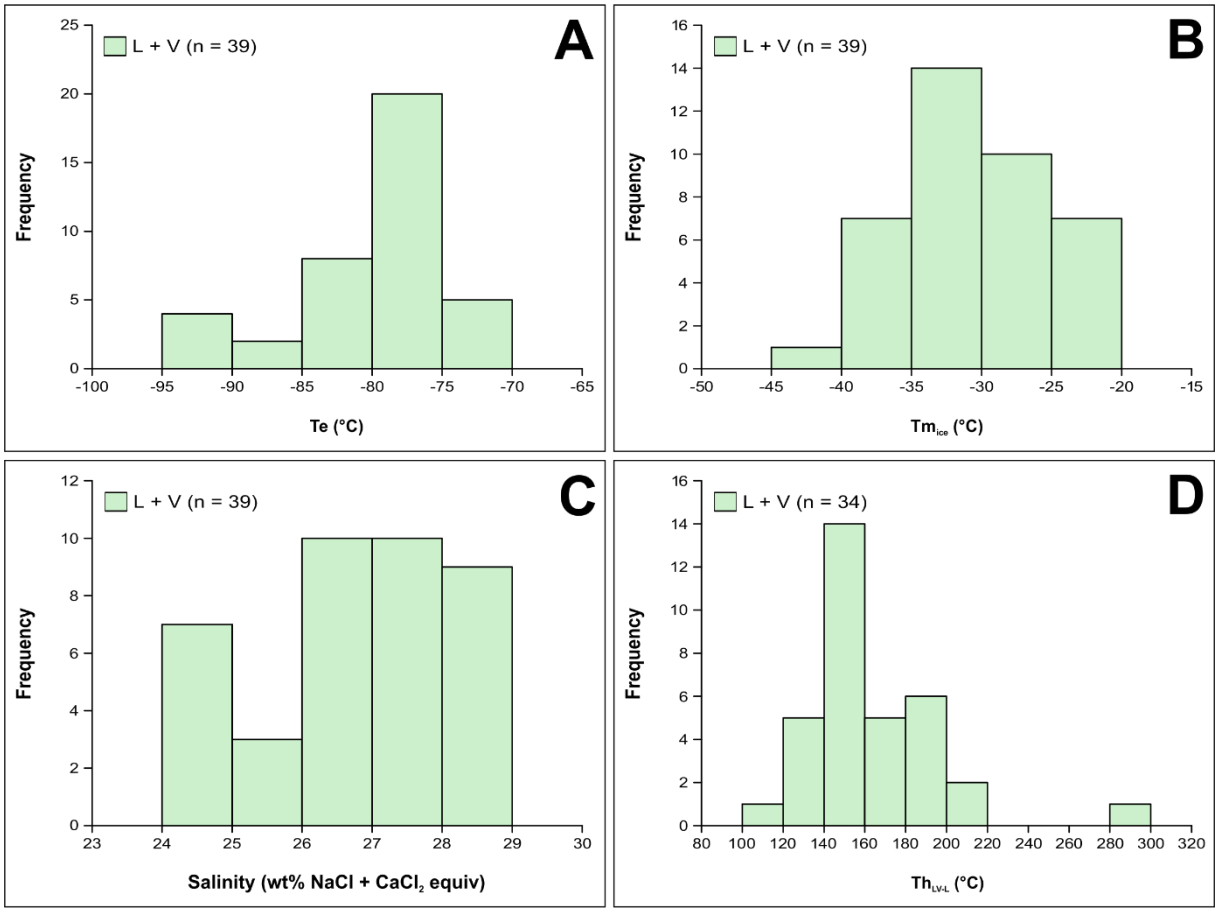

Figure 11. *Microthermometric data obtained from Type 2 ($LH_2O + VH_2O$) fluid inclusions in apatite crystals. (A) First melting temperatures (Te). (B) Ice melting temperatures (Tm_{ice}). (C) Salinities (in wt% NaCl + $CaCl_2$ equiv.) estimated considering $Tm_{ice} = Tm_{hh}$ and following the method of Steele-MacInnis et al. (2011). (D) Total homogenization temperatures (Th_{LV-L}).*

Evidences of metastability among Type 2 fluid inclusions were commonly observed during microthermometric runs. The most noticeable indications of this metastable behavior include several inclusions that have not undergone freezing during supercooling (temperatures below -190°C) and fluid inclusions that could be either single-phase (L_{H_2O}) or two-phase ($L_{H_2O} + V_{H_2O}$) at room temperature (Roedder 1971).

Boron isotopic compositions

Two tourmaline (II) samples from the chlorite alteration zone were selected for B-isotope analyses (**Fig. 12A**). Both crystals displayed no internal zonation in backscattered images (**Figs. 12B-C**). The total range in $\delta^{11}B$ compositions varies between +8.2 and +13.6‰ (**Table 2**), with an average value of +10.46‰ (n = 15). Within a single crystal, no significant isotopic variation was observed (+8.2 to + 11.2‰, n = 9; and +9.6 to 13.6‰, n = 6).

Table 2 *Boron isotopic compositions of tourmalines from the Grota Funda deposit*

Sample	$^{11}B/^{10}B$	Error	$\delta^{11}B$ (‰)[a]	2σ (‰)
GRFUN/1093A-1	4.639	0.00023	13.6	0.05
GRFUN/1093A-2	4.624	0.00022	10.3	0.05
GRFUN/1093A-3	4.626	0.00021	10.8	0.05
GRFUN/1093A-4	4.622	0.00020	10.0	0.04
GRFUN/1093A-5	4.627	0.00020	11.2	0.04
GRFUN/1093A-6	4.620	0.00022	9.6	0.05
GRFUN/1093B-7	4.622	0.00022	10.3	0.05
GRFUN/1093B-8	4.622	0.00021	10.3	0.05
GRFUN/1093B-9	4.620	0.00021	9.7	0.04
GRFUN/1093B-10	4.622	0.00021	10.3	0.05
GRFUN/1093B-11	4.626	0.00020	11.1	0.04
GRFUN/1093B-12	4.623	0.00022	10.8	0.05
GRFUN/1093B-13	4.625	0.00023	11.2	0.05
GRFUN/1093B-14	4.611	0.00024	8.2	0.05
GRFUN/1093B-15	4.617	0.00021	9.4	0.04

1093 – FD029/355.90 m

[a] *Calculated using the International Tourmaline Standard – IAEA B4 ($^{11}B/^{10}B$ = 4.536 and $\delta^{11}B$ = - 8.71‰) as reference.*

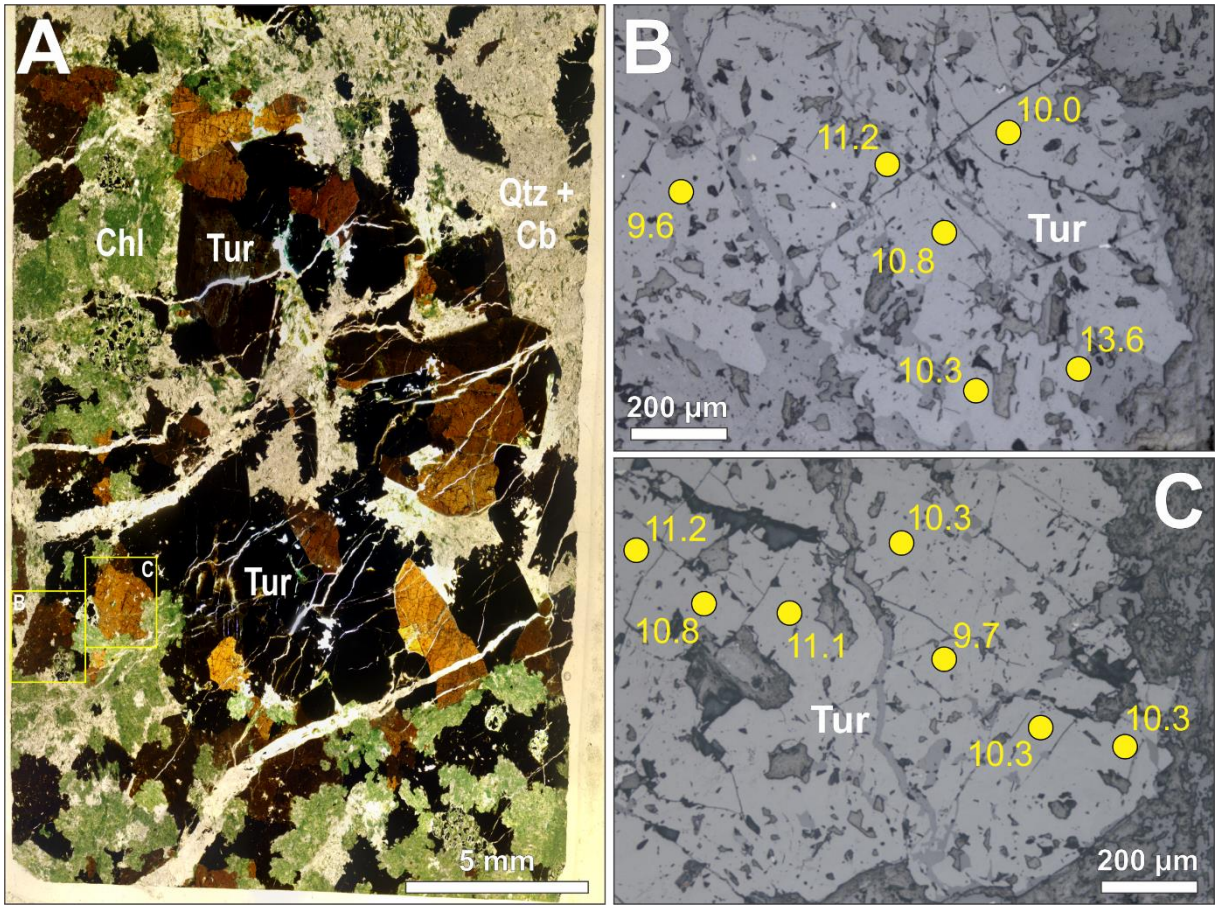

Figure 12. *(A) Thin section overview of the chlorite-tourmaline alteration zone, crosscutted by quartz-carbonate veinlets. In detail, the selected tourmaline crystals for B-isotope analyses. (B) and (C) Backscattered images of the analyzed tourmaline (II) crystals, showing the LA-MC-ICPMS spots and their respective* $\delta^{11}B$ *values. Mineral abbreviations: Cb carbonate; Chl chlorite; Qtz quartz; Tur tourmaline.*

Molybdenite Re-Os dating

Molybdenite from the grunerite-magnetite veins (**Fig. 6B**) has Re abundance of 89.11 ppm (σ = ± 0.55), 55.78 ppm of ^{187}Re (σ = ± 0.35), radiogenic ^{187}Os concentration of 2.40 ppm (σ = ± 0.05), and 2.05 ppb of total common Os (σ = ± 0.25). The ELAN DRC-e ICP-MS analyses conducted in this study yielded a Re–Os model age of 2,530 ± 60 Ma.

DISCUSSIONS

Evolution of the hydrothermal system

The evolution of the Grota Funda hydrothermal system is marked by multiple episodes of hydrothermal alteration and copper (-gold) mineralization. Early sodic-calcic alteration characterizes the initial stage of hydrothermal activity in the deposit, followed by intense Fe-metasomatism, potassic alteration with biotite, chlorite-quartz-tourmaline formation, and late carbonate-quartz veining. Paragenetic associations at Grota Funda are presented in **Fig. 13**.

Sodic-calcic alteration assemblages are extremely common in IOCG systems worldwide and from Carajás, especially in those evolved in deeper crustal levels (Hitzman et al. 1992; Pollard 2001; Monteiro et al. 2007; Melo et al. 2016). At Grota Funda this alteration is marked by the precipitation of hydrothermal albite, with subsequent hastingsite and marialitic scapolite formation, at temperatures probably above 500°C (Oliver et al. 1993; Perring et al. 1999). This is corroborated by geothermometry studies in hornblende and almandine crystals at the Gameleira deposit, which have evidenced an average equilibrium temperature of 540 ± 25°C for the sodic-calcic assemblage (Lindenmayer et al. 2001). Moreover, the presence of marialite in Na-Ca alteration zones evidences that these high temperature fluids also contained high chlorine contents (Vanko and Bishop 1982), which may have enhanced the transport of iron, copper, and gold as chloride complexes in the initial stages of hydrothermal activity at Grota Funda (Williams-Jones et al. 2009; Pokrovski et al. 2013, 2014).

The first stage of copper-gold mineralization (Mineralization I; **Fig. 13**) recognized in the Grota Funda deposit is coeval with intense Fe-metasomatism, which is mainly characterized by massive precipitation of magnetite (I) ± grunerite-almandine-chalcopyrite. In IOCG deposits, these magnetite-rich alteration assemblages typically form from an oxidized fluid at temperatures over 400°C (Skirrow and Walshe 2002; Bastrakov et al. 2007; Rusk et al. 2010; Somarin and Mumin 2014). The transition between Na-Ca alteration and Fe-metasomatism suggests that precipitation of chalcopyrite and gold was possibly facilitated by a decrease in temperature and Cl^- activity, the latter due to early destabilization of scapolite, besides an increase in fO_2 evidenced by the precipitation of magnetite.

Potassic alteration with biotite is well developed at Grota Funda, and its occurrence indicates high K^+ activity in the hydrothermal fluids. In the deposit, potassically-altered zones are commonly associated with mylonitized domains, suggesting that they could have been formed during shearing. Therefore, fluid circulation was structurally-controlled within strongly sheared zones (e.g. Pojuca fault system?) that promoted pervasive fluid–rock interaction. This alteration stage is also accompanied by massive quartz precipitation, which may have been controlled by mixing of high- and low-salinity solutions, once silica solubility tends to decrease with decreasing salinity, temperature and pH (Fournier 1983; Rimstidt 1997). In addition, early destabilization of scapolite may have been promoted by influx of external diluted fluids, favoring subsequent quartz formation.

Similarly to what is observed at Gameleira, two types of biotite were recognized in the Grota Funda deposit: (i) tabular fine- to medium-grained brownish crystals in pervasively-altered zones, and; (ii) fine-grained green biotite flakes, directly associated with mineralized zones (Mineralization II). According to Lindenmayer et al. (2001), the first type represents a Ti-bearing biotite in the Gameleira deposit, whereas the second is F-enriched.

The main sulfide ore (Mineralization II; **Fig. 13**) is represented by mineralized breccia bodies spatially and temporally associated with potassically-altered zones, and mainly characterized by a chalcopyrite(II)-magnetite(II)-pyrrhotite-sphalerite association. This ore assemblage clearly formed under lower fO_2 conditions than the mineralization associated with Fe-metasomatized domains (Mineralization I), although at similar fS_2 (**Fig. 14**). However, the replacement of chalcopyrite by bornite, which is expected at temperatures below 355°C (Amcoff 1988), and the late crystallization of pyrite, are evidences of fluid evolution towards higher fS_2 conditions (**Fig. 14**).

A distinct chlorite alteration assemblage, represented by chlorite ± quartz-tourmaline(II)-magnetite(III)-actinolite-carbonate, overprints previous hydrothermally altered zones. Experimental data indicate that the incipient replacement of biotite by chlorite, observed in this study, requires hydrothermal fluids with relatively low pH (Beane 1994). This is further corroborated by the replacement of tourmaline (II), which is only stable under pH ≥ 6.5 (London et al. 1996), by carbonate in the late stages of hydrothermal activity at Grota Funda. However, the presence of magnetite, instead of hematite, in association with chlorite suggests that the hydrothermal fluids remained under relatively low fO_2 conditions. Considerable temperature decrease probably represented the main mechanism that triggered chalcopyrite precipitation in mineralized zones spatially associated with the chlorite alteration (Liu and McPhail 2005).

The last stage of hydrothermal alteration observed at Grota Funda is characterized by widespread carbonate veining. These veins are mainly constituted of calcite ± quartz-chalcopyrite-pyrite, and were probably generated in a brittle structural regime. According to Lindenmayer et al. (2001), similar veins recognized in the Gameleira area were formed from an acidic fluid at temperatures around 190 ± 10°C.

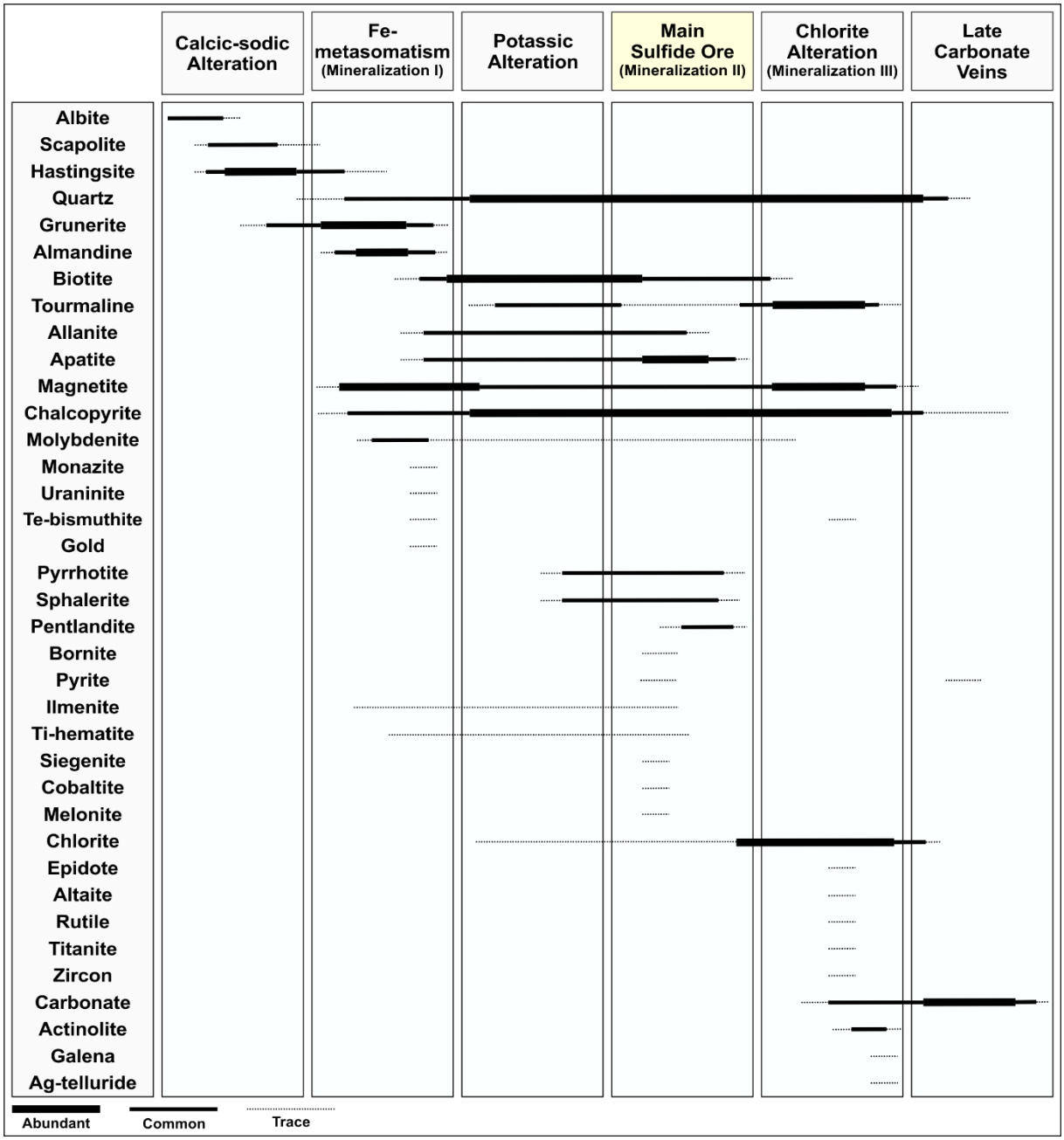

Figure 13. Paragenetic sequence of the Grota Funda hydrothermal system.

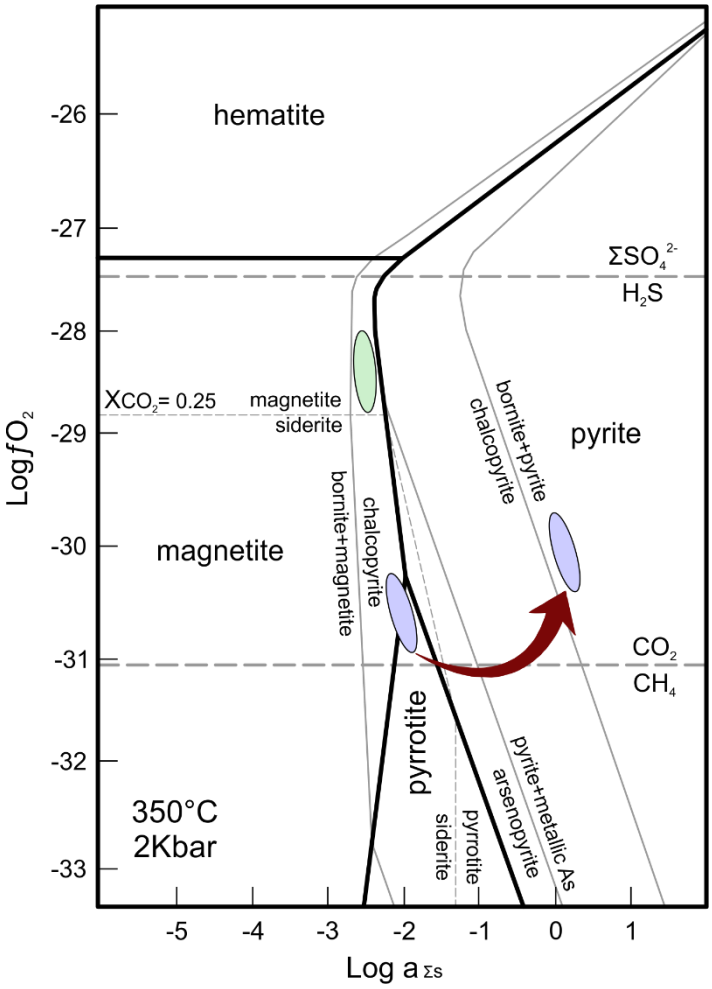

Figure 14. Log fO_2 vs. log $a_{\Sigma s}$ diagram from 350°C and 2 Kbar. Patterned areas represent estimated fO_2 and $a_{\Sigma s}$ conditions for the mineralization associated with Fe-metasomatized zones (light green; Mineralization I) and the main sulfide ore (light blue; Mineralization II). Red arrow indicates the change in $a_{\Sigma s}$ conditions due to the replacement of chalcopyrite by bornite and the late crystallization of pyrite in the main sulfide ore. Stability boundaries for Fe-sulphide and Fe-oxide phases are shown as heavy solid lines. Light solid lines and dashed lines show reaction boundaries for Cu- and As-bearing phases, and carbonate phases (at X_{CO_2} = 0.25), respectively. Heavy dashed lines represent important aqueous redox buffers (modified from Mikucki and Ridley 1993).

The paragenetic evolution of the Grota Funda deposit reflects important changes in the physical-chemical conditions of the hydrothermal fluids. This is mainly illustrated by temperature conditions dropping from 540°C (Na-Ca alteration) to below 200°C (late carbonate veins), accompanied by a decrease in salinity and pH. In this scenario, early and high temperature alteration assemblages (albite, scapolite-hastingsite) were possibly formed

due to circulation of metalliferous and hypersaline fluids, whereas the onset of ore precipitation was probably related to fluid mixing processes, with the participation of relatively dilute (moderate salinity) and cooler fluids. A similar evolutionary trend has been proposed for several IOCG deposits situated in both northern and southern sectors of the Carajás Domain, including Gameleira, Sossego, Igarapé-Bahia, Alvo 118, Bacuri, Salobo, and others (Lindenmayer et al. 2001; Monteiro et al. 2007; Dreher et al. 2008; Torresi et al. 2012; Melo et al. 2014, 2016).

Additionally, the Grota Funda deposit shares other similarities with the IOCG systems characterized in the Carajás Province. Early sodic-calcic alteration succeed by high-temperature iron-enriched assemblages (e.g. grunerite-almandine-magnetite) seems to be an ubiquitous feature presented by IOCG deposits situated in the north portion of the Carajás Domain, as demonstrated at Salobo (Melo et al. 2016), Igarapé-Bahia (Tallarico et al. 2005), Gameleira (Lindenmayer et al. 2001) and Igarapé-Cinzento/GT46 (Silva et al. 2005). In contrast, the predominance of potassic and chlorite alteration zones seems to be characteristic of shallow-emplaced deposits, such as Sossego (Monteiro et al. 2007) and Alvo 118 (Torresi et al. 2012).

Comparatively, both Grota Funda and Gameleira deposits seems to have registered the same types and chronological order of hydrothermal alteration stages. Except for some local-scale particularities, it appears that they share a similar evolutionary history during the Neoarchean (2.5 – 2.6 Ga) with multiple pulses of epigenetic mineralizing events. On the other hand, although situated within the same regional discontinuity these deposits clearly undergone a distinct genetic process than the Pojuca deposit, currently interpreted as a syngenetic ca. 2.7 Ga VMS-type Cu-Zn system.

Fluid evolution and ore genesis

The fluid inclusions analyses conducted on ore-related apatite have revealed that the main sulfide ore zone of the Grota Funda deposit possibly developed from the interaction between highly saline fluids, defined by Type 1 multiphase, saline-aqueous inclusions, and moderate to high salinity (24 to 29 wt.% NaCl + $CaCl_2$ equiv.), low-temperature (113.2°C to 212°C), Ca-Na-rich, CO_2-free aqueous fluids, represented by Type 2 inclusions. These data seem to be in accordance with what is observed in other IOCG systems of the Carajás Domain. According to Xavier et al. (2012), the involvement of highly saline (35−70 wt% NaCl equiv.) and hot (> 500°C) metalliferous brines in the ore forming processes represents a striking feature of these systems, as illustrated at Salobo (Réquia et al. 1995), Igarapé-Bahia

(Dreher et al. 2008), Sossego (Carvalho 2009), Alvo 118 (Torresi et al. 2012), and others. The origin of these metalliferous brines, however, has been a great matter of debate. A magmatic-hydrothermal affiliation with Archean granites has been proposed by several authors (Tallarico et al. 2005; Grainger et al. 2008). In contrast, independent evidence from chlorine and boron isotopes, combined with Cl/Br-Na/Cl systematics, indicate a major contribution from evaporative brines as a source of high salinity in IOCG deposits of the Carajás Province (Chiaradia et al. 2006; Xavier et al. 2008, 2009). Notwithstanding the participation of lower temperature (< 250°C) aqueous fluids of low to intermediate salinity, with or without interaction of aqueous-carbonic ($CO_2 \pm CH_4$; Réquia and Fontboté 2001; Dreher 2004) fluids, seems to predominate in the mineralization stages of most of the Carajás IOCG deposits (Xavier et al. 2012).

The fluid inclusion assemblages at Grota Funda strongly suggest that a fluid mixing process could have represented the main mechanism controlling ore formation. Even though no microthermometric data for Type 1 fluid inclusions was recorded, it is assumed that they could represent the initial highly saline hydrothermal fluids responsible for the formation of widespread Na-Ca alteration in the deposit, and for the transport of Cu(-Au) as chloride complexes during the evolution of the Grota Funda hydrothermal system. The interaction of this metalliferous brine with a lower temperature and relatively diluted fluid (Type 2 fluid inclusions), during the potassic alteration event, may have induced temperature and salinity decrease and, therefore, the ore precipitation.

Sources of boron at Grota Funda

The Grota Funda deposit is mainly hosted by mafic metavolcanic rocks. According to Smith et al. (1995), the average boron content of the mafic oceanic crust is considerably low (5.2 ± 1.5 ppm), with $\delta^{11}B$ values ranging at +3.4 ± 1.1‰. The analyzed tourmaline (II) samples in this study have demonstrated overall B-isotopic compositions between +8.2 and +13.6‰. These data suggest that the Grota Funda host rocks hardly represent the main sources of boron in the deposit. Moreover, the locally high abundance of tourmaline in strongly chloritized zones (up to 70 vol.%) indicate that boron must have been introduced by an externally-derived fluid. Hence, the isotopic composition of tourmaline (II) would be probably dominated by that of the hydrothermal fluid (Pal et al. 2010).

Based on the isotopic composition of potential boron reservoirs (**Fig. 15**; Barth 1993; Marschall and Jiang 2011), the fairly homogeneous positive $\delta^{11}B$ values presented here are compatible with a variety of crustal sources, including metamorphic rocks, marine

carbonates and submarine brines. Consequently, significant influence of magmatic fluids, which represent an isotopically light boron source, is unlikely to have occurred. This is also evidenced by the fact that the $\delta^{11}B$ values of the hydrothermal fluids, in equilibrium with tourmaline, were probably higher than those obtained for tourmaline (II) samples, due to temperature-dependent fractionation effects (Palmer et al. 1992; Meyer et al. 2008; Marschall et al. 2009b). The presence of actinolite in association with chlorite and tourmaline (II), observed in chlorite-altered zones of the Grota Funda deposit, suggests a temperature of formation around 300°C (Browne 1978), which according to the fractionation equation proposed by Meyer et al. (2008) ($\Delta^{11}B_{(Tour\text{-}Fluid)}$ = -4.20 x [1,000/T (K)] + 3.52), predicts a fluid that is approximately 4‰ heavier than tourmaline (II). Hence, the B-isotopic composition of tourmaline (II) obtained in this study would correspond to a fluid with $\delta^{11}B$ values spanning from ~ +12‰ to +18‰. However, it is important to point out that the fractionation of ^{10}B and ^{11}B between tourmaline and the hydrothermal fluid has not yet been calibrated at temperatures below 400°C, and therefore can only be estimated (Meyer et al. 2008; Marschall et al. 2009b).

Marine evaporites were firstly interpreted as the main sources of boron in IOCG systems from the Carajás Province (Xavier et al. 2008). Studies on the Salobo and Igarapé-Bahia deposits have evidenced extremely heavy (> 24‰) boron isotopic compositions of tourmaline (**Fig. 15**), which were interpreted to reflect the initial hydrothermal ore fluid that interacted with marine evaporites. Variations toward lower $\delta^{11}B$ (< 10‰) values, observed in tourmalines from the Acampamento Norte (ACPN) orebody of the Igarapé-Bahia deposit, were then attributed to mixing with fluids containing lighter boron (e.g. magmatic) or a mixed boron source (Xavier et al. 2008). Significantly variable and lower (-8‰ to 11‰) $\delta^{11}B$ values were also obtained for tourmaline from the Sossego deposit, and likewise associated with mixed sources, including isotopically light boron from granitic magmas and heavy boron from marine evaporites (Xavier et al. 2008).

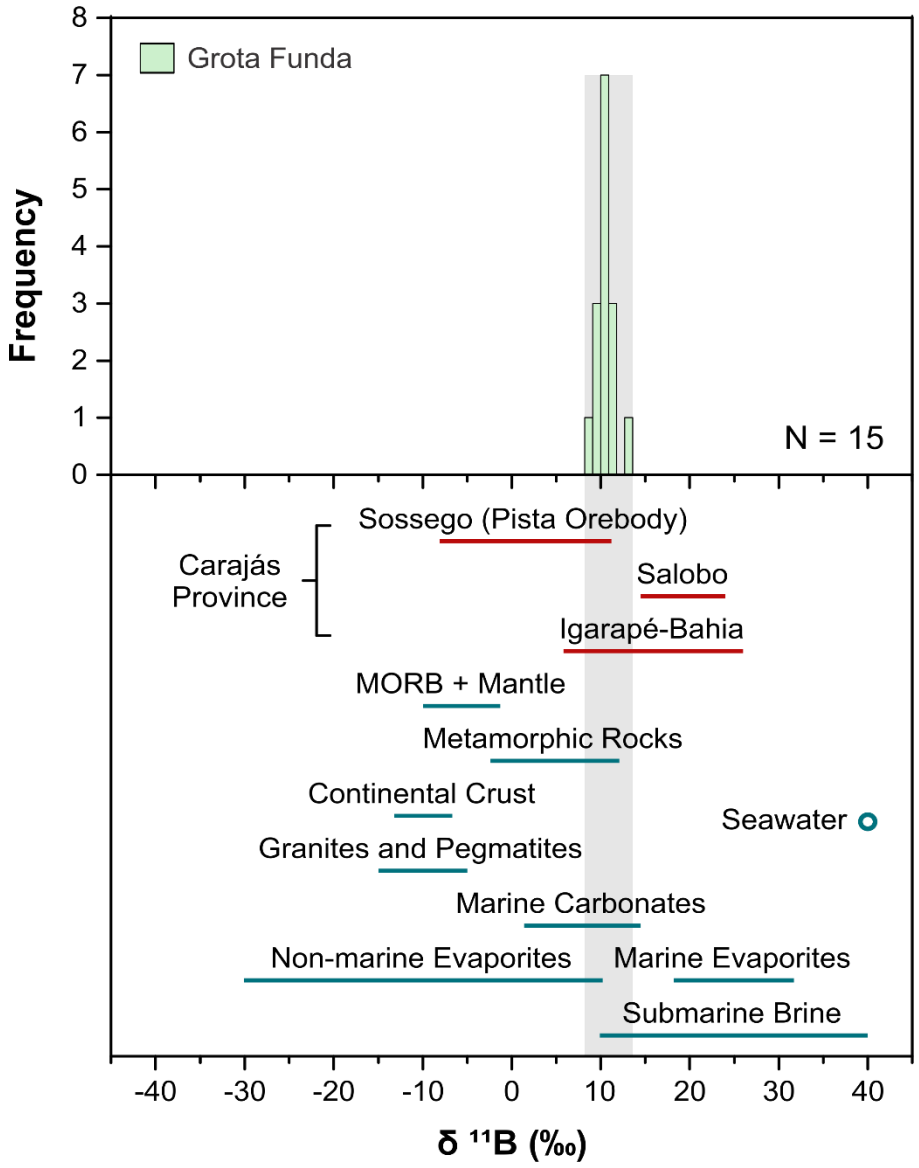

Figure 15. *Histogram of tourmaline boron isotope compositions from the Grota Funda deposit. Ranges of* $\delta^{11}B$ *values for several boron reservoirs in nature (Barth 1993; Marschall and Jiang 2011) and for previously studied IOCG systems from the Carajás Province (Xavier et al. 2008) are shown for reference.*

The participation of non-magmatic ore fluids in the evolution of IOCG deposits from the Carajás Province have also been corroborated by chlorine isotopes data and halogen ratios (e.g. Cl/Br-Na/Cl) in fluid inclusions (Chiaradia et al. 2006; Xavier et al. 2009). According to Chiaradia et al. (2006), the high molar Cl/Br (≥ 4,000) ratios and the near 0‰ $\delta^{37}Cl$ values presented by the ore fluids at Gameleira are indicative of a prevailing evaporitic Cl contribution in the deposit, with a probable participation of magmatic fluids, as supported by other supplementary stable isotopes data (S, O and C). In contrast, isotopic data from the Sossego deposit indicate a mixed origin with participation of mantle-derived magmatic fluids

and basinal brines (Chiaradia et al. 2006). However, the low Cl/Br ratios presented by fluid inclusions of the Igarapé-Bahia and Alvo 118 deposits rule out the dissolution of evaporites as the source of salinity for the Carajás IOCG fluids (Xavier et al. 2009), as initially suggested by boron isotope data (Xavier et al. 2008). Instead, the Cl/Br and Na/Cl data indicate that these fluids may have been derived from seawater evaporation (e.g. bittern fluids), which may have mixed with magma-derived brines (Xavier et al. 2009, 2012, 2013).

In summary, the boron isotopic compositions of tourmaline, when combined with the Cl/Br-Na/Cl ratios in inclusion fluids, point to an important involvement of non-magmatic fluids (e.g., bittern-type basinal fluids) in the ore-forming process of several IOCG deposits of the Carajás Domain (Xavier et al. 2008, 2013). The Grota Funda deposit seems to follow the same trend by sharing a similar boron isotopic signature with other IOCG deposits of the Carajás Domain, especially when compared with the Igarapé-Bahia/Alemão deposit. Therefore, the positive $\delta^{11}B$ values presented by tourmaline of the Grota Funda deposit are likewise attributed to mixed sources, including isotopically heavier boron sourced fluids, possibly represented by highly saline brines (e.g., evolved seawater, formation water or bittern fluids) and light boron leached from the host rocks (e.g mafic metavolcanic rocks).

Timing of IOCG mineralization

Molybdenite from the grunerite-magnetite veins yielded a Re-Os model age of 2,530 ± 60 Ma (σ). According to field and petrographic observations, these veins are correlated with the Fe-enrichment event defined in the early stages of hydrothermal alteration of the Grota Funda deposit. Thus, the intrinsic relation between iron-enriched domains and mineralized zones strongly suggests that the first event of Cu-Au mineralization recognized at Grota Funda took place in the Neoarchean. However, the significance of this mineralizing event, and its implications on the current metallogenic models for the formation of IOCG systems in the Carajás Domain, especially those situated in the northern sector, need to be interpreted with caution.

Moreto et al. (2015a, b) have demonstrated that the IOCG systems in the Southern Copper Belt (Sossego, Cristalino, Alvo 118, Bacaba, Castanha, Visconde, Bacuri and Jatobá deposits) are the result of multiple episodes of hydrothermal activity spanning the Neoarchean (ca. 2.71 – 2.68 Ga) to the Paleoproterozoic (2.0 – 1.88 Ga). In contrast, the currently available geochronological data for the northern sector of the Carajás Domain (**Table 3**) point to an important metallogenic event at ca. 2.57 Ga, which, notably, has not been recorded yet in the southern sector. Evidences that support this event include the mineralization ages obtained for

the Salobo (2,576 ± 8 Ma, Re-Os in molybdenite; Réquia et al., 2003) and Igarapé-Bahia (2,575 ± 12 Ma, U-Pb in monazite; Tallarico et al. 2005) deposits, which are contemporaneous with the emplacement of the Old Salobo (2,573 ± 2 Ma, U-Pb in zircon; Machado et al. 1991) and the Itacaiúnas (2,560 ± 37 Ma; Pb-Pb in zircon; Souza et al. 1996) granites. The obtained ca. 2.53 Ga age for the Cu-Au mineralization at Grota Funda overlaps within error the mineralization ages for the Salobo and Igarapé-Bahia deposits. Moreover, in the Igarapé-Cinzento/GT46 deposit, pegmatite intrusive bodies yielded Re-Os molybdenite ages of 2,554 ± 8 Ma and 2,557 ± 8 Ma (Silva et al. 2005), whereas ore-related molybdenite from the Gameleira deposit recorded an slightly older Re-Os age of 2,614 ± 14 Ma.

Collectively, this set of ages points to a temporal link between the ca. 2.5 Ga granitic magmatism and IOCG genesis in the northern sector of the Carajás Domain. According to Melo et al. (2016), however, the ca. 2.5 Ga age may reflect an important tectono-thermal event that could be related to the reactivation of the Carajás and Cinzento strike-slip fault systems at ca. 2.6 Ga (Pinheiro and Holdsworth 1997).

Noteworthy, Cu-bearing quartz-grunerite veins, and late sulfide-biotite veins from the Gameleira deposit yielded whole rock Sm-Nd isochron ages of 1,839 ± 15 Ma (MSWD = 0.83), and 1,700 ± 31 Ma (MSWD = 2.3), respectively, whereas brown biotite from the metavolcanic host rocks recorded a minimum ^{40}Ar-^{39}Ar age of 1,734 ± 8 Ma for the pervasive potassic alteration (Pimentel et al. 2003). According to Pimentel et al. (2003) these ages provide a strong evidence that the mineralizing fluids at Gameleira were possibly derived from, or intensively interacted with Paleoproterozoic (ca. 1.8 Ga) granites analogous to the Pojuca granite. A similar style of potassic alteration with biotite has been recognized in the Grota Funda deposit, suggesting that a regional-scale episode of hydrothermal activity could have affected both deposits. Consequently, it would be expected that biotite from the Grota Funda deposit would present Paleoproterozoic ages similar to those of Gameleira. In this scenario, the previously established Neoarchean (ca. 2.5 Ga) system would have been overprinted by a Paleoproterozoic hydrothermal event.

Table 3 *Geochronological data for regional units and IOCG deposits from the northern sector of the Carajás Domain, Carajás Province*

	Sample	Age (Ma)	Method	Reference
Regional Units				
	Migmatite (Xingu Complex)	2,859 ± 2	U-Pb in zircon	Machado et al. (1991)
	Migmatite (Xingu Complex)	3,066 ± 6.6	U-Pb in zircon	Delinardo da Silva (2014)
	Mafic granulites (Pium Complex)	3,002 ± 14	U-Pb in zircon	Pidgeon et al. (2000)
	Itacaiúnas granite	2,560 ± 37	Pb-Pb in zircon	Souza et al. (1996)
Northern IOCG deposits				
Igarapé-Cinzento/GT46				
	Gray granite	2,612 ± 2	U-Pb in monazite	Silva et al. (2005)
Host rocks	Pink and gray granites	2,668 ± 100	Sm-Nd (whole rock)	Silva et al. (2005)
	Basalts and gabbro	2,686 ± 87	Sm-Nd (whole rock)	Silva et al. (2005)
	Ore breccia and hydrothermal sample from the Salobo deposit	1,752 ± 77	Sm-Nd (whole rock)	Silva et al. (2005)
	Biotite (Potassic alteration)	1,858 ± 7	^{40}Ar-^{39}Ar in biotite	Silva et al. (2005)
Ore	Molybdenite from pegmatitic granite	2,554 ± 8	Re-Os in molybdenite	Silva et al. (2005)
	Molybdenite from pegmatitic granite	2,557 ± 8	Re-Os in molybdenite	Silva et al. (2005)
	Molybdenite from granite	2,600 ± 8	Re-Os in molybdenite	Silva et al. (2005)
	Molybdenite from amphibolite	2,711 ± 9	Re-Os in molybdenite	Silva et al. (2005)
Salobo				
	Magnetite-rich rock	2,551 ± 2	U-Pb in monazite	Machado et al. (1991)
	Old Salobo granite	2,573 ± 2	U-Pb in zircon	Machado et al. (1991)
	Granitic vein	2,758	U-Pb in zircon	Machado et al. (1991)
Host rocks	Foliated amphibolite (metamorphism)	2,761 ± 3	U-Pb in zircon	Machado et al. (1991)
	Rocks with post-ore alteration	2,950 ± 25	U-Pb in zircon	Melo et al. (2016)
	Cascata gneiss	2,763 ± 4.4	U-Pb in zircon	Melo et al. (2016)
	Old Salobo granite	2,547 ± 5.3	U-Pb in zircon	Melo et al. (2016)

Table 3 *(continued)*

	Sample	Age (Ma)	Method	Reference
Salobo				
Ore	Molybdenite	2,562 ± 8	Re-Os in molybdenite	Réquia et al. (2003)
	Molybdenite	2,576 ± 8	Re-Os in molybdenite	Réquia et al. (2003)
	Bornite–chalcopyrite leachates	2,579 ± 71	Pb-Pb (sulphides)	Réquia et al. (2003)
	Salobo ore	2,535 ± 8.4	U-Pb in zircon	Melo et al. (2016)
	Salobo ore	2,452 ± 14	U-Pb in monazite	Melo et al. (2016)
Igarapé-Bahia				
Host rocks	Mafic metavolcanic rock	2,758 ± 75	Sm-Nd (whole rock)	Galarza et al. (2003)
	Mafic metavolcanic rock	2,748 ± 34	U-Pb in zircon	Tallarico et al. (2005)
	Mafic metavolcanic rock	2,745 ± 1	Pb-Pb in zircon	Galarza et al. (2008)
Ore	Monazite from ore breccia	2,575 ± 12	U-Pb in monazite	Tallarico et al. (2005)
	Chalcopyrite (mafic metavolcanic rock)	2,756 ± 24	Pb-Pb in chalcopyrite	Galarza et al. (2008)
	Chalcopyrite (hydrothermal breccia)	2,772 ± 46	Pb-Pb in chalcopyrite	Galarza et al. (2008)
	Chalcopyrite (mafic intrusive rock)	2,777 ± 22	Pb-Pb in chalcopyrite	Galarza et al. (2008)
Gameleira				
Host rocks	Amphibolite (metamorphism)	2,732 ± 2	U-Pb in zircon	Machado et al. (1991)
	Quartz diorite	2,705 ± 2	Pb-Pb in zircon	Galarza & Macambira (2002)
	Meta-andesite[1]	2,719 ± 80	Sm-Nd (whole rock)	Pimentel et al. (2003)
	Metagabbro and cogenetic meta-andesite[1]	2,757 ± 81	Sm-Nd (whole rock)	Pimentel et al. (2003)
	Biotite (potassic alteration) from meta-andesite	1,734 ± 8	^{40}Ar-^{39}Ar in biotite	Pimentel et al. (2003)

[1] *Also interpreted as host rocks of the Pojuca deposit*

Table 3 *(continued)*

	Sample	Age (Ma)	Method	Reference
Gameleira				
Ore	Quartz–grunerite–gold vein	1,839 ± 15	Sm-Nd (whole rock)	Pimentel et al. (2003)
	Ore-related molybdenite	2,614 ± 14	Re-Os in molybdenite	Marschik et al. (2005)
Grota Funda				
Ore	Molybdenite from grunerite-magnetite veins	2,530 ± 60	Re-Os in molybdenite	This study
Pojuca[2]				
Host Rocks/Ore	Amphibolite separates	2,732 ± 2	U-Pb in zircon	Machado et al. (1991)

[2] *VMS-type Cu-Zn deposit*

However, the emplacement of the Paleoproterozoic Pojuca granite (1,874 ± 2 Ma, U-Pb in zircon; Machado et al. 1991) in the Pojuca-Gameleira-Grota Funda trend suggests that a diffusion-driven thermal reset, especially in the ^{40}Ar-^{39}Ar system, could have occurred. At temperatures over 300°C, for example, partial or total resetting of the ^{40}Ar-^{39}Ar isotopic system in biotite is expected due to significant thermally activated argon diffusion (Chiaradia et al. 2013). Assuming that biotite from pervasively potassically-altered zones of both Gameleira and Grota Funda deposits formed previously (e.g. Neoarchean?), the thermal effect caused by emplacement of the Pojuca granite could have reset the ^{40}Ar-^{39}Ar system. Therefore, the ages obtained through this method would not represent the timing of biotite crystallization itself, but instead would reflect the cooling history of the mineral after the granite emplacement.

CONCLUSIONS

The Grota Funda deposit, together with the Gameleira and Pojuca deposits, lies along a regional WNW-ESE-striking shear zone (Pojuca Fault System), in the northwestern portion of the Carajás Domain. In the deposit area, metavolcanic rocks attributed to the Igarapé-Pojuca Group represent the main hosts to the copper (-gold) mineralization.

The hydrothermal alteration sequence of the Grota Funda deposit encompasses: (i) an early sodic-calcic alteration, represented by albite, hastingsite and scapolite, followed by; (ii) intense Fe-metasomatism, with massive precipitation of magnetite, grunerite and almandine; (iii) potassic alteration with biotite, accompanied by quartz formation and spatially associated with the main sulfide ore zone; (iv) widespread chlorite alteration, with associated quartz, tourmaline, actinolite and carbonate; (v) late carbonate-quartz veining developed during brittle deformation. Copper (-gold) mineralizations have also been recognized associated with Fe-metasomatized and chlorite-altered zones. Molybdenite from grunerite-magnetite veins yielded a Re-Os model age of 2,530 ± 60 Ma, which is interpreted as a mineralization age coeval with the Fe-metasomatism.

The main sulfide ore occurs predominantly as breccia bodies, being subordinately recognized in veinlets, fracture infillings and as disseminations. Ore paragenesis includes primarily chalcopyrite, magnetite, pyrrhotite, pentlandite, sphalerite, with minor ilmenite, Ti-hematite, siegenite, cobaltite and melonite. The association chalcopyrite-magnetite-pyrrhotite-sphalerite indicates precipitation under low fS_2 and fO_2 conditions, whereas the replacement of chalcopyrite by bornite, and the late crystallization of pyrite, are evidences of fluid evolution towards higher fS_2 conditions.

The paragenetic evolution of the Grota Funda deposit points to significant changes in the physical-chemical conditions of the hydrothermal fluids, such as temperature decrease from 540°C (Na-Ca alteration) to below 200°C (late carbonate veins), accompanied by a decrease in salinity and pH. The early and high temperature alteration assemblages (albite, scapolite-hastingsite) may be intrinsically related to regional circulation of deep-seated hypersaline and hot metalliferous fluids, which transported metals as chloride complexes, whereas the onset of ore precipitation resulted from significant influx of relatively dilute (moderate salinity) and cooler fluids.

Overall, the fluid inclusion data for the Grota Funda deposit point to a trend in fluid evolution which apparently involved the interaction between highly saline hydrothermal fluids with cooler and relatively dilute fluids. This process may have induced temperature and

salinity decrease, and consequently, the precipitation of the main sulfide ore. Boron isotopic compositions of tourmaline from the chlorite alteration zone also provide strong evidence for a possible involvement of isotopically heavier boron sourced fluids, possibly represented by highly saline brines (e.g., evolved seawater, formation water or bittern fluids) and light boron leached from the host rocks (e.g mafic metavolcanic rocks).

REFERENCES

Almeida JAC, Dall'Agnol R, Dias SB, Althoff FJ (2010) Origin of the Archean leucogranodiorite-granite suites: Evidence from the Rio Maria terrane and implications for granite magmatism in the Archean. Lithos 120:235–257. doi: 10.1016/j.lithos.2010.07.026

Amcoff O (1988) Experimental replacement of chalcopyrite by bornite: Textural and chemical changes during a solid-state process. Mineralium Deposita 23:286–292. doi: 10.1007/BF00206409

Andao D, Hongliao H, Ningwan Y, et al (1995) A Study of the Rhenium-Osmium Geochronometry of Molybdenites. Acta Geologica Sinica 8:171–181.

Araújo OJB, Maia RGN, Jorge-João XS, Costa JBS (1988) A megaestruturação da folha Serra dos Carajás. In: VII Congresso Latino Americano de Geologia. Belém, pp 324–333

Avelar VG, Lafon JM, Correia Jr. FC, Macambira EMB (1999) O magmatismo arqueano da região de Tucumã - Província Mineral De Carajás: Novos resultados geocronológicos. Revista Brasileira de Geociências 29:453–460.

Barros CEM, Macambira MJB, Barbey P, Scheller T (2004) Dados isotópicos Pb-Pb em zircão (evaporação) e Sm-Nd do Complexo Granítico Estrela, Província Mineral de Carajás, Brasil: Implicações petrológicas e tectônicas. Revista Brasileira de Geociências 34:531–538.

Barros CEM, Sardinha AS, Macambira MJB, et al (2009) Structure, petrology, geochemistry and zircon U/Pb and Pb/Pb geochronology of the synkinematic archean (2.7 Ga) A-type granites from the Carajás Metallogenetic Province, northern Brazil. The Canadian Mineralogist 47:1423–1440. doi: 10.3749/canmin.47.6.1423

Barth S (1993) Boron isotope variations in nature: a synthesis. Geologische Rundschau 82:640–651. doi: 10.1007/BF00191491

Bastrakov EN, Skirrow RG, Davidson GJ (2007) Fluid evolution and origins of iron oxide Cu-Au prospects in the Olympic Dam district, Gawler Craton, South Australia. Economic Geology 102:1415–1440. doi: 10.2113/gsecongeo.102.8.1415

Beane RE (1994) A graphic view of hydrothermal mineral stability relations. In: Leintz DR (ed) Alteration and Alteration Processes associated with Ore-forming Systems, v. 11. Geological Association of Canada, Short Course Notes, pp 1–30

Browne PRL (1978) Hydrothermal alteration active geothermal fields. Annual Review of Earth and Planetary Science 6:229–250.

Carvalho ER (2009) Caracterização geológica e gênese das mineralizações de óxido de Fe-Cu-Au e metais associados na Província Mineral de Carajás: Estudo de caso do depósito de Sossego. University of Campinas

Carvalho JMA (2004) Distritos Mineiros do Estado do Pará. DNPM/CPRM, Belém

Chi GX, Ni P (2007) Equations for calculation of NaCl/(NaCl + CaCl2) rations and salinities from hydrohalite-melting and ice-melting temperatures in the H2O-NaCl-CaCl2 system. Acta Petrologica Sinica 23:33–37.

Chiaradia M, Banks D, Cliff R, et al (2006) Origin of fluids in iron oxide-copper-gold deposits: Constraints from δ37Cl, 87Sr/86Sr and Cl/Br. Mineralium Deposita 41:565–573. doi: 10.1007/s00126-006-0082-6

Chiaradia M, Schaltegger U, Spikings R, et al (2013) How Accurately Can We Date the Duration of Magmatic-Hydrothermal Events in Porphyry Systems? - An Invited Paper. Economic Geology 108:565–584.

Crawford ML (1981) Fluid inclusions in metamorphic rocks - low and medium grade. In: Hollister LS, Crawford ML (eds) Short Course in Fluid Inclusions: Application to Petrology. Mineralogical Association of Canada, Calgary, pp 157–181

CVRD/CMM (1972) Distrito ferrífero da Serra dos Carajás. In: XXVI Congresso Brasileiro de Geologia. SBG-Núcleo Norte, Belém, pp 78–80

Dall'Agnol R, Oliveira MA, Almeida JAC, et al (2006) Archean and paleoproterozoic granitoids of the Carajás Metallogenic Province, eastern Amazon Craton. In: Symposium on magmatism, crustal evolution and metallogenesis of the Amazonian craton. Belém, pp 99–150

Dardenne MA, Ferreira Filho CF, Meirelles MR (1988) The role of shoshonitic and calc-alkaline suites in the tectonic evolution of the Carajás District, Brazil. Journal of South American Earth Sciences 1:363–372. doi: 10.1016/0895-9811(88)90023-5

Delinardo da Silva MA (2014) Metatexitos e diatexitos do Complexo Xingú na região de Canaã dos Carajás: Implicações para a evolução mesoarqueana do Domínio Carajás. Universidade de Campinas

Dias GS, Macambira MB, Dall'Agnol R, et al (1996) Datações de zircões de sill de metagabro: Comprovação de idade arqueana da Formação Águas Claras, Carajás, Pará. In: V Simpósio de Geologia da Amazônia. SBG, Belém, pp 376–378

DOCEGEO (1988) Revisão litoestratigráfica da Província Mineral de Carajás - Litoestratigrafia e principais depósitos minerais. In: XXXV Congresso Brasileiro de Geologia. SBG, Belém, pp 11–54

Dreher AM (2004) O depósito primário de Cu-Au de Igarapé-Bahia, Carajás: Rochas fragmentárias, fluidos mineralizantes e modelo metalogenético. Universidade Estadual de Campinas

Dreher AM, Xavier RP, Taylor BE, Martini SL (2008) New geologic, fluid inclusion and stable isotope studies on the controversial Igarapé Bahia Cu-Au deposit, Carajás Province, Brazil. Mineralium Deposita 43:161–184. doi: 10.1007/s00126-007-0150-6

Feio GRL, Dall'Agnol R, Dantas EL, et al (2013) Archean granitoid magmatism in the Canaã dos Carajás area: Implications for crustal evolution of the Carajás province, Amazonian craton, Brazil. Precambrian Research 227:157–185. doi: 10.1016/j.precamres.2012.04.007

Feio GRL, Dall'Agnol R, Dantas EL, et al (2012) Geochemistry, geochronology, and origin of the Neoarchean Planalto Granite suite, Carajás, Amazonian craton: A-type or hydrated charnockitic granites? Lithos 151:57–73. doi: 10.1016/j.lithos.2012.02.020

Ferreira Filho CF, Cançado F, Correa C, et al (2007) Mineralizações estratiformes de PGE-Ni associadas a complexos acamadados em Carajás: os exemplos de Luanga e Serra da Onça. In: Rosa-Costa LT, Klein EL, Viglio EP (eds) Contribuições à geologia da Amazônia, v. 5. SBG-Núcleo Norte, Belém, pp 1–14

Fournier RO (1983) Active hydrothermal systems as analogues of fossil systems. In: Eaton G (ed) The Role of Heat in the Development of Energy and Mineral Resources in the Northern Basin and Range Province. Geothermal Resources Council, Davis, pp 263–284

Gabriel EO, Oliveira DC (2014) Geologia, petrografia e geoquímica dos granitoides arqueanos de alto magnésio da região de Água Azul do Norte, porção sul do Domínio Carajás, Pará. Boletim do Museu Paraense Emílio Goeldi - Série Ciências Naturais 9:533–564.

Galarza MA, Macambira MJB (2002) Geocronologia e evolução crustal da área do depósito de Cu-Au Gameleira, Província Mineral de Carajás (Pará), Brasil. Revista do Instituto de Geociências da USP 2:143–159.

Galarza MA, Macambira MJB, Moura CA V. (2003) Geocronologia Pb-Pb e Sm-Nd das rochas máficas do depósito Igarapé Bahia, Província Mineral de Carajás (PA). In: VII Simpósio de Geologia da Amazônia. p CD-ROM

Galarza MA, Macambira MJB, Villas RN (2008) Dating and isotopic characteristics (Pb and S) of the Fe oxide-Cu-Au-U-REE Igarapé Bahia ore deposit, Carajás mineral province, Pará state, Brazil. Journal of South American Earth Sciences 25:377–397. doi: 10.1016/j.jsames.2007.07.006

Grainger CJ, Groves DI, Tallarico FHB, Fletcher IR (2008) Metallogenesis of the Carajás Mineral Province, Southern Amazon Craton, Brazil: Varying styles of Archean through Paleoproterozoic to Neoproterozoic base- and precious-metal mineralisation. Ore Geology Reviews 33:451–489. doi: 10.1016/j.oregeorev.2006.10.010

Hirata WK, Rigon JC, Kadekaru K, et al (1982) Geologia regional da Província Mineral de Carajás. In: I Simpósio de Geologia da Amazônia. SBG/NO, Belém, pp 100–110

Hitzman MW, Oreskes N, Einaudi MT (1992) Geological characteristics and tectonic setting of proterozoic iron oxide (Cu-U-Au-REE) deposits. Precambrian Research 58:241–287. doi: 10.1016/0301-9268(92)90121-4

Hou KJ, Li YH, Xiao YK, et al (2010) In situ boron isotope measurements of natural geological materials by LA-MC-ICP-MS. Chinese Science Bulletin 55:3305–3311. doi: 10.1007/s11434-010-4064-9

Huang X-W, Qi L, Gao J-F, Zhou M-F (2013) First Reliable Re-Os Ages of Pyrite and Stable Isotope Compositions of Fe(-Cu) Deposits in the Hami Region, Eastern Tianshan Orogenic Belt, NW China. Resource Geology 63:166–187. doi: 10.1111/rge.12003

Huhn SRB, Macambira MJB, Dall'Agnol R (1999a) Geologia e geocronologia Pb-Pb do Granito Alcalino Planalto, Região da Serra do Rabo, Carajás-PA. In: VI Simpósio de Geologia da Amazônia. SBG-Núcleo Norte, pp 463–466

Huhn SRB, Souza CIJ, Albuquerque MC, et al (1999b) Descoberta do depósito Cu(Au) Cristalino: geologia e mineralização associada - Região da Serra do Rabo - Carajás - PA. In: VI Simpósio de Geologia da Amazônia. SBG-Núcleo Norte, Manaus, pp 140–143

Lindenmayer ZG, Pimentel MM, Ronchi LH, et al (2001) Geologia do depósito de Cu-Au de Gameleira, Serra dos Carajás, Pará. In: Jost H, Brod JA, Queiroz ET (eds) Caracterização de depósitos auríferos em distritos mineiros. DNPM/ADIMB, Brasília, pp 81–139

Liu W, McPhail DC (2005) Thermodynamic properties of copper chloride complexes and copper transport in magmatic-hydrothermal solutions. Chemical Geology 221:21–39. doi: 10.1016/j.chemgeo.2005.04.009

Lobato LM, Rosière CA, Silva RCF, et al (2005) A mineralização hidrotermal de ferro da Província Mineral de Carajás: Controle estrutural e contexto na evolução metalogenética da província. In: Marini OJ, Queiroz ET, Ramos BW (eds) Caracterização de depósitos minerais em distritos mineiros da Amazônia. DNPM/CT-Mineral/ADIMB, Brasília, pp 21–92

London D, Morgan GB, Wolf MB (1996) Boron in granitic rocks and their contact aureoles. In: Grew ES, Anovitz LM (eds) Boron: Mineralogy, Petrology and Geochemistry, v. 33. Mineralogical Society of America. Reviews in Mineralogy, pp 299–330

Macambira EMB, Ferreira Filho CF (2002) Fracionamento magmático dos corpos máfico-ultramáficos da Suíte Intrusiva Cateté – sudeste do Pará. In: Klein EL, Vasquez ML, Rosa-Costa LT (eds) Contribuições à geologia da Amazônia, v. 3. SBG-Núcleo Norte, Belém, pp 105–114

Macambira EMB, Vale AG (1997) São Félix do Xingu: folha SB.22-Y-B, Estado do Pará, escala 1:250.000. Texto Explicativo. In: Programa Levantamentos Geológicos Básicos do Brasil (PLGB). CPRM, Brasília, p 344

Machado N, Lindenmayer Z, Krogh TE, Lindenmayer D (1991) U-Pb geochronology of Archean magmatism and basement reactivation in the Carajás area, Amazon shield, Brazil. Precambrian Research 49:329–354. doi: 10.1016/0301-9268(91)90040-H

Markey R, Stein H, Morgan J (1998) Highly precise Re-Os dating for molybdenite using alkaline fusion and NTIMS. Talanta 45:935–946. doi: 10.1016/S0039-9140(97)00198-7

Marschall HR, Jiang SY (2011) Tourmaline isotopes: No element left behind. Elements 7:313–319. doi: 10.2113/gselements.7.5.313

Marschall HR, Meyer C, Wunder B, et al (2009) Experimental boron isotope fractionation between tourmaline and fluid: Confirmation from in situ analyses by secondary ion mass spectrometry and from Rayleigh fractionation modelling. Contributions to Mineralogy and Petrology 158:675–681. doi: 10.1007/s00410-009-0403-8

Marschik R, Mathur R, Ruiz J, et al (2005) Late Archean Cu-Au-Mo mineralization at Gameleira and Serra Verde, Carajás Mineral Province, Brazil: Constraints from Re-Os molybdenite ages. Mineralium Deposita 39:983–991. doi: 10.1007/s00126-004-0450-z

Marschik R, Mathur R, Ruiz J, et al (2002) An Archean Re-Os molybdenite age for the Gameleira Cu-Au-Mo mineralization, Carajás Province, Brazil. Geological Society of America Abstract With Programs 34:337.

Medeiros Neto FA, Villas RNN (1985) Geologia da jazida de Cu-Zn do corpo 4E-Pojuca, Serra dos Carajás. In: II Simpósio de Geologia da Amazônia. SBG-Núcleo Norte, Belém, pp 97–112

Meirelles MR (1986) Geoquímica e petrologia dos jaspilitos e rochas vulcânicas associadas, Grupo Grão-Pará, Serra dos Carajás. UnB

Meirelles MR, Dardenne MA (1991) Vulcanismo basáltico de afinidade shoshonítica em ambiente de arco arqueano, Grupo Grão-Pará, Serra Dos Carajás - Pará. Revista Brasileira de Geociências 21:41–50.

Melo GHC, Monteiro LVS, Moreto CPN, et al (2014) Paragenesis and evolution of the hydrothermal Bacuri iron oxide-copper-gold deposit, Carajás Province (PA). Brazilian Journal of Geology 44:73–90. doi: 10.5327/Z2317-4889201400010007

Melo GHC, Monteiro LVS, Xavier RP, et al (2016) Temporal evolution of the giant Salobo IOCG deposit, Carajás Province (Brazil): Constraints from paragenesis of hydrothermal alteration and U-Pb geochronology. Mineralium Deposita 52:709–732. doi: 10.1007/s00126-016-0693-5

Meyer C, Wunder B, Meixner A, et al (2008) Boron-isotope fractionation between tourmaline and fluid: An experimental re-investigation. Contributions to Mineralogy and Petrology 156:259–267. doi: 10.1007/s00410-008-0285-1

Mikucki EJ, Ridley JR (1993) The hydrothermal fluid of Archean lode-gold deposits at different metamorphic grades: compositional constraints from ore and wallrock alteration assemblages. Mineralium Deposita 28:469–481.

Monteiro LVS, Xavier RP, Carvalho ER, et al (2007) Spatial and temporal zoning of hydrothermal alteration and mineralization in the Sossego iron oxide–copper–gold deposit, Carajás Mineral Province, Brazil: paragenesis and stable isotope constraints.

Moreto CPN, Monteiro LVS, Xavier RP, et al (2015a) Neoarchean and paleoproterozoic iron oxide-copper-gold events at the Sossego deposit, Carajás Province, Brazil: Re-Os and U-Pb geochronological evidence. Economic Geology 110:809–835. doi: 10.2113/econgeo.110.3.809

Moreto CPN, Monteiro LVS, Xavier RP, et al (2015b) Timing of multiple hydrothermal events in the iron oxide–copper–gold deposits of the Southern Copper Belt, Carajás Province, Brazil. Mineralium Deposita 50:517–546. doi: 10.1007/s00126-014-0549-9

Moreto CPN, Monteiro LVS, Xavier RP, et al (2011) Mesoarchean (3.0 and 2.86 Ga) host rocks of the iron oxide-Cu-Au Bacaba deposit, Carajás Mineral Province: U-Pb geochronology and metallogenetic implications. Mineralium Deposita 46:789–811. doi: 10.1007/s00126-011-0352-9

Mougeot R, Respaut JP, Brique L, et al (1996) Geochronological constraints for the age of the Águas Claras Formation (Carajás Province, Pará, Brazil). In: XXXIX Congresso Brasileiro de Geologia. SBG, Salvador, pp 579–581

Neves MP (2006) Estudos isotópicos (Pb-Pb, Sm-Nd, C e O) do depósito Cu-Au do Sossego, Província Mineral de Carajás. Universidade Federal do Pará

Nogueira ACR, Truckenbrodt W, Pinheiro RVL (1995) Formação Águas Claras, Pré-Cambriano da Serra dos Carajás: Redescrição e redefinição litoestratigráfica. Boletim do Museu Paraense Emílio Goeldi - Série Ciências da Terra 7:177–277.

Oliver NHS, Cartwright I, Wall VJ, Golding SD (1993) The stable isotope signature of kilometre-scale fracture dominated metamorphic fluid pathways, Mary Kathleen, Australia. Journal of Metamorphic Geology 11:705–720. doi: 10.1111/j.1525-1314.1993.tb00182.x

Pal DC, Trumbull RB, Wiedenbeck M (2010) Chemical and boron isotope compositions of tourmaline from the Jaduguda U (-Cu-Fe) deposit, Singhbhum shear zone, India: Implications for the sources and evolution of mineralizing fluids. Chemical Geology 277:245–260. doi: 10.1016/j.chemgeo.2010.08.008

Palmer MR, London D, Morgan VI GB, Babb HA (1992) Experimental determination of fractionation of 11B/10B between tourmaline and aqueous vapor: A temperature- and pressure-dependent isotopic system. Chemical Geology 101:123–129. doi: http://dx.doi.org/10.1016/0009-2541(92)90209-N

Perring CS, Pollard PJ, Blake KL, et al (1999) Metallogeny of the Lightning Creek Cu-Au prospect, Mount Isa Inlier, Australia. In: Stanley CJ, Rankin AH, Bodnar RJ (eds) Mineral deposits: processes to processing. Balkema, Rotterdam, pp 413–416

Pimentel MM, Lindenmayer ZG, Laux JH, et al (2003) Geochronology and Nd isotope geochemistry of the Gameleira Cu – Au deposit, Serra dos Carajás, Brazil: 1.8 - 1.7 Ga hydrothermal alteration and mineralization. Journal of South American Earth Sciences 15:803–813.

Pinheiro RVL, Holdsworth RE (1997) Reactivation of Archaean strik-slip fault systems, Amazon region, Brazil. Journal of the Geological Society of London 154:99–103.

Pinheiro RVL, Kadekaru K, Soares AV, et al (2013) Carajás, Brazil - a short tectonic review. In: XIII Simpósio de Geologia da Amazônia. Belém, pp 1086–1089

Pokrovski GS, Akinfiev NN, Borisova AY, et al (2014) Gold speciation and transport in geological fluids: insights from experiments and physical-chemical modelling. Geological Society, London, Special Publications 402:9–70. doi: 10.1144/SP402.4

Pokrovski GS, Borisova AY, Bychkov AY (2013) Speciation and transport of metals and metalloids in geological vapors. Reviews in Mineralogy and Geochemistry 76:165–218. doi: 10.2138/rmg.2013.76.6

Pollard PJ (2001) Sodic (-calcic) alteration in Fe-oxide-Cu-Au districts: an origin via unmixing of magmatic H2O-CO2-NaCl ± CaCl2-KCl fluids. Mineralium Deposita 36:93–100.

Pollard PJ (2006) An intrusion-related origin for Cu-Au mineralization in iron oxide-copper-gold (IOCG) provinces. Mineralium Deposita 41:179–187. doi: 10.1007/s00126-006-0054-x

Qi L, Zhou M-F, Gao J, Zhao Z (2010) An improved Carius tube technique for determination of low concentrations of Re and Os in pyrites. Journal of Analytical Atomic Spectrometry 25:585–589. doi: 10.1039/b919016c

Qi L, Zhou M-F, Wang CY, Sun M (2007) Evaluation of a technique for determining Re and PGEs in geological samples by ICP-MS coupled with a modified Carius tube digestion. Geochemical Journal 41:407–414. doi: 10.2343/geochemj.41.407

Réquia K, Fontboté L (2001) The Salobo iron oxide copper-gold hydrothermal system, Carajás mineral province, Brazil. Geological Society of America Abstract With Programs 33:2.

Réquia K, Stein H, Fontboté L, Chiaradia M (2003) Re-Os and Pb-Pb geochronology of the Archean Salobo iron oxide copper-gold deposit, Carajás mineral province, northern Brazil. Mineralium Deposita 38:727–738. doi: 10.1007/s00126-003-0364-1

Réquia K, Xavier RP, Figueiredo BR (1995) Evolução paragenética, textural e das fases fluidas no depósito polimetálico de Salobo, Província Mineral de Carajás, Pará. Boletim do Museu Paraense Emílio Goeldi - Série Ciências da Terra 7:27–39.

Rimstidt JD (1997) Gangue mineral transport and deposition. In: Barnes HL (ed) Geochemistry of Hydrothermal Ore Deposits, 3rd edn. Wiley, New York, pp 435–487

Rodrigues DS, Oliveira DC, Macambira MJB (2014) Geologia, geoquímica e geocronologia do Granito Mesoarqueano Boa Sorte, município de Água Azul do Norte, Pará – Província Carajás. Boletim do Museu Paraense Emílio Goeldi - Série Ciências Naturais 9:597–633.

Roedder E (1984) Fluid Inclusions. Mineralogical Society of America. Reviews in Mineralogy, Washington

Roedder E (1971) Metastability in Fluid Inclusions. In: IMA-IAGOD Meetings ’70, IAGOD Vol. The Society of Resource Geology, pp 327–334

Ronchi LH, Lindenmayer ZG, Araújo JC, Baecker CA (2001) Assinatura granítica das inclusões fluidas relacionadas ao depósito de Cu-Au de Gameleira, Carajás, PA. In: VII Simpósio de Geologia da Amazônia.

Rusk B, Oliver N, Blenkinsop T, Zhang D (2010) Physical and chemical characteristics of the Ernest Henry iron oxide copper gold deposit, Cloncurry, Queensland, Australia: Implications for IOCG genesis. In: Porter TM (ed) Hydrothermal Iron Oxide Copper-Gold & Related Deposits: A Global Perspective, v.3, Advances in the Understanding of IOCG Deposits. PGC Publishing, Adelaide, pp 201–218

Sardinha AS, Barros CEM, Krymsky R (2006) Geology, geochemistry, and U-Pb geochronology of the Archean (2.74 Ga) Serra do Rabo granite stocks, Carajás Metallogenetic Province, northern Brazil. Journal of South American Earth Sciences 20:327–339. doi: 10.1016/j.jsames.2005.11.001

Saueressig R (1988) Depósito de cobre e zinco do Corpo Quatro, Pojuca. In: XXXV Congresso Brasileiro de Geologia. SBG, Belém, pp 115–119

Schoenberg R, Nägler TF, Kramers JD (2000) Precise Os isotope ratio and Re – Os isotope dilution measurements down to the picogram level using multicollector inductively coupled plasma mass spectrometry. International Jounral of Mass Spectrometry 197:85–94.

Schwarz M, Frantz JC (2013) Depósito de Cu-Zn Pojuca Corpo Quatro: IOCG ou VMS? Pesquisas em Geociências 40:5–19.

Shirey SB, Walker RJ (1995) Carius Tube Digestion for Low-Blank Rhenium-Osmium Analysis. Analytical Chemistry 67:2136–2141. doi: 10.1021/ac00109a036

Silva AC, Dall'Agnol R, Guimarães FV, Oliveira DC (2014) Geologia, petrografia e geoquímica de Associações Tonalíticas e Trondhjemíticas Arqueanas de Vila Jussara, Província Carajás, Pará. Boletim do Museu Paraense Emílio Goeldi - Série Ciências Naturais 9:13–45.

Silva MG, Teixeira JBG, Pimentel MM, et al (2005) Geologia e mineralizações de Fe-Cu-Au do Alvo GT46 (Igarapé Cinzento), Carajás. In: Marini OJ, Queiroz ET, Ramos BW (eds) Caracterização de depósitos minerais em distritos mineiros da Amazônia. Brasília, pp 94–151

Skirrow RG, Walshe JL (2002) Reduced and oxidized Au-Cu-Bi iron oxide deposits of the Tennant Creek Inlier, Australia: An integrated geologic and chemical model. Economic Geology 97:1167–1202. doi: 10.2113/gsecongeo.97.6.1167

Smith HJ, Spivack AJ, Staudigel H, Hart SR (1995) The boron isotopic composition of altered oceanic crust. Chemical Geology 126:119–135. doi: 10.1016/0009-2541(95)00113-6

Somarin AK, Mumin AH (2014) P-T composition and evolution of paleofluids in the Paleoproterozoic Mag Hill IOCG system, Contact Lake belt, Northwest Territories, Canada. Mineralium Deposita 49:199–215. doi: 10.1007/s00126-013-0482-3

Souza SRB, Macambira MJB, Sheller T (1996) Novos dados geocronológicos para os granitos deformados do Rio Itacaiúnas (Serra dos Carajás, PA): implicações estratigráficas. In: V Simpósio de Geologia da Amazônia. SBG, Belém, pp 380–383

Steele-MacInnis M, Bodnar RJ, Naden J (2011) Numerical model to determine the composition of H2O-NaCl-CaCl2 fluid inclusions based on microthermometric and microanalytical data. Geochimica et Cosmochimica Acta 75:21–40. doi: 10.1016/j.gca.2010.10.002

Stein HJ, Sundblad K, Markey RJ, et al (1998) Re-Os ages for Archean molybdenite and pyrite, Kuittila-Kivisuo, Finland and Proterozoic molybdenite, Kabeliai, Lithuania: Testing the chronometer in a metamorphic and metasomatic setting. Mineralium Deposita 33:329–345. doi: 10.1007/s001260050153

Tallarico FHB (2003) O cinturão cupro-aurífero de Carajás, Brasil. Universidade Estadual de Campinas

Tallarico FHB, Figueiredo BR, Groves DI, et al (2005) Geology and SHRIMP U-Pb geochronology of the Igarapé Bahia deposit, Carajás copper-gold belt, Brazil: An Archean (2.57 Ga) example of Iron-Oxide Cu-Au-(U-REE) mineralization. Economic Geology 100:7–28. doi: 10.2113/100.1.0007

Tallarico FHB, McNaughton NJ, Groves DI, et al (2004) Geological and SHRIMP II U-Pb constraints on the age and origin of the Breves Cu-Au-(W-Bi-Sn) deposit, Carajás, Brazil. Mineralium Deposita 39:68–86. doi: 10.1007/s00126-003-0383-y

Teixeira JBG (1994) Geochemistry, petrology, and tectonic setting of the archean basaltic and dioritic rocks from the N4 Iron deposit, Serra dos Carajás, Pará, Brazil. Penn State University

Teixeira JBG, Lindenmayer ZG, Silva MG (2010) Depósitos de Óxido de Fe, Cu-Au de Carajás. In: Brito RSC, Silva MG, Kuyumjian RM (eds) Modelos de depósitos de cobre do Brasil e sua resposta ao intemperismo, 1 ed. CPRM, Brasília, pp 15–48

Teixeira MFB, Dall'Agnol R, Silva AC, Santos PA (2013) Geologia, petrografia e geoquímica do Leucogranodiorito Pantanal e dos leucogranitos arqueanos da área a norte de Sapucaia, Província Carajás, Pará: Implicações petrogenéticas. Boletim do Museu Paraense Emílio Goeldi - Série Ciências Naturais 8:291–323.

Tonarini S, Pennisi M, Adorni-Braccesi A, et al (2003) Intercomparison of boron isotope and concentration measurements. Part I: Selection, preparation and homogeneity tests of the intercomparison materials. Geostandards Newsletter 27:21–39. doi: 10.1111/j.1751-908X.2003.tb00710.x

Torresi I, Xavier RP, Bortholoto DFA, Monteiro LVS (2012) Hydrothermal alteration, fluid inclusions and stable isotope systematics of the Alvo 118 iron oxide-copper-gold deposit, Carajás Mineral Province (Brazil): Implications for ore genesis. Mineralium Deposita 47:299–323. doi: 10.1007/s00126-011-0373-4

Trendall AF, Basei MAS, De Laeter JR, Nelson DR (1998) SHRIMP zircon U-Pb constraints on the age of the Carajás formation, Grão Pará Group, Amazon Craton. Journal of South American Earth Sciences 11:265–277. doi: 10.1016/S0895-9811(98)00015-7

VALE (2017) Produção da Vale no 4T16.

VALE (2009) Revisão na tipologia de minério do Depósito Pólo.

Vanko DA, Bishop FC (1982) Occurrence and origin of marialitic scapolite in the Humboldt lopolith, N.W. Nevada. Contributions to Mineralogy and Petrology 81:277–289. doi: 10.1007/BF00371682

Vasquez ML, Rosa-Costa LT, Silva CMG, et al (2008) Geologia e Recursos Minerais do Estado do Pará: Sistema de Informações Geográficas - SIG: texto explicativo dos mapas Geológico e Tectônico e de Recursos Minerais do Estado do Pará. Escala 1:1.000.000. CPRM, Belém

Villas RN, Neves MP, Moura C V., et al (2006) Estudos isotópicos (Pb, C e O) no depósito Cu-Au do Sossego, Província Mineral de Carajás. In: IX Simpósio de Geologia da Amazônia. SBG-Núcleo Norte, Belém, p [CD-ROM]

Williams-Jones AE, Bowell RJ, Migdisov AA (2009) Gold in solution. Elements 5:281–287. doi: 10.2113/gselements.5.5.281

Winter CJ (1994) Geology and base-metal mineralization associated with Archean iron-formation in the Pojuca Corpo Quatro Deposit, Carajás, Brazil. University of Southampton

Wirth KR, Gibbs AK, Olszewski Jr. WJ (1986) U-Pb ages of zircons from the Grão-Pará Group and Serra dos Carajás Granites, Pará, Brazil. Revista Brasileira de Geociências 16:195–200.

Xavier RP, Monteiro LVS, Moreto CPN, et al (2012) The iron oxide copper-gold systems of the Carajás mineral province. Economic Geology 16:433–454.

Xavier RP, Monteiro LVS, Souza Filho CR, et al (2010) The iron oxide copper-gold deposits of the Carajás Mineral Province, Brazil: An update and critical review. In: Porter TM (ed) Hydrothermal Iron Oxide Copper-Gold & Related Deposits: A Global Perspective, v.3, Advances in the Understanding of IOCG Deposits. PGC Publishing, Adelaide,

Xavier RP, Rusk B, Emsbo P, Monteiro LVS (2009) Composition and source of salinity of ore-bearing fluids in Cu-Au systems of the Carajás Mineral Province, Brazil. In: 10th SGA Biennial Meeting. SGA, Townsville, pp 272–274

Xavier RP, Trumbull RB, Wiedenbeck M, Monteiro LVS (2013) Sources of mineralizing fluids in Cu-Au systems from the Carajás Mineral Province (Brazil): constraints from in-situ microanalysis of hydrogen and boron isotopes in tourmaline. In: 12th SGA Biennial Meeting. Uppsala, pp 1402–1405

Xavier RP, Wiedenbeck M, Trumbull RB, et al (2008) Tourmaline B-isotopes fingerprint marine evaporites as the source of high-salinity ore fluids in iron oxide copper-gold deposits, Carajás Mineral Province (Brazil). Geology 36:743–746. doi: 10.1130/G24841A.1

Yang SY, Jiang SY, Palmer MR (2015) Chemical and boron isotopic compositions of tourmaline from the Nyalam leucogranites, South Tibetan Himalaya: Implication for their formation from B-rich melt to hydrothermal fluids. Chemical Geology 419:102–113. doi: 10.1016/j.chemgeo.2015.10.026